Multiphysical study of cladding failure detection in Sodium cooled Fast Reactors

Congjin Ding

THÈSE

Pour obtenir le grade de

DOCTEUR DE L'UNIVERSITÉ GRENOBLE ALPES

Spécialité : MEP : Mécanique des fluides Energétique, Procédés

Arrêté ministériel : 25 mai 2016

Présentée par

Congjin DING

Thèse dirigée par **Phillipe FILLIATRE** et **Lionel DESGRANGES**

préparée au sein du **CEA Cadarache**
dans **l'École Doctorale I-MEP2 - Ingénierie - Matériaux, Mécanique, Environnement, Energétique, Procédés, Production**

Etude multiphysique de la détection des ruptures de gaine dans les réacteurs rapides refroidis au sodium

Multiphysical study of cladding failure detection in Sodium cooled Fast Reactors

Thèse soutenue publiquement le **22 septembre 2022,**
devant le jury composé de :

Monsieur Pablo RUBIOLO
PROFESSEUR, Université Grenoble Alpes, Président
Madame Teodora RETEGAN VOLLMER
PROFESSEUR, Chalmers University of Technology, Rapporteure
Monsieur Benoît GALL
PROFESSEUR, Institut Pluridisciplinaire Hubert Curien, Rapporteur
Monsieur Kan WANG
PROFESSEUR, Tsinghua University, Examinateur
Monsieur Phillipe FILLIATRE
DIRECTEUR DE RECHERCHE, CEA Cadarache, Directeur de thèse
Monsieur Lionel DESGRANGES
Professeur à l'INSTN, CEA Cadarache, Encadrant de thèse

CEA/DES/IRESNE/DER/SPESI/LDCI DO 2022-082 du 29/06/2022

Contents

List of Figures

List of Tables

Abbreviations

ASTRID	Advanced Sodium Technological Reactor for Industrial Demonstration
BOL	Beginning of life
CEA	French Alternative Energies and Atomic Energy Commission
CEFR	China Experimental Fast Reactor
DND	Delayed neutrons detection system (Détection des Neutrons Différés)
DNP	Delayed neutron precursors
DRG	Gas detection system (Détection des Ruptures de Gaine)
EOL	End of life
FBTR	Fast Breeder Test Reactor
FGR	Fission gas release
FP	Fission products
FSRP	Fuel-Sodium Reactions Products
GFR	Gas-cooled fast reactor
GIF	Generation IV International Forum
HTF	Hydraulic Transfer Function
JHR	Jules Horowitz Reactor
JOG	Joint Oxyde-Gaine
LFR	Lead-cooled fast reactor
LRG	Pin failure location system (Localisation des Ruptures de Gaine)
OSR	Oxide-Sodium Reaction
PFBR	Prototype Fast Breeder Reactor
PRISM	Power Reactor Innovative Small Module
PWR	Pressurized water reactor
R&D	Research and Development
RG	Fuel pin failure (Rupture de gaine)
SFR	Sodium cooled fast reactors

General introduction

Since the beginning of the new century, new energy demands have arisen, and global warming due to fossil fuels has become a significant issue [108]. People have had more new thinking about the use of nuclear energy, which now provides about 10% of the world's electricity from about 440 power reactors, and it is the world's second-largest source of low-carbon power, as shown in Fig. 1. At the levels of "deep decarbonization" that have been widely discussed in international policy deliberations - for example, a 2050 emissions target for the electric sector that is well below 50 grams of carbon dioxide per kilowatt-hour of electricity generation (gCO_2/KWh) - including nuclear in the mix of capacity options helps to minimize or constrain rising system costs, which makes attaining stringent emissions goals more realistic [30].

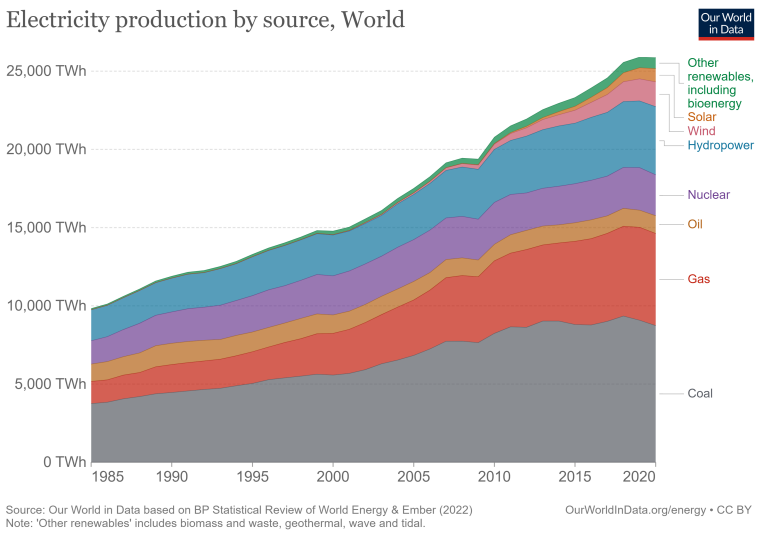

Figure 1: World electricity production by source.

In the future development of nuclear energy, it is necessary not only to improve safety and economy continuously but also to upgrade the treatment of nuclear fuel supply and nuclear waste disposal. Better use of natural resources and reducing the long-lived wastes are the main factors contributing to the renewed interest in fast breeder reactors [148]. The Generation IV International Forum

(GIF) was established in 2000 to coordinate research and development work for Generation IV nuclear energy systems [36]. The Generation IV nuclear energy systems comprise nuclear reactor technologies that could be deployed by the mid-21st century and present significant advancements in economics, safety, reliability, and sustainability over currently operating reactors [141].

There are six types of reactors in the Gen-IV nuclear energy system, which include sodium-cooled fast reactors (SFR), lead-cooled fast reactors (LFR), gas-cooled fast reactors (GFR), supercritical water reactors, ultra-high temperature gas-cooled reactors and molten salt fast reactors. Among them, SFR featured a fast-spectrum reactor and closed fuel recycle system. The primary mission of the SFR is to improve resource utilization, management of high-level wastes, and management of plutonium and other actinides. Moving to SFR reactors would then highly reduce the need for natural uranium and therefore increase the self-sufficiency in uranium of countries in high nuclear energy development [122].

Safety and reliability are essential for developing and operating Gen-IV SFRs. The level of increased safety to be achieved in SFR requires the development of instrumental means intended to monitor the radioactive material confinement barriers, which are in order: the fuel cladding, the primary circuit, and the reactor building containment. During the operation of SFR, there might be fuel pin failures [92], which represent a crack or a rupture on the cladding, which is the first confinement barrier of the fuel inside the reactor core. The release of fissile materials from fuel pin failure can result in coolant channel blockages which may impede the sodium cooling of the fuel and eventually lead to a threat to the core integrity in SFR.

Marked by historic achievements with the deployment of RAPSODIE, PHENIX, and SUPERPHENIX, France focused on SFR development, where it has significant experience, feedback, and maturity. Although the construction of the ASTRID project was abandoned in 2019, research and development on fast reactors persisted, which allowed France to maintain and improve its expertise in the technology and ensured a restart at any time.

The "clean sodium concept" is demanded for SFR in France to assure the reliability of the reactor. A contamination measuring system has to be designed in order to continuously search for the release of fission products by a fuel pin failure [115]. This thesis work is part of monitoring the fuel cladding failure and aims to have an overall view of the fuel pin failure detection in SFR due to its significance. Historically, two complementary and independent functions have been dedicated to monitoring and managing these leakages through cladding. It's about:

- Fission gas signal will be monitored by the DRG system (Gas detection sys-

tem), which is the first signal released when there is a crack on the cladding.

- Neutron signal will be detected in the DND system (Delayed neutron detection system) when the cladding crack is enlarged. The neutron signal is related to the breached fuel size in the sodium. When the neutron signal reaches the threshold, the reactor is shut down.

From the perspective of detection system design, due to the different monitoring purposes and release characteristics of fission products in gas and neutron detection, the key parameters for detection system design will be different. In order to evaluate conception choices for this system and optimize detection system design, a comprehensive view is sought from a fuel and detection perspective. Based on the safety requirements of the SFR, I will study in this thesis a general approach to comprehensively describe the cladding failure and induced contamination detection of sodium cooled fast reactors. Basically, I will conceive a general model based on descriptions of physical and chemical phenomena; then, I will use experimental data from past reactors to test the model and provide new interpretations of the data; hopefully, I will give some guidelines for new systems in future reactors.

This thesis is built around seven chapters:

- The chapter 1 of this manuscript will propose a synthetic description of the main characteristics of fuel pin failure in SFR;
- The chapter 2 will be devoted to historical instrumental methods designed to monitor cladding ruptures. A roadmap to address the thesis problem will therefore be presented;
- The chapter 3 and chapter 4 will be dedicated to the modeling of the whole gas detection system, including the fission gas release, the transfer function of the system, and the detector efficiency;
- The chapter 5 and chapter 6 will focus on the neutron detection system, including the modeling of the transfer process of fission products and the analysis of release mechanisms due to the fuel pin behavior.
- The chapter 7 will discuss the methodology applications and improvements.

The general conclusions will highlight the main results of this work, for which perspectives will be presented.

Chapter 1

Fuel pin failure in sodium cooled fast reactor

This chapter begins with the requirements of the GEN IV reactor, and the advantages of sodium cooled fast neutron reactors in order to meet the current energy and environmental challenges. The main types and projects of SFR research and development are introduced, especially the historic achievements with the deployment of RAPSODIE, PHENIX, and SUPERPHENIX in France. The core components of SFR are stated, including the fuel pin, coolant, and the core, as the basic knowledge of the thesis.

SFR must demonstrate increased safety compared to its predecessors, particularly concerning the problems of cladding failures. The significance of fuel pin failure monitoring in SFR is presented, and the difference between pin failure problems in water reactors is explained. Then the characteristic of fuel pin failure evolution and the release mechanism of fission products are illustrated.

1.1 Development of SFR

Several frameworks of reflection have been undertaken in order to define the nuclear systems that could meet the energy needs of tomorrow. The fourth-generation (Gen-IV) nuclear energy system aims to catalyze global research and development to bring out the nuclear systems of the future, which target economics, safety, sustainability, and nuclear non-proliferation:

- Economics means a significant price advantage over other energy sources during the lifetime. The total power generation cost must be more competitive than the other power generation methods in the region or country where the plant is located.
- Safety means excellent safety and reliability, including very low core breakage probability and damage. For any credible cause-cause event, the Gen-IV reactor does not suffer severe core damage and must be demonstrated through a comprehensive reactor experiment.
- Sustainability means meeting clean air targets and efficiently using fuel resources while producing electricity. Reduce and effectively manage nuclear waste, reduce the burden on operations and related personnel, and thus improve public and environmental protection.
- Advantages are addressed for fast reactors in the creation of a more reliable mode of nonproliferation in the closed nuclear fuel cycle in comparison with the existing fully open and partially closed fuel cycles of thermal reactors [10].

In the development of Gen-IV reactors, SFR has the most comprehensive technological basis due to experience gained worldwide and the operation of several experimental, prototype, and commercial size reactors [64] [15]. For example, SFR has been selected as the reference fast reactor concept in the U.S., France, and Japan. SFR technology evaluation relies significantly on the substantial base technology development programs within each country, and it has already been developed to commercial or near the commercial scale, unlike the other reactors [118]. In the past years, the demonstration and prototype SFRs such as PFR (UKAEA), PHENIX (France), BN-350 (Kazakhstan), SUPERPHENIX (France), BN-600 (Russia), and Monju (Japan) have established technology bases; pioneering experience was acquired by experimental SFRs including Fermi (USA), EBR-II (USA), FFTF (USA), DFR (UKAEA), Rapsodie (France), BR-5/10 (Russia), BOR-60 (Russia), Joyo (Japan), FBTR (India) [8].

Sodium cooled reactors could be categorized into loop and pool types, as shown in Fig. 1.1 and Fig. 1.2. In the pool type, the primary coolant is contained in the main reactor vessel, which therefore includes the reactor core and a heat exchanger. In the loop type, the heat exchangers are outside the reactor tank. Pool and loop type reactors in the world are shown in Tab. 1.1. From the viewpoint of operational experiences in the prototype class, BN-350 had operational experiences. Monju is the only existing reactor as the loop prototype. For the pool type, PFR, Phenix, and BN-600 accumulated operational experiences. BN-600 is still in operation, and PFBR and BN-800 have started operation. As the next-generation reactors, PRISM, BN-1200, and PGSFR have selected the pool type. JSFR has adopted the loop type, reducing construction costs with innovative technologies [102]. As a whole, the pool-type sodium-cooled fast reactor seems to be the most promising concept in the current state of our knowledge and of European baseline design and safety requirements [105].

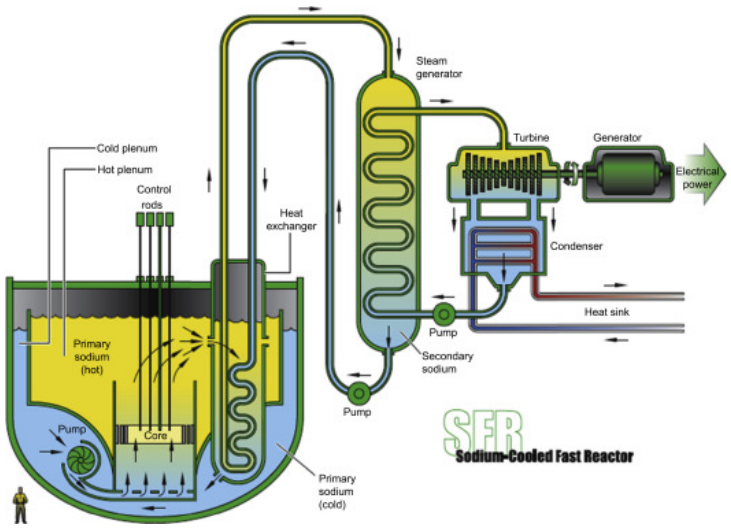

Figure 1.1: Sodium-cooled fast reactor system (pool type) [102].

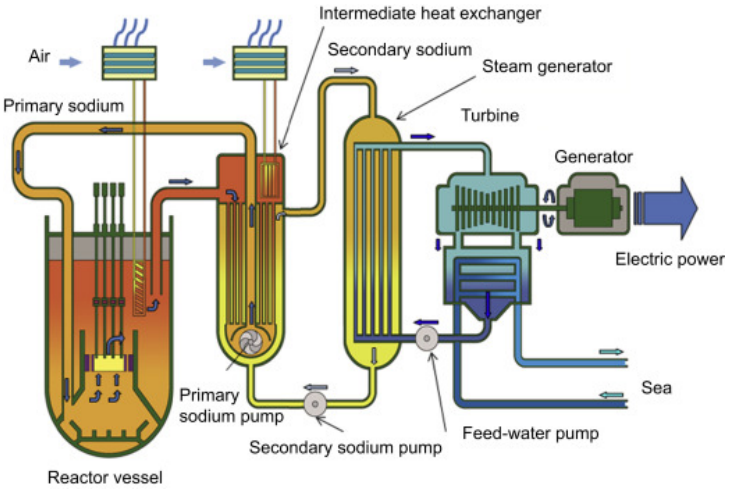

Figure 1.2: Sodium-cooled fast reactor system (loop type) [102].

Table 1.1: Pool and loop type reactors in the world [102].

	Pool	Loop
United States	EBR-II	EBR-I, Fermi, SEFOR, CRBR,FFTF
United Kingdom	PFR	DFR
France	PHENIX, SUPERPHENIX	Rapsodie
Germany		KNK II, SNR-300
Russia	BN-600, BN-800	BOR-60, BN-350
India	PFBR	FBTR
China	CEFR	
Japan		Joyo, Monju

The SFR research and development (R&D) has been in the limelight in several countries, mainly France, China, Russia, the United States, Japan, India, and South Korea [43]. There have been several projects in the world:

- Reactors currently in service: the BN 600/800 reactor in Russia; the China Experimental Fast Reactor (CEFR) project;
- In integrated commissioning stage: the 500 MWe Prototype Fast Breeder Reactor (PFBR) in India;
- Worked but being repaired: restart of Joyo in Japan;
- Ongoing projects: a commercial version with a power output of 1200 MWe (BN-1200) in Russia; a 310 MWe reactor known as PRISM (Power Reactor Innovative Small Module) in the US [139]; a 390 MWth/150 MWe prototype SFR is considered in South Korea;

- Abandoned: French industry has opted for the development of a Generation IV reactor prototype based on the SFR concept via ASTRID, the Advanced Sodium Technological Reactor for Industrial Demonstration project [68] [145] [52]. The project ASTRID was abandoned in August 2019, but France has always maintained a base of technical skills capable of ensuring a concrete restart of the sector at any time.

1.2 History of SFR in France

In France, the first experimental SFR was RAPSODIE, located in Cadarache. The construction of this reactor with an initial power of 20 MWth began in 1962. The main design lines (assemblies, materials, vessel, intermediate exchangers) were validated and maintained on RAPSODIE, and the breeding capacity of fast neutron reactors has been demonstrated.

The first PHENIX divergence occurred on August 31, 1973, at the Marcoule site. The objectives of this reactor were to continue research on the acquisition of knowledge on the operation of SFRs. PHENIX connected to the network with an electrical power of 250 MWe (563 MWth) on December 13, 1973, demonstrating the industrial viability. The plant then entered into research programs on managing high-level and long-lived waste to demonstrate the feasibility of transmutation of minor actinides. The feedback accumulated over the 35 years of operation of the PHENIX power plant has made it possible to understand a certain number of phenomena and develop solutions. In the context of these studies, it has been shown that the radioactive releases from the SFR technology are extremely low, with dosimetry lower by a factor of ten than that of the existing water reactor fleet. PHENIX was withdrawn from the network in March 2009.

In 1970, Italy, Germany, and France agreed to build and operate a European SFR-type reactor in France, SUPERPHENIX, which started in September 1985. SUPERPHENIX was the most successful reactor in this sector, with an electrical power of 1240 MWe (3000 MWth). The primary purpose of this project was to demonstrate the feasibility of an industrial-scale SFR and mastery of the physics of large cores. SUPERPHENIX was shut down in 1997. This prototype had perfectly integrated the experience of the PHENIX and RAPSODIE reactors and had made it possible to consolidate its viability.

1.3 SFR core components

1.3.1 The fuel pin and assembly

The core design in SFR must maintain a high power density in order to compensate for the low fission cross sections by fast neutrons. This requires a core design in the form of closed hexagonal tubes, forming assemblies. Each assembly contains a bundle of fuel pins by helical spacer wires. Thus, the coolant can circulate between the fuel pins and extract the heat from the fission reactions. However, this tight geometry can, in the event of the release of fuel material outside the cladding, cause partial plugging of the assembly. As an example, the core of the PHENIX reactor was composed of 121 fissile assemblies with 217 fuel pins per assembly. In total, this represents 26257 fuel pins, all of which have a potential risk of rupture. During the operational period of the PHENIX reactor (1973-2009), there have been 42 gas pin failures, 15 of them being open pin failures [24].

The fuel pin comprises sintered cylindrical pellets, solid or annular, with diameters varying between 4 and 7 mm and containing combustible oxide (generally $(\mathrm{U,Pu})\mathrm{O}_2$). Upper and lower free volumes, initially filled with helium at atmospheric pressure, are intended to collect the gaseous fission products released by the fuel during irradiation, sometimes up to over 90 % of generated gases. The internal pressure of the pins is higher than the sodium pressure, which is contrary to PWR. The pellets and these volumes, also called fission gas plenum, are enveloped by a tight cladding, with a thickness of around 0.5 mm, constituting the first confinement barrier for the fissile material. A fuel/cladding gap of approximately 200 to 300 μm is planned to anticipate any geometric changes in the fuel under irradiation.

In summary, the fuel pin in SFR is generally structured as a cladding constituting the first fuel containment barrier; a fissile column of pellets of uranium and plutonium mixed oxides; a gap between pellets and cladding; fission gas plenum (one or two). The fuel assembly and fuel pin designs in SFR are shown in Fig. 1.3 [104].

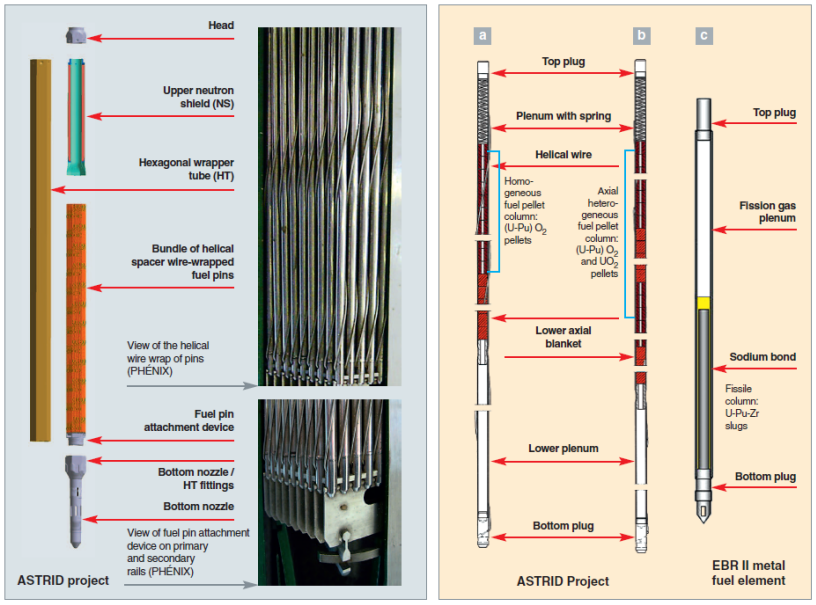

Figure 1.3: The fuel assembly and fuel pin designs in SFR [104].

1.3.2 The sodium coolant

Fast neutron reactors have the particularity of having a small core (compact) and very high specific powers (hundreds to thousands of kW per liter). Therefore, only liquid metals can be used and achieve such heat flux. Among the liquid metals available, sodium is a privileged candidate and is distinguished by many advantages [104]:

- Thermal properties: it allows the extraction of specific powers as high as 1000 to 2000 kW per liter. In addition, while it is only liquid at 98 °C, its boiling temperature is 883 °C at atmospheric pressure, which offers operation over a wide temperature range without the need for pressurization,
- Neutron properties: sodium has good neutron transparency with a capture probability of 4.34 barns for fast neutrons,
- Abundance of resources: it is very widespread in nature and is obtained by electrolysis of salt,
- Not very corrosive in controlled condition: sodium interacts very little with the structure of the reactor.

However, sodium has several disadvantages that must be protected against:

- Strong chemical reactivity with oxygen and water: this reactivity can lead to sodium fires in contact with the air in the event of leaks outside the vessel

or to explosions in contact with water at the level of the steam generators. Nevertheless, this risk is minimized by reinforcing the primary and secondary circuits by making them more airtight and resistant.

- An affinity with the fuel oxide: in the event of a cladding rupture, the sodium can penetrate inside the fuel pin and come into contact with the mixed oxide to form sodium urano-plutonate $Na_3(U, Pu)O_4$, which is a corrosion layer formation. This phenomenon will be introduced later in detail.

- An increase in neutron reactivity when the coolant boils. This problem can be managed by a core concept compensating for this effect: CFV core (core with low reactivity effect in case of sodium drainage) [21] [146].

1.3.3 The core

The core, where the chain reaction and energy production occur, is immersed in the main vessel filled with sodium. For a pool-type SFR, the sodium temperature at the inlet of the core is approximately 400 °C. This temperature reaches 550 °C on an average at the core outlet. The hot primary sodium then flows into an intermediate exchanger, which transfers the heat of the primary sodium to the sodium of a second independent system called the "secondary system". After cooling, the primary sodium is returned to the core inlet by a supply pump (the primary pump) which is also immersed in the main vessel.

The main vessel is topped by a slab used as a cover. The slab includes a rotating plug above the core to allow insertion and removal of the subassemblies and to allow the penetration of the core control rod mechanisms and the core measuring devices. The sodium is inerted by an argon cover gas plenum located above the free level of sodium.

1.4 The significance of fuel pin failure monitoring in SFR

Following the Fukushima accident, safety targets have been reviewed and enhanced by safety authorities in various countries to meet more stringent requirements. Safety criteria evolution for Generation-IV reactors is a crucial component for the design of future sodium cooled fast reactors.

One of the safety demands in SFR is the need for a fast cladding failure detection system in order to minimize fuel pin damage by the reaction with sodium, as well as radionuclide spreading in the secondary coolant circuit, and the need

to extract any assembly affected by a cladding failure due to the impossibility to operate the reactor with a damaged fuel.

There have been experiments on fuel and cladding failures, as shown in Tab. 1.2. Most of reactors have used a fuel consisting of uranium and plutonium oxide, with an excellent operating experience feedback. The other fuels used are enriched uranium oxide (BN-600), carbide (FBTR), and metallic fuels in U.S. reactors. Nitride fuels have also been tested on several reactors, among which BN-600. PHENIX has experienced 15 open cladding failures until 1988 [104].

Table 1.2: Cladding failures on the various reactors.

	PHENIX	PFR	BN-350	BN-600	KNK II
Number of open cladding failures	15	21	high number at the beginning of life	high number at the beginning of life	5

1.4.1 Consequence of fuel pin failure

The cladding failures in SFR result in not only the release of fission products to the primary coolant, but they could also lead to propagation of core damage [128].

In the event of an open cladding failure, the reaction with fuel leads to dissemination of fission products in primary sodium and the reactor cover gas, with the following potential consequences:

- contamination of the primary circuit and fuel, which results in more difficult conditions for maintenance and repair;
- deposited fuel particles lead to coolant channel plugging [72].

Therefore, the emission of fission products from failed pins should be restricted and the detection and characterization of fuel pin failure in SFR should be improved.

1.4.2 Fuel pin failure in SFR compared to PWR

Since fuel pin failures also exist in Pressurized water reactor (PWR) and the technology of failure detection in PWR is well developed, e.g. in [29], [54], [16], [55], [77], [78], I would like to compare the the difference of the fuel pin failure condition in SFR and PWR, to see if there is some cladding failure detection experience that can be learned.

I summarized the difference of fuel pin failure condition in SFR and PWR:

- The fuel pins are located tighter inside a hexagonal lattice in SFR, no possibility of transverse flow as in PWR. As a result, the leakage of fissile material could lead to blockage in SFR;
- The pressure difference between the interior of the fuel pin and the coolant is of opposite signs;
- The reaction between sodium and the exposed fuel, the oxide sodium reaction, makes a higher risk of fissile matter dissemination in the primary coolant;
- Due to water corrosion on the primary circuit, the contamination of coolant in PWR is already high in normal condition. The failure of few rods does not affect so much the radiologic concerns, which is contrary to SFR. The limitation of contamination of primary components (pumps, IHX, etc.) in SFR is possible to reduce human exposure during maintenance operation.

Thus the detection need for cladding failures in SFR is different from PWR:

- In PWR, several amounts of pin failure are allowed for operation and the detection for the cladding failure is intermittent and long term detection.
- In SFR, the "clean sodium concept" is demanded and dissemination of fissile matters in the primary coolant is prevented. It is necessary to shut down the reactor as soon as severe cladding failures are detected. The detection system is continuous online monitoring.

Thus it is difficult to compare release mechanisms and detection techniques in SFR and PWR, because of water contamination, transverse circulation, less pressure within the cladding than water and different modes of corrosion.

1.5 Characteristic of fuel pin failure

In order to study the detection of fuel pin failure, the characteristics of fuel pin evolution and fission product release during cladding failure should be clarified firstly.

1.5.1 Evolution of the fuel pin failure

The performance and failure modes of oxide fuel depend on various irradiation effects: (1) fuel restructuring and grain growth affect the fission gas release and fuel creep characteristics; (2) as-fabricated porosity migration is responsible for the

formation of the central cavity and it affects fuel thermal conductivity; (3) fission gas retention and release affect the radial distribution of total porosity and fission gas bubble induced fuel swelling; (4) fission product swelling includes solid fission product and fission gas bubble swelling, and it affects the radial porosity profile and fuel dimensions; (5) fuel-cladding gap condition affects the fuel temperatures; (6) irradiation-induced cladding swelling affects the cladding dimensions and density. The failure modes include the plastic straining of the cladding due to internal fission gas pressure and differential expansion between the fuel and cladding, and the cladding melting due to excessive temperatures [128].

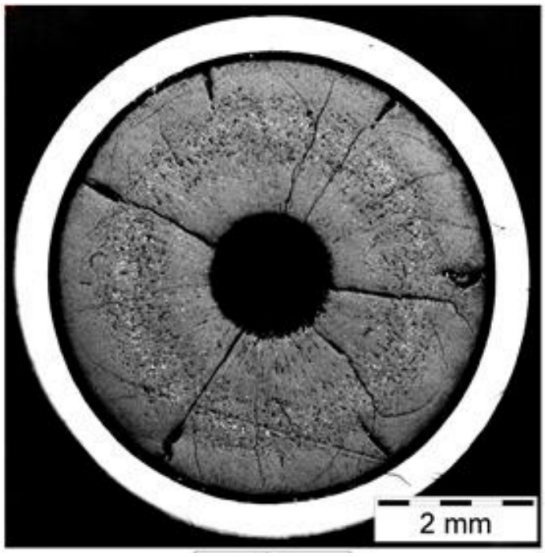

Figure 1.4: A cross section of irradiated oxide fuel pin in PHENIX reactor (Normal stage) [106].

There are four stages of the fuel pin failure evolution, e.g. [65], as shown below:

- Normal: This stage is defect-free. The sodium coolant is clean. A cross section of irradiated oxide fuel pin in PHENIX reactor is shown in Fig. 1.4 [106].
- Crack: This stage only leads to leakage of gaseous fission products.
- Narrow rupture: A narrow rupture may be subsequent to a crack in case it undergoes several thermal expansions due to various power variations. Delayed neutron precursors (DNP) release and the oxide-sodium reaction (OSR) happens [13].
- Wide rupture: The oxygen atoms feeding the oxide-sodium reaction mainly come from the inner fuel pellet, which continuously flows along the fuel oxide

at the rupture location. There are particles of fissile material released into primary circuit. A post irradiation examination image of fuel pin failure in PHENIX reactor is shown in Fig. 1.5.

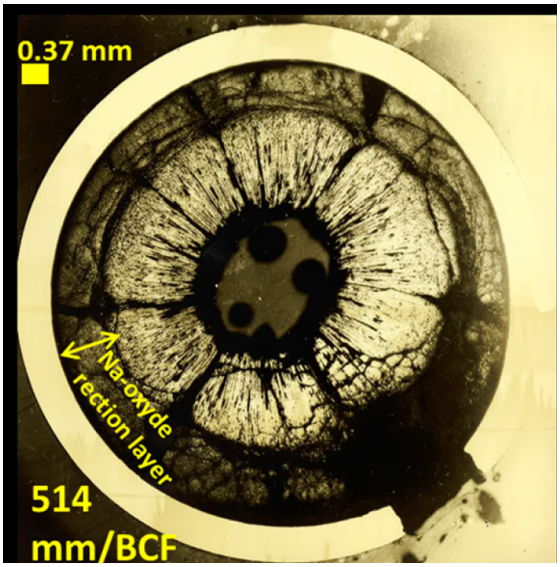

Figure 1.5: A post irradiation examination image of fuel pin failure in PHENIX reactor (Wide rupture stage) (from CEA internal report, 2016).

1.5.2 Fission products

The fission products created during the burn up can be classified, according to their physical-chemical nature, into five categories [59] [49]:

- Solid fission products: Y, La, Ce, Pr, Nd, Pm, Sm, Eu, Gd. They are soluble in the fuel matrix $(Pu, U)O_2$ and hardly migrate therein.
- Fission products forming metallic precipitates: Mo, Tc, Ru, Rh, Pd, Ag, Cd, In, Sn, Sb, Te. These precipitates appear at high burn up and at high temperature. They are manifested by white inclusions of a few micrometers in an area mid-radius of the pellet.
- Fission products forming oxide precipitates (solid or volatile alkaline): Rb, Cs, Sr, Ba, Zr, Nb. Some of these products (Cs and Rb) are volatile at the fuel temperature but can be liquid at the cladding.
- Volatile halogens: I, Br. Depending on the temperature, volatile halogens can be in the solid, liquid or gaseous state. At the cladding temperature, these fission products are gaseous (boiling temperature at 183 °C for I, at 58 °C for Br), which play an important role in the properties of the fuel and in the corrosion effects.

- Gaseous fission products: Xe, Kr. Generally located at the periphery of the pellet and insoluble in the fuel matrix, these gases are collected in the gas plenum in the cladding.

The fission products interested in the cladding failure detection are mainly gaseous fission products in gas detection; and volatile halogens, some of which are delayed neutron precursors (DNP), in neutron detection.

1.5.3 Release of fission gas

A crack failure is accompanied only by the emission of fission gases but not generating a DNP release, which means that there is not yet a contact between fuel and sodium (sodium does not enter due to the viscosity if the crack is too narrow). This damage may prevail in the reactor over weeks or months until it develops into a narrow rupture by extension or by one or several secondary failures. During the burn up, most of the gaseous fission products, about 80 % to 90 % [45], will be released from the fuel pin and be accumulated in fission gas plenum, which is the gas expansion volume inside the fuel pin. For most conditions in SFR, when there is a crack on the cladding, the gaseous fission products in the gas plenum will be released instantaneously through the crack because of the pressure difference between the fuel and the coolant.

After the first instantaneous release, there might be stable and continuous release, or intermittent release with oscillated activity. Analysis of fission gas releases during this period can be used to monitor rupture propagation [72].

1.5.4 Release mechanisms of DNP

During the narrow rupture, there will be a direct contact between fuel and sodium. The release mechanisms for the fission products mainly include direct recoil, knock out and diffusion. For delayed neutron precursors (DNP), all the isotopes decay so rapidly that the distribution near the surface is not affected by the knock out process thus knock out is negligible [84]. So direct recoil and diffusion calculation will be focused on.

Release by recoil is considered to be an athermal mechanism, i.e. not driven by a thermal diffusion mechanism, but proportional to the fission rate and fission yield and independent of the decay constant for radioactive species [150]. Therefore recoil can be considered as a release mechanism of stationary state.

Compared to direct recoil, thermal diffusion release depends on the temperature and the environmental conditions. The evolution of fuel conditions (corrosion

layer formation, joint oxyde gaine, gas burst, etc.) may have an influence for the diffusion release of the fission products.

1.5.5 Corrosion layer formation

An important phenomenon during the fuel evolution which may change the diffusion behaviour is the corrosion layer formation [24], as shown in Fig. 1.6. When there is a rupture on the cladding, sodium will penetrate inside the the fuel pin through the crack followed by exchange of sodium between inside and outside the fuel pin. $(U, Pu)O_2$ reacts with sodium to form sodium urano-plutonate, which is the corrosion layer. The reaction of corrosion layer formation takes place at the periphery of the fuel pin and is stopped when the oxygen potential is low enough to reach equilibrium [59]. Then the corrosion layer will be stable. Because the thermal conductivity of corrosion layer is lower than the oxide fuel [130], it will change the fuel temperature condition during the process of formation.

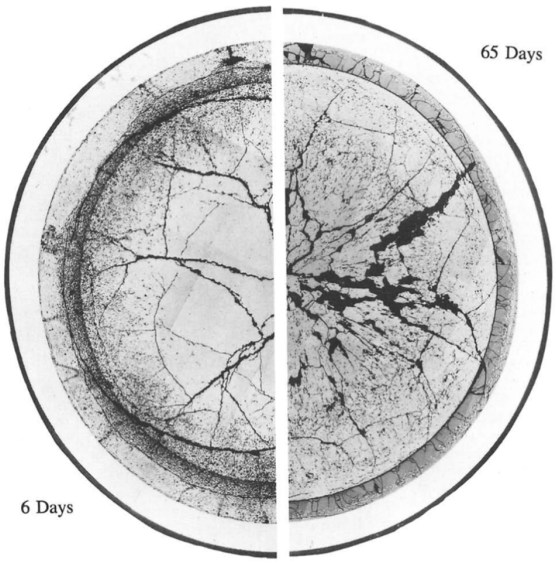

Figure 1.6: Fuel sodium reaction product - the corrosion layer [130].

1.5.6 JOG formation

During the burn up, there is another phenomenon: volatile fission products migrate towards the cold region of the fuel pin due to volatility and axial temperature gradient; then they accumulate between fuel and cladding where a bonding layer is formed, which is called JOG (Joint Oxyde Gaine) [120].

Cs_2MoO_4(liq) is the main constituent of JOG. Its chemical interaction with liquid sodium is of prime interest. Cesium can react with fuel and form JOG according to:

$$2Cs(g) + O_2(g) + MoO_2(s) \rightarrow Cs_2MoO_4(liq) \tag{1.1}$$

Cesium can also react with fission product iodine according to:

$$Cs(g) + \frac{1}{2}I_2(g) \rightarrow CsI(liq) \tag{1.2}$$

The free energy of formation of CsI is quite negative. This reaction should proceed nearly to completion [103]. Cesium is soluble in sodium and sodium replaces cesium in most cesium compounds of the periphery. Upon contact between liquid sodium and CsI in the JOG layer, iodine is expected to form mostly sodium iodide NaI and elemental cesium, largely in gaseous form. NaI is stable in in liquid sodium [14]. Compounds such as Na-I and Na-Te can be formed after sodium penetration.

1.6 Conclusion

Fast neutron reactors are a technological solution that meets the growth of energy needs, the sustainability of resources, the fight against the proliferation of nuclear weapons and respect for the environment. Objectives for a sustainable nuclear power which plays its part in the energy mix have been defined by the GIF IV international forum.

Safety and availability requirements have been set for SFRs, include close monitoring of any leakage tightness of the first containment barrier, namely the fuel cladding. Detecting these cladding ruptures at an early stage would enable the operator to better assess the fuel performance, to predict fuel evolution and to judge the advisability of a possible withdrawal.

The fuel pin failure evolution and the release mechanisms of fission products have been described in this chapter. The detection methods and device will be introduced in the next chapter.

Chapter 2

The detection methodology and the research status

After having underlined the importance of monitoring cladding failures to meet the safety and availability requirements of an SFR, as well as describing the fuel pin failure evolution and behavior, detection methods and their research status will be interested in. Thus, in this chapter, the detection system in SFR especially in the PHENIX reactor will be introduced, including different detection methods and the detectors in gas and neutron detection; the detected cladding failure cases in the PHENIX reactor will be summarized.

The instrumentation experience feedback of cladding rupture detection will be presented through a bibliographic study. The lessons learned from this study will make it possible to formulate the problem of the thesis and define the research methodology.

2.1 PHENIX reactor and the detection system

The process design and principle of the cladding failure detection system are similar in different countries. Due to the rich experience gained from cladding failure detection experiments in PHENIX reactor in France, this chapter will mainly present the detection methods and failure cases in PHENIX reactor.

PHENIX is a pool-type sodium-cooled fast reactor composed of a main primary reactor vessel, three secondary sodium circuits, three tertiary water/steam circuits, and one turbine [97] [147]. PHENIX nominal power was 560 MWt/250 MWe [134]. The main reactor vessel is 11.8 m in diameter and 9.8 m in height, filled with 800 tonnes of sodium, as shown in Fig. 2.1. A safety vessel surrounds the main vessel as an additional barrier in case of sodium leakage. The roof is a 0.06 m depth structure closing the top of the main vessel to ensure a tight barrier. Argon fills the upper space between the sodium and the roof [135]. Depleted uranium oxide is used as an axial blanket in the lower and upper parts of the fuel pins. The fuel in the active core is composed of (U-Pu)O_2 mixed oxide.

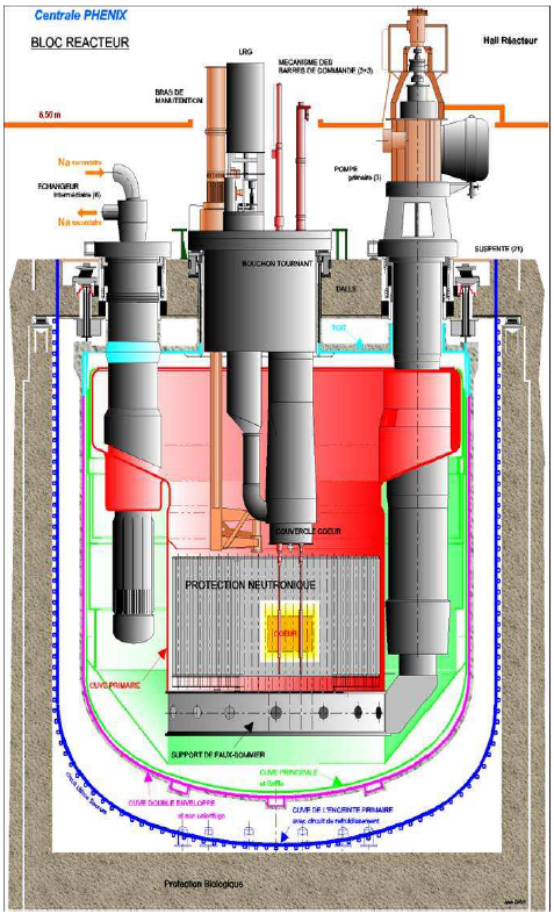

Figure 2.1: PHENIX primary circuit [135].

Detection and monitoring methods are selected in priority so as to detect each

of the cladding failures for the purpose of mitigating consequences on the power reactor's operation. This continuous monitoring covers all of the major families of neutron, thermal hydraulic, mechanical and chemical measurements.

The detection system in PHENIX reactor is related to the fuel pin failure evolution, which consists of mainly two parts, as shown in Fig. 2.2:

- DRG system (Détection des Ruptures de Gaine) (Gas detection system): DRG system is located in the cover gas. Because gas signal is the first signal that can be detected when there is a cladding failure, the aim of DRG system is to detect the failure as soon as possible.
- DND system (Détection des Neutrons Différés) (Neutron detection system): DND system is located in the sodium coolant. Because neutron signal is related to the breached fuel area exposed to the coolant, a threshold of the maximum breached size is set up to avoid the fissile material release in the coolant. Normally a neutron signal increase means that the rupture becomes more severe. If the DND signal corresponding to the rupture size reaches to the threshold, the reactor will be shut down.

There is also a LRG system (Pin failure location system) (Localisation des Ruptures de Gaine) aimed at locating the pin failure both in gas and neutron system.

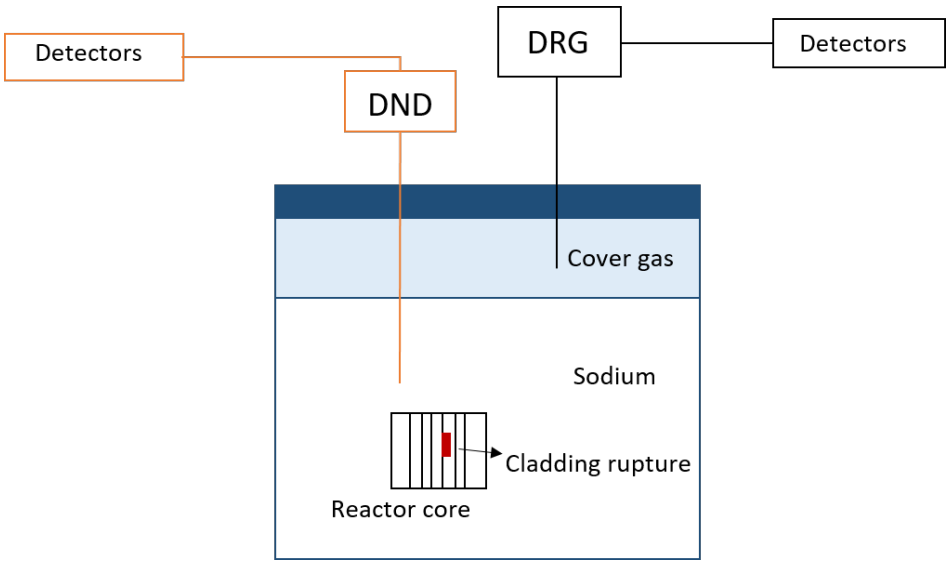

Figure 2.2: General scheme of DRG - DND detection system in PHENIX reactor.

The signal retrieved in the detection system is related to the fuel pin evolution stages. In summary, gas signals can be detected due to fission gas emissions during the crack stage. If the failure turns out to be more severe, neutron signals can be

retrieved, which are emitted by delayed neutron precursors (DNP) during narrow rupture. For a wide rupture, an emergency shut down will be immediately ordered.

Three time periods of signals are defined associated to different stages of fuel pin failure evolution, as shown in Fig. 2.3:

- t1: the duration of irradiation of the fuel pin without gas signal detection;
- t2: the duration of fission gas detection without DND signal;
- t3: the duration of irradiation with a permanent DND signal.

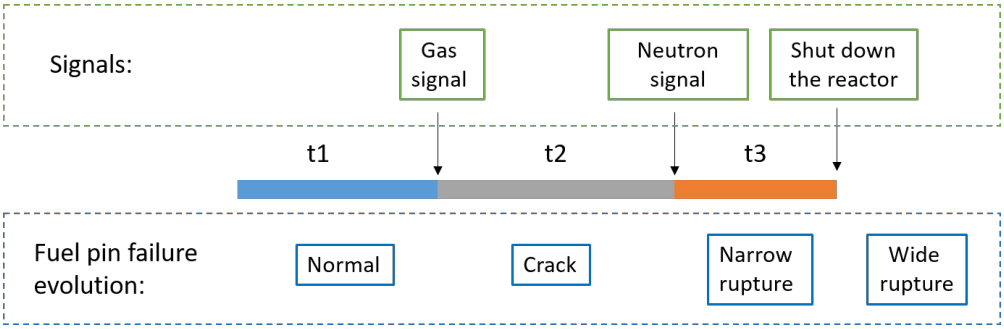

Figure 2.3: Different periods of signal associated with the fuel pin failure evolution.

2.1.1 DRG detection system

When there is a fuel pin failure in a SFR, which means a crack happens on the cladding, gaseous fission products will be released outside the cladding through the crack. Then the detection system can detect these gases. The crack with gaseous fission products release will be at the first stage of fuel pin failure thus the aim of the gas detection is to detect (DRG system) and locate (LRG system) the gas as soon as possible.

The DRG system can provide information regarding the size of the failure and predict in advance the potential for evolution into an open failure [129] [49]. The detection of fission products present in the cover gas is practiced by diverse techniques: gamma spectroscopy [113]; gas chromatography [109]; ionization chamber [20]; mass spectrometer for stable xenon isotopes [71]; precipitator and scintillation counter [46]; tagging and xenon adsorption on activated carbon [1]. It became apparent in almost all cases that the methods of integral energy, such as ionization chamber and precipitator, are the robust methods and attain the highest availability, whilst gamma spectroscopy furnishes detailed information which can hardly be dispensed with [72]. The main instrumentation methods are listed in Tab. 2.1.

Table 2.1: Instrumentation of pool type SFR cover gas monitoring system [72].

Reactor	Ge/ Ge(Li)	Ion. chamb.	Mass spectr.	Precipit.	Scint. counter	Tagging	Xe adsorp.
PHENIX	yes	yes	yes	no	no	part.	no
SPX	yes	yes	no	no	no	no	no
PFR	yes	no	no	yes	no	part.	no
EBR-II	yes	no	yes	no	no	yes	yes
BN-600	yes	yes	no	yes	yes	no	no
CEFR	yes	no	no	yes	yes	yes	no

The general scheme of DRG system in PHENIX reactor is illustrated in Fig. 2.4 and the detailed DRG-LRG system is shown in Fig. 2.5. DRG can detect gaseous fission products release by monitoring the activity in the cover gas. The DRG gas circuit of PHENIX is distinct from the scanning and purification circuit of the cover gas of the reactor. The analysis of the cover gas previously rid of sodium aerosols is carried out permanently by an ionization chamber with circulation MX 32 (overall measure of activity), by a gamma spectrometry (selective activity measurement) and by an ENSPECT device (measurement of stable isotope contents and identification of gas markers).

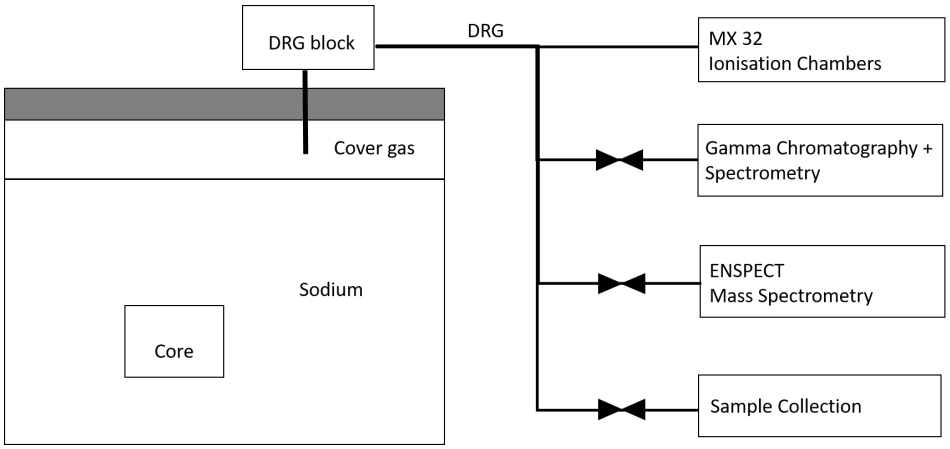

Figure 2.4: General scheme of DRG system in PHENIX reactor.

The main detectors for gaseous fission products are shown below:

- A global activity measurement: it aims to continuously assessment of the total activity of the cover gas. This measurement is carried out using circulating ionization chambers, supplied by the electric current from the β and γ decays of the gas. Ionization chambers MX 32 are used in PHENIX: they are assigned to the DRG cover gas to supply continuous overall value of the activity.

- A selective measurement by gamma spectrometry (e.g. Germanium HP diode): it allows an isotopic analysis of the radioactive fission gases, responsible for the evolution of the signal in one of the ionization chambers. This measurement, provided by a spectrometer, makes it possible to monitor the progress of any cladding rupture giving rise to the release of gaseous fission products. Gamma spectrometry is used in PHENIX to make the identification of gaseous fission products via a periodic measurement (1 time a day) and on demand.

- A selective measurement by mass spectrometry: it makes it possible to quantify the concentration of certain stable isotopes of xenon and krypton. Upstream of the measuring device, separation of rare fission gases, produced in small quantities, and argon, taken in large quantities, is carried out by chromatography and cryogenic trapping. In the event of cladding failure, the concentration ratio between stable and radioactive rare gases makes it possible to pre-locate the leaking assembly by evaluating the burn up rate [49].

- The gas tagging method: it is an effective identification technique that uses isotopic analysis of krypton (Kr) and xenon (Xe) contained in the Ar cover gas, using mass spectrometry for detection [69]. Prior to operation of the reactor, certain amounts of Kr and Xe gases are loaded into the fuel pins with unique isotopic ratios. A fuel failure event can be identified in an assembly unit by measurement of these isotopic ratios of the leaked Kr and Xe gases contained in the Ar cover gas [71], which was only partly used in PHENIX reactor.

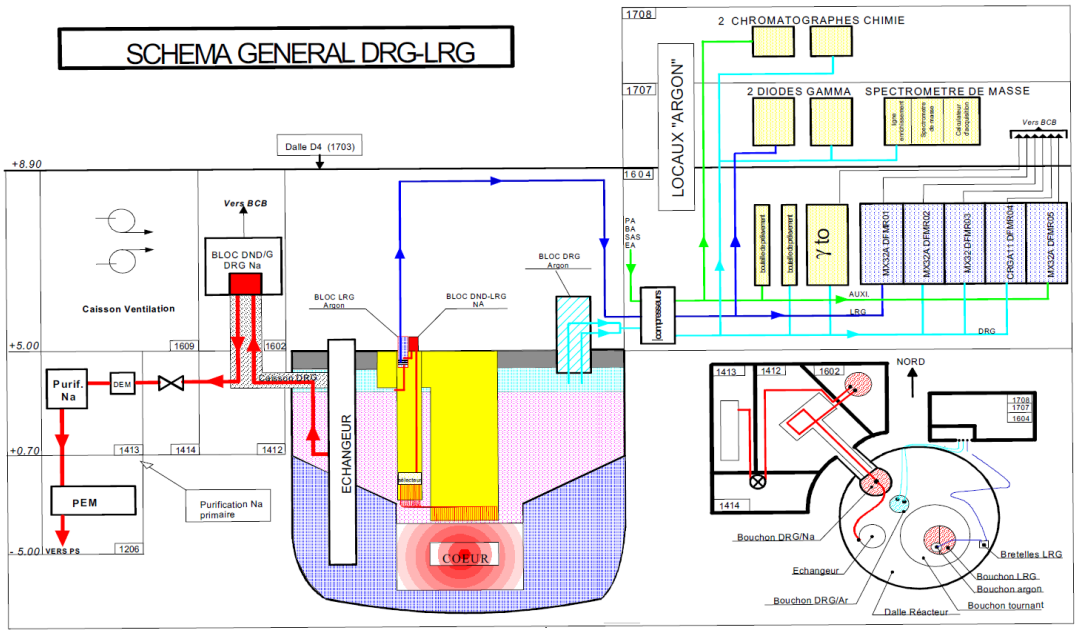

Figure 2.5: DRG-LRG system (from CEA internal report, 2008).

The main background signal in DRG detection system includes two isotope sources:

- ^{41}Ar, with a half-life of 110 minutes, is produced by ^{41}K (n,p) ^{41}Ar and ^{40}Ar (n, γ) ^{41}Ar. It emits β- particles with an average energy of 464 keV and γ radiation at a characteristic energy of 1294 keV.

- ^{23}Ne, with a half-life of 37.2 seconds, is produced by ^{23}Na (n, p) ^{23}Ne. It emits β- particles with an average energy of 1898 keV and γ radiation at a characteristic energy of 440 keV.

Due to the short half-life of ^{23}Ne, the activity can be reduced by the delay line. After the delay line (around 12 minutes), the background of ^{23}Ne is negligible. Thus the main background signal is ^{41}Ar. The order of magnitude of background signal is 0.01 Ci/m^3 in PHENIX reactor.

2.1.2 DND detection system

Generally there are two concepts of DND detection system design:

- ex-vessel detection (remote DND concept): it is used in PHENIX reactor. The primary sodium withdrawal is done at the level of the six intermediate exchangers. Each sampling line ensures a sample of the sodium circulating in the heart. A length of sampling lines and an equivalent flow rate of pumps imply a transit time on the six circuits. Each sampling line joins its

measurement volume for the detection of any delayed neutrons, the output of which flows into a return line common to the six starting circuits.

- in-vessel detection (an integrated DND concept): it has been tested on Superphénix and actively studied in the ASTRID project. DNP induced additional signal within the primary sodium itself. The signal comes from neutrons emitted by DNP, the amount of which depending on the hydraulic transfer function (HTF) gives the concentration of stable particles, transported by sodium flow, reaching the vicinity of the sensor with respect to time [40]. Initially, the motivations of the integrated DND lie in the reduction of the response time (approximately 6 seconds) while limiting the circulation of primary sodium outside the vessel. In a second step, these modifications lead to a reduction in costs and an ease of installation of the detectors.

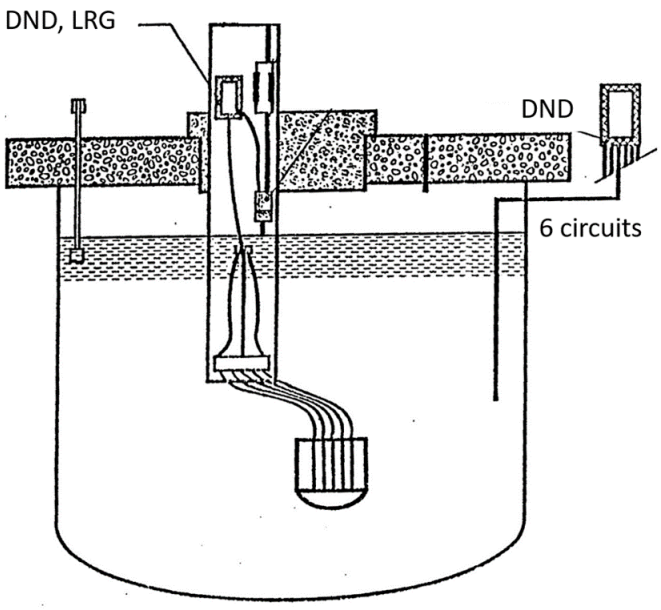

Figure 2.6: General scheme of DND system in PHENIX (from PHENIX internal report, 1978).

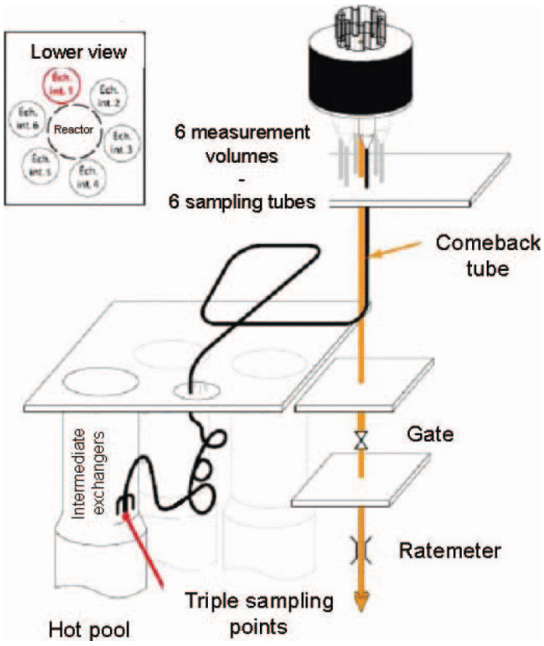

Figure 2.7: DND system sampling loop [25].

In PHENIX reactor, the neutron detection system is composed by delayed neutron detection system DND (Détection des Neutrons Différés) and localisation system LRG (Localisation des Ruptures de Gaine) system, as shown in Fig. 2.6. DND system is carried out by means of 6 sodium samples taken from the reactor vessel and sodium samples are continuously extracted from the outlet of fuel assemblies; LRG system is for locating the cladding ruptures. DND system sampling loop and the schematic view are shown in Fig. 2.7 and Fig. 2.8. A traditional design of the DND system is composed of a sodium volume about 3 liters surrounded by a few centimetres of lead shielding and polyethylene moderator. Three ^{3}He proportional counters assure the thermal neutron detection. When a cladding rupture reaches a DND threshold signal deemed critical, the emergency stop is automatically triggered.

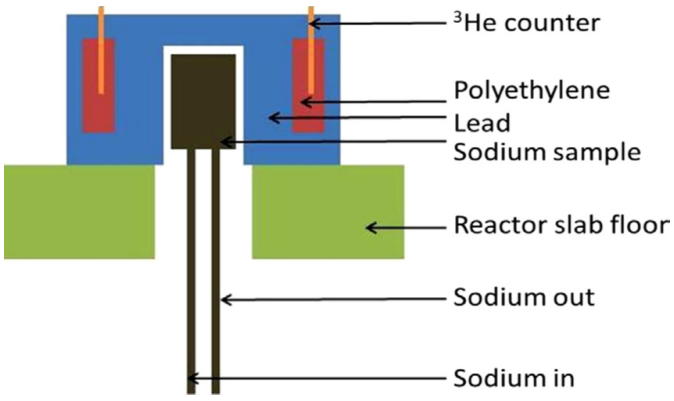

Figure 2.8: DND system schematic view [115].

DND signal indicates the breached size of the fuel pin. The geometric surface of the exposed fuel in cm^2 detected in DND system S_{DND} is calibrated by the equivalent recoil surface (S_{rec}). The definition of S_{rec} is based on the assumption that recoil is the only phenomenon (athermal mechanism, no time dependence at the time scale of rupture detection and follow-up) and the fuel is directly in contact over S_{rec} with the sodium flow. The threshold of the DND signal to shut down the reactor has been set to 2.5 cm^2 of S_{DND} or 25 cm^2 of S_{rec}. It's worth noting that this calibration is for the engineering scenario. Thus there is no direct connection between S_{rec} and the real breached surface if other mechanisms than recoil come into play.

The main background source in the DND detection system is the original pollution (tramp uranium) of the cladding during the fuel design. The order of magnitude of the background signal is 150-200 c/s in the PHENIX reactor.

2.1.3 Summary of detected cladding failure cases in PHENIX reactor

With the DRG and DND detection system, experiments of fuel pin failure have been implemented in PHENIX reactor. Among approximately 150,000 fuel pins irradiated in PHENIX during its 36 years of operation, only 15 open cladding failures occurred (none in Superphenix), half of which occurred on experimental fuel pins irradiated beyond the "standard" characteristics [52]. The fuel pin failure cases with different t1, t2 and t3 in PHENIX are listed in Fig. 2.9.

N°	Ass	Début irrad°	Fin irrad°
RG1	CPA 268	29/03/1976	01/05/1979
RG2	DCI 3106	12/07/1978	26/01/1981
RG3	KCI 6402	09/07/1976	09/07/1981
RG4	DCC1101	25/01/1976	10/08/1981
RG5	CPD 409	26/06/1981	25/02/1982
RG6	CPD 416	21/08/1980	24/04/1982
RG7	DCI 4908	12/01/1980	07/10/1982
RG8	DCI 108	13/08/1983	21/05/1985
RG9	KCI 6414	22/08/1981	29/10/1985
RG10	KCI 6413	22/08/1981	29/10/1985
RG11	CPD 6018	08/02/1986	05/03/1986
RG12	CPE 6016	08/02/1986	03/08/1987
RG13	CPE 6005	23/10/1985	21/08/1987
RG14	DCI 3124	23/06/1985	02/03/1988
RG15	CPA 5037	15/06/1986	17/06/1988

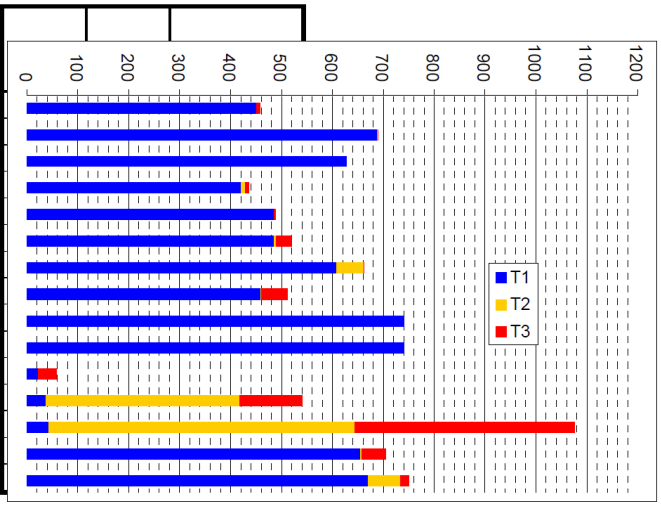

Figure 2.9: Fuel pin failure cases with different t1, t2 and t3 in PHENIX reactor (from CEA internal report, 2008).

Since there is no dedicated experiment for signal analysis, re-analysis of data

previously collected in PHENIX reactor is the main approach in this thesis. However, since the cladding failures are rare during reactor operation and the signals recorded in the industry framework are not used for research purposes, limited data are available. The information of cladding failure cases in PHENIX is shown in Tab. 2.2 and Tab. 2.3.

Table 2.2: Summary of fuel information of cladding failure cases in PHENIX.

Case No.	Fuel pin type	Time	Cladding	Reactor parameters (MWth)	Linear power (W/cm)	Burn up (%)	Rupture (mm)
1	EA	01.05.79 -16 cycle	316	589	359	8.6	30
2	EA	26.01.81 -22 cycle	316 Ti	570	293	11.7	440
3	EC	09.07.81 -23 cycle	316 Ti	/	/	11.4	440
4	SA	10.08.81 -23 cycle	316	/	/	7	48
5	SA	25.02.82 -25 cycle	316	582	347	8.9	50
6	SA	24.04.82 -26 cycle	316	377	349	9.1	55&35
7	EA	07.10.82 -27 cycle	316	380	258	7.6	50
8	EA	21.05.85 -33 cycle	15-15 Ti	394	241	7.8	60&50
9	EC	29.10.851 -35 cycle	Inconel 706	525	280	12.2	390
10	EC	29.10.85 -35 cycle	Inconel 706	525	280	11.8	408
11	SA	05.03.86 -36 cycle	15-15 Ti	575	409	0.35	20
12	SA	03.08.86 -41 cycle	15-15 Ti	526	239.8	5.693	many 20&15 &16&25
13	SA	21.08.86 -41 cycle	15-15 Ti	583	312	5.262	10
14	EA	02.03.88 -43 cycle	Inconel 706	580	326	11.56	480
15	SA	17.06.88 -44 cycle	15-15 Ti	transitional regime	355	9.02	5

EA: Experimental Assembly, EC: Experimental Capsules, SA: Standard Assembly.

Table 2.3: Summary of signal information of cladding failure cases in PHENIX.

Case No.	t1/t2/t3	Gas signal max (Ci/m^3)	DND signal max (cm^2)	Detection notes
1	451d/8h/6h	5	0.3	Rather slow slope of the DND signal before normal shutdown.
2	688d/42h/28min	2	2.5	The rapid evolution of the neutrons before the emergency stop.
3	627d/39min/8min	/	/	Major rupture led to emergency stop.
4	421d/192h/6h48	/	/	/
5	486d/6.34h/2h46	8	1	A second gas release during neutron signals.
6	485.6d/4.1d/30h	7	1	Slow evolution before shut down.
7	609d/52d/1h31	1	1	Observed a gas emission stop, followed by a neutron rapid increase.
8	459.5d/8h/51h30	0.8	1	Slow evolution before shut down.
9	740d/4min/6min	0.3	2.5	Major rupture led to emergency stop, gas and neutron emission at the same time.
10	740d/4min/6min	0.3	2.5	Same as case No.9.
11	22d/7min/36h	0.05/8	2.5	Gas and neutron emission at the same time.
12	37d/380d/123d	4	3	Long t3 at normal power.
13	42d/602d/18d	4	2.5	With many operations and had two stays in internal storage before.
14	655d/64h30/48h	1.5	1	Gas emission before neutron.
15	670d/64d/16h	1.8/4	0.15	Voluntary shutdown for maintenance work.

The information of fuel pin failure cases in PHENIX reactor is summarised below:

- The longest neutron emission time (t3) was obtained during a plateau operation of RG (Rupture de gaine, fuel pin failure in french) 6 and RG 8 (at reduced power), and RG 12 (at nominal power). Similar release regime is observed: 1) gas emission without neutron; 2) neutron emission without gas. The similarity is also found by the shape of the defects on the needle: 2 distinct cracks, each about 50 mm long.

- The duration of the neutron emission (t3) is less than 10 minutes of RG 3, RG 9&10.

- RG 11 had two types of neutron evolution at normal power: first, less than 0.5 cm^2 DND for 36 h, the second very fast from 0.5 to 2.5 cm^2. Two release regimes are observed: 1) neutron emission without gas; 2) very significant gas emission at the time of the neutron evolution. In RG 11, the first gas and neutron emission appeared at the same time.

- The appearance of the first neutron signal appeared on a transient or at the end of it: RG 6, RG 9&10, RG 3 and RG 12.

Generally the fuel pin failures are identified in 3 groups:

1. Major cracks or ruptures are concerned, which led to the emergency stop: RG 2 (440 mm), RG 3 (400 mm), RG 9&10.
2. A single defect on the cladding, with a crack of about 50 mm (RG 1, RG 4, RG 5 and RG 7), ended by a normal reactor shutdown.
3. Two separate cracks of equal importance: RG 6 (55/35 mm) and RG 8 (60/50 mm), with slow evolution of the neutron signal up to 1 cm^2 (RG 6) or 2 cm^2 (RG 8) before the scheduled shutdown.

The fuel pin failure is rare from the operating experience [8]. Thus the experiment data of gas and neutron signal from these open pin failures in PHENIX reactor, as well as the post irradiation examination photos of cladding rupture are important documents for signal characteristic and failure pin behavior.

2.2 Research status of SFR fuel pin failure detection in different countries

Then the bibliography study was made, and the research status of SFR fuel pin failure detection in the world was summarised in order to determine the aim of this thesis work.

2.2.1 France

The general instrumentation of the reactor must make it possible to monitor the physical quantities of the core. In the context of French sodium fast reactors, the instrumentation and, more particularly, the monitoring and online diagnosis have been enhanced [74]. The methodologies in nuclear measurements and instrumentation with applications in reactors are developed [18] [56]. Plenty of research has been done within the Astrid project:

Coulon et al. conducted a simulation study and discussed the privileged ways to design ex-vessel DND systems [27]; presented the experiment done at the French PHENIX and showed the adaptive ADONIS gamma spectrometry system set on primary sodium coolant sample could be clad failure detection system for future SFR [25].

Jammes et al. worked on the fission chamber technology in SFR, which plays a key role in neutron instrumentation [73] [75].

Rohée et al. optimized the DND device with both Monte-Carlo simulations and experiment in order to improve the detection capability, which results highlight the potential for a low-noise DND system based on graphite moderation [114] [115].

Filliatre et al. proposed a new type of pot with a coil shape which has the better performances with respect to the detector response to delayed neutrons and optimized the hydraulic part of the design of the DND detection block [42]; made an estimation of the signal received in-vessel detection system, discussed possible solutions to improve this sensitivity and made the hypothesis testing study [40].

Garti et al. studied the contribution of a low background instrumentation by means of a Compton suppression system integrated into the SFR measuring device [49] [51].

2.2.2 Other countries

In Japan, Fukano identified four possible mechanisms of fuel element failure propagation from adventitious fuel pin failure (FEFPA) and developed a safety assessment code. An assessment on FEFPA of Japanese prototype fast breeder reactor (Monju) was performed using this methodology [46]. Aizawa et al. investigated a tagging-gas (Tag) system in failed fuel detection and location (FFDL) system of Japan Sodium-cooled Fast Reactor (JSFR) [1] [2]. Iwata et al. evaluated the availability of resonance ionization mass spectrometry (RIMS) to the failed fuel identification technique in the fast reactors [71]. Schematic drawing of failed fuel detectors in Monju is shown in Fig. 2.10.

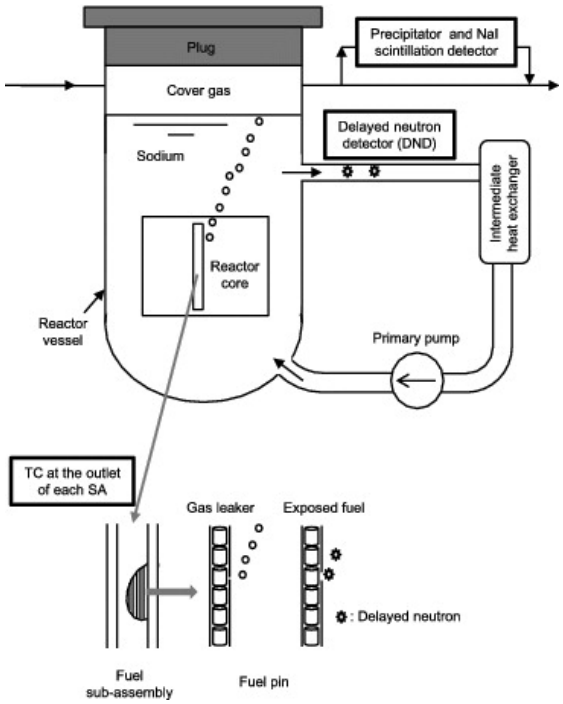

Figure 2.10: Schematic drawing of failed fuel detectors in Monju. [46].

In China, Yewang et al. introduced the tag gas method and its applications in fuel failure detection system of China Experimental Fast Reactor (CEFR) [151], which is an important method for fuel failure location using mass spectrometry. The schematic of tag gas location system in CEFR is shown in Fig. 2.11. Rui and Shu-ming studied models of fission gas release and migration and established a program calculating the number of failed fuel pins in different power [116]. Liu and Qiu improved the delayed neutron detection station and detector and proposed a calculation model and developed a code of the failed fuel detection system of CEFR [86].

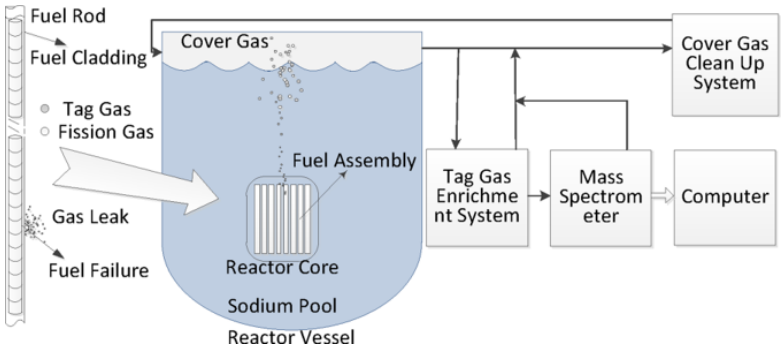

Figure 2.11: Schematic of tag gas location system in CEFR. [151].

In India, Mitra et al. studied dispersion of fission product noble gases using turbulent diffusion equation for the case of release of active cover gas from a lo-

cation inside reactor containment building of Fast Breeder Test Reactor (FBTR) and estimated the time-evolution of the gross gamma activity concentration at a detector location [96]. Ramanathan et al. studied the efficiency of separating inactive krypton and xenon noble gases with argon purge out of liquid sodium in failed fuel localization module in the Prototype Fast Breeder Reactor (PFBR) [109]. Bachchan et al. proposed a revised simulation methodology of delayed neutron signal estimation involving various steps of neutronics and thermal hydraulics calculations, which is considered to be a pre-requisite for the program of experimental demonstration of bulk DND system in PFBR [11]. A schematic of delayed neutron detection during random pin wet rupture is shown in Fig. 2.12.

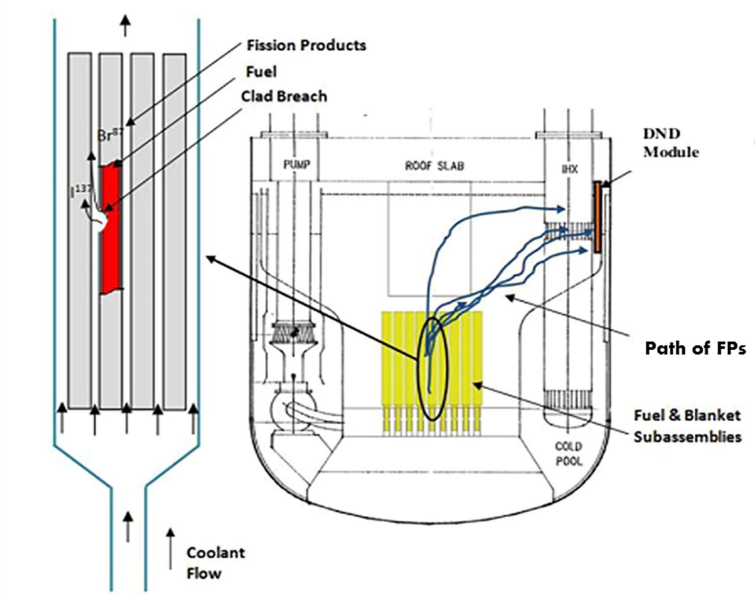

Figure 2.12: Schematic of delayed neutron detection during random pin wet rupture in PFBR [11].

In Russia, the failed fuel pin claddings in the BN-600 reactor operation have been described and results of a large series of experiments at the BR-10 on fuel pin behaviour are discussed [140]. Albutova and Lukyanov developed a regression model for determination of the background level for the sector fuel cladding leak detection system of BN-600 and studied the dependence of background on the reactor operational parameters [3]. Rogozhkin et al. developed a procedure for numerical modeling of the transport of delayed neutron precursors for monitoring the seal-tightness of the cladding and verified it on full-scale reactor problems [112].

In the United States, cladding failure simulation tests have been performed in fuel element rupture detector (FERD) in Experimental Breeder Reactor II (EBR-II) with simulated failures and normal detection system [125] [126]. The methods

have been devised for annunciating and clearly identifying these failures in EBR-II [82].

2.3 Problematic and methodology of the thesis

To summary the research above, several detection methods and detector technology have been studied and improved; the specific thermal hydraulics transfer process has been calculated; the experiments of fuel pin failure have been implemented. But it can be found that once fission products leave a breached cladding, their activity which is eventually measured by the detection systems appears critically dependent on their transit path through the primary sodium and, for fission gases, depends on movement through the cover gas space. Modeling of this transport is important to determine the required sensitivity of failure detectors, and to set prudent shutdown limits for activity in operating plants. It lacks much required data, and is very dependent on the particular reactor plant configuration [72]. A more systematic study and analysis considering the entire detection process is wished for future design.

Therefore, I would like to define a general methodology to make a comprehensive description of the fission products release and detection system, which can be applied to reactors with the core configuration. Under the guidance of the methodology, I can derive the key parameters for the conception choice, with both the numerical modeling and previous experiment data analysis, from two perspectives of fuel behavior and the detected signal, which can support detection system design of future SFRs.

During the operational period of the PHENIX reactor (1973-2009), there were a total of 42 gas pin failures and 15 open-pin failures [135]. Up to now, the experimental data obtained at PHENIX have been used in an operational manner in order to conduct the reactor. I will do the documentary study of the experiment data in PHENIX reactor and do the simulation on the basis of the following physical model.

In order to build a physical model to describe the whole detection process, I define a generic equation of the detected signal:

$$D_{signal}(t) = \sum_{i=FP} R_i(t) * F_i(t) \times E_i + \sum_{j=BI} Q_j(t) * T_j(t) \times E_j \tag{2.1}$$

The first term in Eq. 2.1 is about fission products detection: with i the isotopes of fission products (FP); $D_{signal}(t)$ is the detected signal of the detector; $R_i(t)$ the fission products released from the cladding rupture; $F_i(t)$ the transfer function, a mathematical description of the transportation from the cladding

rupture to the detector; E_i the detection efficiency for the fission products.

The second term is related to the background signal: with j the background isotopes (BI); Q_j the quantity of background isotopes in the reactor; $T_j(t)$ the transfer function of background isotopes to the detector; E_j the detection efficiency for the background isotopes.

Basically, in a contamination measurement system, the detected signal $D_{signal}(t)$ will be obtained to understand the released signal $R_i(t)$ by fission products. The efficiency of the whole system will depend on the transfer function $F_i(t)$ and detection efficiency E_i.

However, in previous detection experience of the SFR reactors, e.g. RAPSODIE, PHENIX, SUPERPHENIX, the analysis of the signal was lacking and the interpretation of signal evolution related to fuel pin behaviour was ambiguous. From the perspective of detection system design, due to the different monitoring purposes and release characteristics of fission products in gas and neutron detection, the key parameters for detection system design will be different.

Therefore, I would like to develop a general methodology of detection process through the theoretical analysis and numerical modeling of $R_i(t)$ and $F_i(t)$ and E_i as well as the experiment data study of $D_{signal}(t)$, in order to comprehend the release characteristics of the fission products; clarify the relation between $D_{signal}(t)$ and $R_i(t)$; determine the key parameters of gas and neutron detection systems respectively; optimize the detection system design of SFR in the future.

Corresponding to the different situations of fuel pin failure and the released fission products in gas and neutron detection, I devised two scenarios to describe the release and detection process respectively. The research will be implemented under these two scenarios:

- The first scenario is for crack on the cladding only with fission gas leakage, shown in Fig. 2.13. In this condition, the whole process will be: during the reactor operating, the fission gases are produced and diffused in the fuel pin. Part of the fission gas will be released from the fuel pin and be accumulated in fission gas plenum, a gas expansion volume inside the cladding [45]. When there is a crack failure on the cladding, the fission gas accumulated in the gas plenum in the cladding will release through the crack, go through the sodium coolant, and finally will be transported into the cover gas. Then the activity in the cover gas will be increased. The gas detection system makes the sampling in the cover gas and the fission gases are transported to the detector continuously, which will monitor the gas activity.

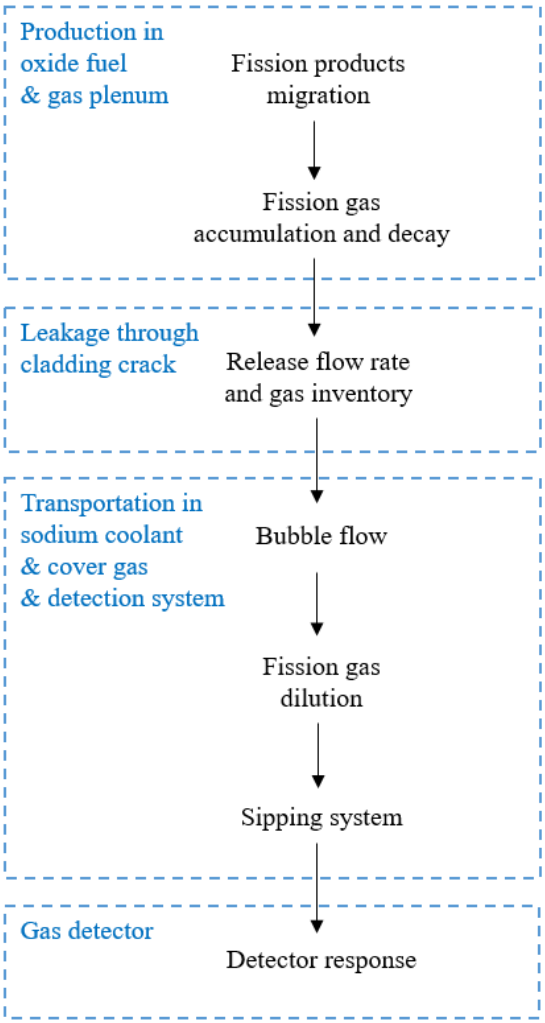

Figure 2.13: Scenario for crack only with fission gas leakage.

- The second scenario is for narrow rupture with fission product leakage, shown in Fig. 2.14. In this condition, the sodium will flow through the cladding rupture and fission products will be released from the fuel pin to the sodium coolant directly and continuously. Some of the fission products can emit delayed neutrons, which are delayed neutron precursors (DNP). DNP will be transported by sodium and the sipping system of the neutron detection system. Then neutron detector will detect the neutron signal. One phenomenon needs to be noticed in this scenario: during the DNP release, the sodium in contact with fuel will induce a oxide-sodium reaction (OSR). The sodium urano-plutonate may accelerate the DNP release or increase the cladding swelling and then enlarge the primary crack.

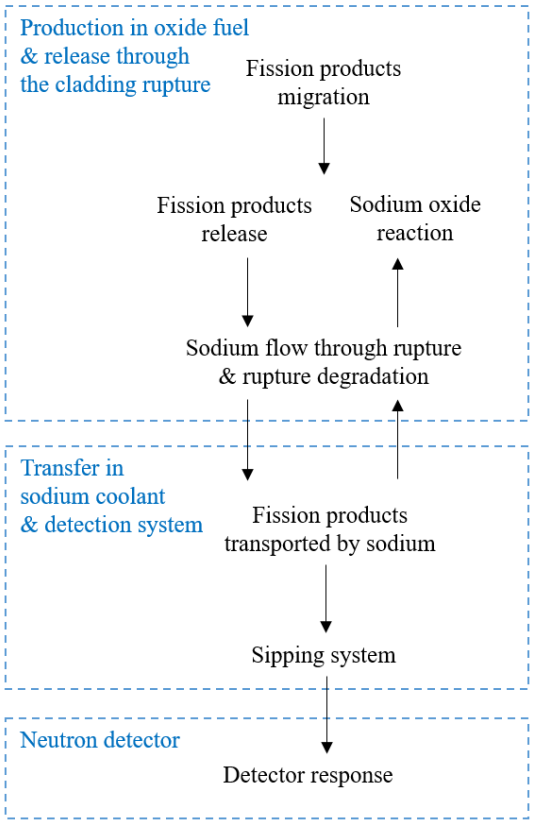

Figure 2.14: Scenario for narrow rupture with fission product leakage.

To answer the problem of the thesis, I propose a study in several chapters:

In chapter 3, I will apply the equation to the gas detection and I will study the transfer function $F_i(t)$ to predict the time broadening introduced by the transportation process. I will assess the transfer function by a comparison between the modeling results and the experiment data in PHENIX reactor. Then I will study the application of the transfer function such as deconvolution process.

In chapter 4, I will develop a general methodology for gas detection modeling: I will deduce the detected signal $D_{signal}(t)$ based on the research of transfer function $F_i(t)$, combined with the numerical modeling of fission gas release rate $R_i(t)$ and detector (ionization chamber) efficiency E_i, aimed to look for early detection of small cladding failure in SFR. I will analyse the reliability of early detection of DRG system and will propose the recommendations for the future design of SFR detection system.

In chapter 5, I will apply the equation to the neutron detection. Due to the release mechanism of delayed neutron precursors depends on the fuel behaviour, I will model the entire system of $F_i(t)$ and E_i with the basic release of direct recoil. I will point out the key parameters of detection system and will discuss the fuel properties that may affect neutron detection.

In chapter 6, I will model the enhanced thermal diffusion release $R_i(t)$ due to corrosion layer formation during the fuel evolution, in order to interpret the neutron signal time evolution and to have a better prediction to the breached fuel area. I will discuss other impacts of corrosion layer formation on detection system and will explain some phenomena of experiment data.

In chapter 7, I will propose the potential ways to apply the methodology to the new reactor designs.

Chapter 3

Transfer function determination in gas detection system

As presented in chapter 1 and chapter 2, SFRs are required to remain contamination free to maintain the reliability of the reactor. The release of fission products from a cladding failure is monitored by a detection system. Gaseous fission products release will be at the first stage of failure and will be detected by the gas detection system, which is DRG system.

In this chapter, I will apply the general equation Eq. 2.1 defined in chapter 2 to DRG system to describe the detection process, according to the developed crack scenario with fission gas release. Among the terms in the equation, the transport process will introduce a time broadening to the signal and modeling of the transport is important to determine the required sensitivity of failure detectors. But the formulation of this transport procedure is lacking in the literature, thus I will firstly study the transportation process of the fission gas in DRG system, which is the transfer function $F_i(t)$ in Eq. 2.1. The modeling of the whole process of gas detection will be performed in the next chapter.

I will propose a model for the transfer function according to the scheme of gas detection system. Then I will develop a general formulation of the transfer function and evaluate it through the modeling with PHENIX reactor parameters and the comparison with the experiment data.

3.1 Introduction

As introduced in Sec. 2.3, a general methodology is searched for to make a comprehensive description of the fission products release and detection system. Thus a scenario is developed to describe the whole process of gas detection system, as illustrated in Fig. 3.1. The scenario can be divided in mainly 5 stages:

1. Fission gas production and accumulation in the gas plenum;
2. Gas leakage flux through the crack;
3. Transportation through the sodium flow, cover gas and sampling pipes up to the detector;
4. Detector efficiency for different isotopes;
5. Sources of background signal.

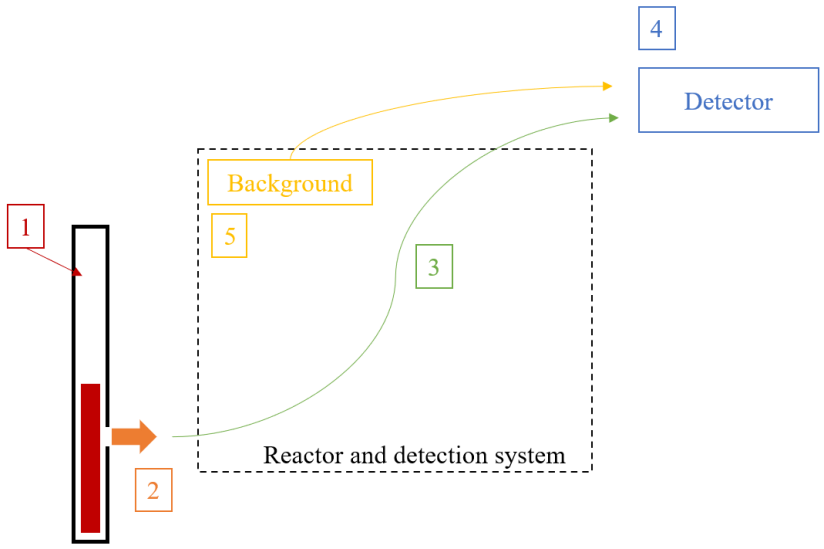

Figure 3.1: The scenario of fission gas release and detection.

Through literature review, several stages can be modeled under theoretical guidance, e.g. fission gas release can be modeled by fuel performance codes and detector efficiency can be modeled by Monte Carlo particle transport simulation codes. However, proposals for formulating transport procedures are lacking in the literature. Therefore, stage 3, the transport of fission gas from the fuel rods to the detectors, will be investigated first.

The transportation process of DRG system is described by a transfer function, which convolutes the entry signal to form the observed signal. In other words, the

detected signal can be seen as the convolution of the released gas and a transfer function, which involves reactor and detection system specifications such as the sodium flow rate or the cover gas volume. The main effect of that convolution is to introduce a time broadening between the fission products release at pin failure and the arrival near the detector, which has to be assessed in order to obtain the proper interpretation of the detected signal. The larger the time broadening, the smaller the maximum detected value can be achieved for a given quantity of released fission gas, so the worse the sensibility of the detection system.

For the crack cases with fast opening, the gas release in a SFR is expected to be nearly instantaneous with respect to the observed time evolution of the detector signal due to the pressure difference between fuel pin and the sodium coolant. It is expected that the observed signal is mostly given by the transfer function. Therefore, new insights are gained into the PHENIX data and I will select some cases as experimental evaluations of the transfer function.

The goal of the chapter is to set up a model for the transfer function in order to predict the time broadening of the observed signal; then the results are compared to the PHENIX case to assess how quantitatively predictive it is and to determine a transfer function. Although the study will make use of PHENIX data, the determined transfer function will be a general formulation which can be applied to other reactors and to guide the conception choice for the future design.

3.2 Isotopes of interest in DRG system: fission gases

In order to build the model of transfer function, the isotopes of interest of the fission gases need to be clarified. There are 2 types of gaseous fission products, which are mainly Xenon and Krypton isotopes:

- radioactive fission gas monitored by ionization chamber and gamma spectrometry;
- stable isotopes monitored by mass spectrometry, including:

  ^{128}Xe, ^{129}Xe, ^{130}Xe, ^{131}Xe, ^{132}Xe, ^{134}Xe, ^{136}Xe;

  ^{82}Kr, ^{83}Kr, ^{84}Kr, ^{86}Kr.

Due to the ionization chamber is mainly used in the global monitoring in the cover gas and the mass spectrometry is rarely used in PHENIX reactor, there is experiment data for the radioactive detection. For the purpose of transfer function

determination using the experiment data, the radioactive isotopes will be focused on in this study.

The inventory of short-lived gaseous radioactive isotopes is shown in Tab. 3.1 [149], and the decay path of the main isotopes interested are shown in Appendix A. During transportation, the short-lived isotopes may decay to other isotopes. Changes in quantity need to be taken into account.

Table 3.1: The inventory of short-lived radioactive isotopes.

Isotope (half life)	Origin (half life)	End product
^{133}Xe (5.3 d)	^{133}I (20.8 h)	^{133}Cs
^{135m}Xe (16 min)	^{135}I (6.6 h)	^{135}Ba
^{135}Xe (9.2 h)	^{135}I (6.6 h)	^{135}Ba
^{138}Xe (17 min)	^{138}I (6.2 s)	^{138}Ba
^{85m}Kr (4.4 h)	^{85}Br (2.9 min)	^{85}Rb
^{87}Kr (1.3 h)	^{87}Br (55.6 s)	^{87}Sr
^{88}Kr (2.8 h)	^{88}Br (16.3 s)	^{88}Sr

The accumulation of the fission gas in the fuel pin during the burn up is calculated:

$$\frac{dN_f}{dt} = y\tau/2 - \lambda N_f \tag{3.1}$$

The integral of Eq. 3.1 is made, the number of atoms produced in the fuel as the evolution of time is obtained:

$$N_f(t) = \frac{y\tau/2}{\lambda}(1 - e^{-\lambda t}) \tag{3.2}$$

In Eq. 3.1 and Eq. 3.2, where N_f is the number of atoms of fission gas; y is the cumulative fission yield of the considered fission products for fast neutrons; τ is the number of fission events per second, which depends on the linear power of the core; t is the time during the whole burn up.

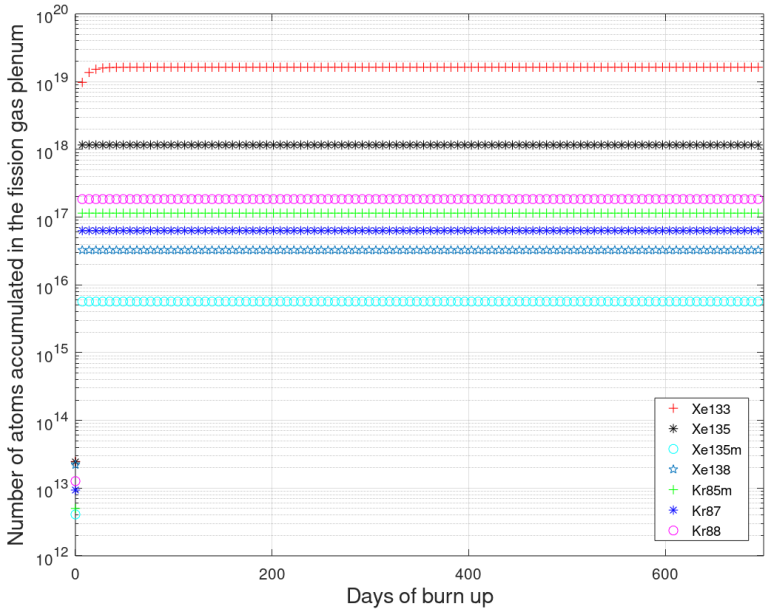

Figure 3.2: Number of atoms accumulated in the fission gas plenum.

The number of atoms of short-lived isotopes accumulated in the fission gas plenum are shown in Fig. 3.2. It can be observed that short-lived fission gases reach a constant equilibrium at the beginning of life. The ^{133}Xe is the dominant isotope with largest number of atoms. The second significant one is ^{135}Xe, which has one tenth of the quantity of ^{133}Xe but is relatively important among the short-lived gaseous fission products. When there is a crack on the cladding, it is generally considered that the gaseous fission products accumulated in the fission gas plenum will be released outside the cladding through the crack because of the pressure difference [45]. Thus ^{133}Xe (5.3 d) and ^{135}Xe (9.2 h) are the main fission gases released into the cover gas.

3.3 Model of the transfer function

3.3.1 Scheme of fission gas transfer

A simplified scheme is built by taking into account fission gas dilution and time broadening, to describe the fission gas release (FGR) transport process. In this section, the transfer function is a predictive modeling in aim to study the time broadening.

When there is a crack on the cladding, the fission gas will be released rapidly into the sodium coolant circuit because of the pressure difference. There will be two forms of gas, either in solution in the sodium or in bubbles which eventually

go into the cover gas. The solubility of Krypton and Xenon in liquid sodium at 700 K and 0.1 MPa is calculated by Eq. 3.3. According to the Henry's law, the amount of dissolved gas in a liquid is proportional to its partial pressure above the liquid. The amount of dissolved Xenon and Krypton in sodium depends on the partial pressure of Xenon and Krypton above sodium.

$$x(g)P = x(l)K \tag{3.3}$$

In Eq. 3.3, where $x(g)$ is the number of moles of Xenon and Krypton per number of moles of Argon in the cover gas; P is the absolute pressure above the sodium, thus $x(g)P$ is the partial pressure of the fission gas above; $x(l)$ is the number of moles of Xenon and Krypton per number of moles of Sodium; K is Henry constant for Xenon and Krypton, derived from the data in [124] [123], which is 4.8×10^{11} MPa and 1.4×10^{10} MPa respectively.

The calculated fraction of Xenon and Krypton dissolved in sodium is 1.0×10^{-8} and 4.0×10^{-7} respectively, which are both very low. It can be concluded that most of the fission gas will be released into the cover gas. To simplify the transport process, for the predictive calculation the hypothesis can be made that all of the FGR goes into the cover gas. Finally the fission gas in cover gas will be sampled into the DRG gas block and be transported to the detection chamber. The activity will be measured by the detectors.

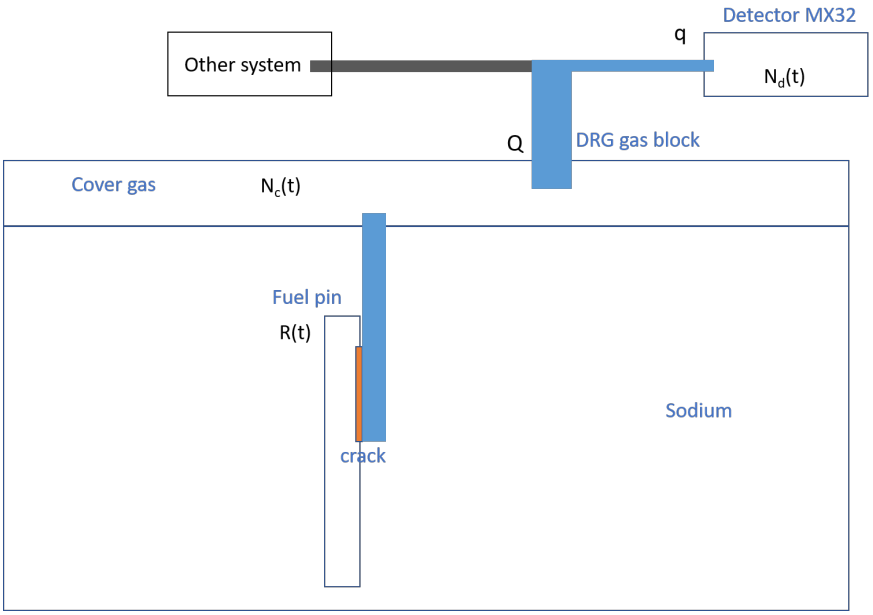

Figure 3.3: The scheme of fission gas release from the fuel pin to DRG detection system.

The scheme of FGR from the fuel pin to DRG detection system is shown

in Fig. 3.3. $R(t)$ is the FGR from the fuel pin, in the unit of number of atoms per second. The FGR will go through the crack, shown in orange in Fig. 3.3, to the sodium coolant, then will be transported into the cover gas. With the simplification mentioned above, this process is represented by the blue tube leading to the cover gas directly. Then the FGR will dilute in the cover gas. N_c is the number of atoms released in cover gas. The sipping system of DRG block samples the FGR from the cover gas, thus the FGR will then flow into the detection chamber, represented by the blue tube leading to the detector. The total flow rate removing the fission gas in the cover gas is Q; the flow rate to the detector is q.

3.3.2 Transfer function

Based on the scheme of FGR from the fuel pin to DRG detection system, the conservation equation of the number of atoms of FGR in the cover gas at moment t is derived, using the framework proposed in [94]. The conservation balance in the cover gas can be expressed as:

$$\frac{\mathrm{d}N_c}{\mathrm{d}t}(t) = R(t) - \frac{Q}{V_c}N_c(t) \tag{3.4}$$

The same balance in the detector can be expressed as:

$$\frac{\mathrm{d}N_d}{\mathrm{d}t}(t) = \frac{q}{V_c}N_c(t) - \frac{q}{V_d}N_d(t) \tag{3.5}$$

In Eq. 3.4 and Eq. 3.5, R represents the FGR from the fuel pin; Q is the total gas flow rate in the cover gas; q is the gas flow rate to the detector; N_c is the number of atoms in the cover gas; N_d is the number of atoms in the detector; V_c is the volume of cover gas; V_d is the volume of detector chamber.

$q = \alpha\, Q$ $(0 < \alpha < 1)$ is defined and the Laplace transform is applied to Eq. 3.4 and Eq. 3.5, R can be expressed as a function of N_d:

$$R(s) = (\frac{V_c}{\alpha Q}s^2 + [\frac{V_c}{V_d} + \frac{1}{\alpha}]s + \frac{Q}{V_d})N_d(s) \tag{3.6}$$

Applying the inverse Laplace transform:

$$R(t) = \frac{V_c}{\alpha Q}\frac{\mathrm{d}^2N_d}{\mathrm{d}t^2}(t) + (\frac{V_c}{V_d} + \frac{1}{\alpha})\frac{\mathrm{d}N_d}{\mathrm{d}t}(t) + \frac{Q}{V_d}N_d(t) \tag{3.7}$$

The transfer function $F(s)$ is defined to express the relation between R and N_d:

$$N_d(s) = F(s)R(s) \tag{3.8}$$

$$F(s) = \frac{1}{As^2 + Bs + C} = \frac{1}{A[(s+a)^2 - b^2]} \tag{3.9}$$

With

$$A = \frac{V_c}{\alpha Q}, B = \frac{V_c}{V_d} + \frac{1}{\alpha}, C = \frac{Q}{V_d} \tag{3.10}$$

$$a = \frac{B}{2A}, b = \sqrt{(\frac{B}{2A})^2 - \frac{C}{A}} \tag{3.11}$$

Then the transfer function formula can be induced:

$$f(t) = \frac{1}{Ab} \times e^{-at} \times \sinh(bt) \tag{3.12}$$

Eq. 3.12 can be simplified and it can be obtained:

$$f(t) = \frac{\alpha V_d}{\alpha V_c - V_d} \times (e^{-\frac{Q}{V_c}t} - e^{-\frac{\alpha Q}{V_d}t}) \tag{3.13}$$

The transfer function Eq. 3.13 is a general formulation of the problem, which is derived from the physical descriptions, it can be applied for different detection setups.

For short-lived isotopes, the radioactive decay of the fission gas during the transfer process needs to be taken into account, thus the mass balance equations in Eq. 3.4 is rewritten and Eq. 3.5 by adding decay items. Then the mass balance equations with the decay constant can be derived:

$$\frac{\mathrm{d}N_c}{\mathrm{d}t}(t) = R(t) - \frac{Q}{V_c}N_c(t) - \lambda N_c(t) \tag{3.14}$$

$$\frac{\mathrm{d}N_d}{\mathrm{d}t}(t) = \frac{q}{V_c}N_c(t) - \frac{q}{V_d}N_d(t) - \lambda N_d(t) \tag{3.15}$$

λ is the average decay constant for all the fission gas isotopes taking into account the quantity fraction, calculated by:

$$\lambda = \sum_{i=FG} \omega_i \lambda_i \tag{3.16}$$

ω_i is the fraction of each fission gas isotope in the total gas quantity, which is studied in Sec. 3.2. The main isotopes are ^{133}Xe (5.3 d) and ^{135}Xe (9.2 h), and the quantity of ^{133}Xe is around ten times of ^{135}Xe.

Then the transfer function will be:

$$f(t) = \frac{\alpha V_d}{\alpha V_c - V_d} \times [e^{-(\frac{Q}{V_c}+\lambda)t} - e^{-(\frac{\alpha Q}{V_d}+\lambda)t}] \tag{3.17}$$

Since V_c is much larger than V_d, the time broadening of transfer function is

mainly depends on Q and V_c.

For the case of instantaneous release, the FGR from the fuel pin is a Dirac peak, it can be obtained:

$$N_d(t) = f(t) \tag{3.18}$$

To assess how quantitatively predictive the model is, the transfer function to a specific case is applied in Sec. 3.4. The transfer function modeling results based on Eq. 3.17 are presented in Sec. 3.4.3.

3.4 Evaluation of transfer function in the PHENIX case

An experimental case in PHENIX reactor is chosen as an assessment study in this section. Among 15 open-pin failures, RG 14 is chosen as a defective fuel pin study case because it only has gas leakage at the first period of release and the FGR is expected to be nearly instantaneous, in the time scale of seconds, with respect to the observed time evolution. The clean signals and mechanisms with clear explanations in this case help to determine a transfer function.

3.4.1 The RG 14 case study

In the fuel pin with the fission process, the fission gas can be released by recoil and knock-out as well as thermal diffusion to the gas plenum. For fast reactor, because of the high temperature, steep temperature gradient and the high burn up, the fraction of FGR in the fission gas plenum is about 80 % to 90 % [45]. In other words, during the burn up without any failure, most of the gaseous fission products will be released from the fuel pin and be accumulated in fission gas plenum, which is the gas expansion volume inside the cladding. The crack in RG 14 was brittle and large which means the crack occurred rapidly. The gaseous fission products in the gas plenum will be released outside the cladding through the crack instantaneously because of the pressure difference between the fuel and the coolant.

The post irradiation examination photo for the crack is shown in Fig. 3.4, taken from the PHENIX internal report, which is a long and straight breach, with relatively large width around 0.5 mm. Its length is approximately 480 mm, which is a relatively long crack. The pin failure happened in the end of life with high burn up of 11.56 %, probably due to embrittlement of cladding by the radiation damage. Brittle crack is known to occur rapidly. The crack observation is consistent with

the instantaneous gas signal detection.

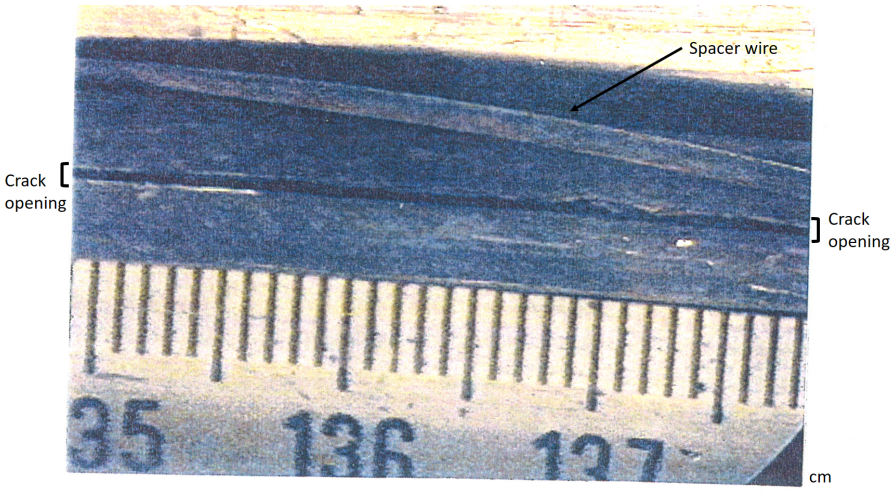

Figure 3.4: Post irradiation examination photo in RG 14 (from PHENIX internal report, 1995).

Thus the assumption of a Dirac peak for the burst release can be justified in the case of RG 14. As a consequence, the observed signal of RG 14 can be regarded as an experimental measurement of the transfer function.

3.4.2 Gas signal of RG 14

The RG 14 cladding crack occurred on the experimental assembly in 1988. The first gas emission was detected on February 26 at 13h00. The first major release of fission gas corresponds to the instantaneous leakage of a cladding. Then the internal pressure suddenly drops and the cover gas activity rapidly rises to a maximum of 1.5 Ci/m^3 due to the arrival of fission gases.

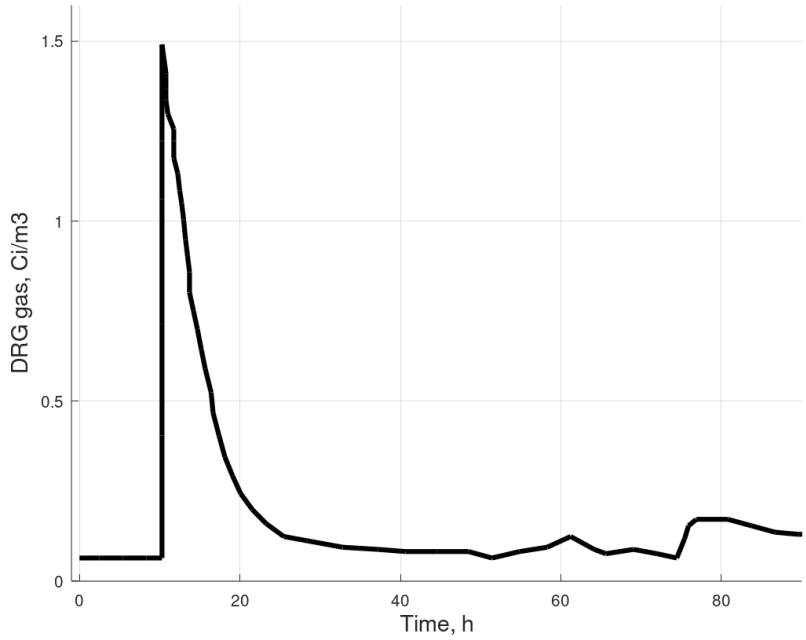

Figure 3.5: The signal of the first period fission gas release detected by MX 32 in RG 14.

The signal of the first period fission gas release detected by MX 32 is shown in Fig. 3.5. It can be observed that the gas signal is expected to be an instantaneous release with time broadening during the first release and then has some time evolution. In order to assess the transfer function, only the first period gas release is studied.

Then the transfer function derived in Sec. 3.3 is applied to RG 14 case and compared the modeling results with RG 14 experiment data.

3.4.3 Modeling prediction and comparison with experiment data

In order to do the assessment of the transfer function, the transfer function modeling results and the comparison with the experiment data in RG 14 are shown in this section.

The transfer function is applied to our specific case RG 14, with the total flow rate in the cover gas Q (5.0 l/s), the flow rate to MX 32 detector q (0.2 l/s),as well as volume data V_c (40 m^3) of the cover gas and V_d (0.09 l) of the detector chamber.

As shown in Fig. 3.6, the red curve is the transfer function modeling according to Eq. 3.13, with Q equal to 5.0 l/s. The result shows that the radioactive decay

only has a limited influence on the transfer function because the main isotope is ^{133}Xe (5.3 d) with relatively long half-life.

To make the comparison, a coefficient is multiplied to make these curves have the same maximum activity value, which is 1.5 Ci/m^3. An offset is also added to the modeling because a continuous emission of 0.06 Ci/m^3 was detected after the first burst.

Then it can be observed that the shape of the transfer modeling curve is consistent with the experiment data, which has the same order of magnitude of the time broadening and the same shape of exponential decreasing. It can be concluded that the model proposed is able to model the time broadening quantitatively and the transfer function is validated.

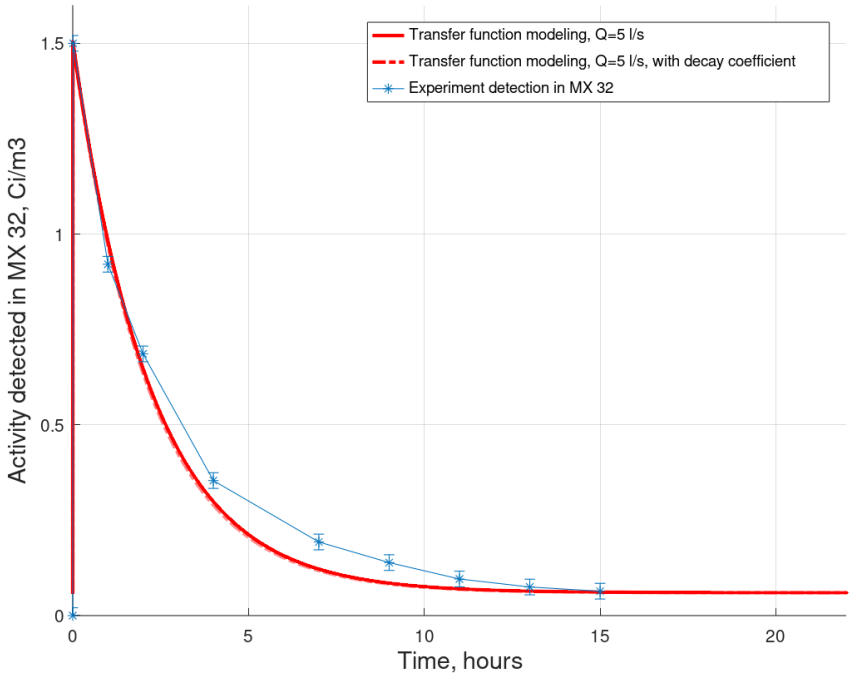

Figure 3.6: The fission gas activity in MX 32 and the transfer function modeling result comparison.

3.5 Conclusion

In this chapter, a model for the transfer function of the gas detection process, making it possible to predict the time broadening of the observed signal, has been proposed. Taking the actual specifications of the reactor, it matches well with the PHENIX reactor experimental data, with the same order of magnitude of the time broadening and the same shape of exponential decreasing. As a result, the

transfer function is validated by a comparison between the modeling result and the experimental data.

In conclusion, the transfer function of gas detection system has been determined, which is a general formulation can be applied to other reactors and to guide the conception choice for the future design. This part of the work has been published in [33]. On the basis of this determined transfer function, I will develop a general methodology to describe the whole gas detection system in the next chapter.

Chapter 4

General methodology for the whole gas detection modeling

In this chapter, I will develop a generic methodology which is applicable to arbitrary SFR gas detection system, based on the transfer function determined in the last chapter. I will define an equation to describe the whole detection system consisted of several modules, including: fission gas quantity accumulated in the fuel gas plenum, the gas leakage flux through the crack, the transportation from the fuel pin to the detector; the detector sensibility to different isotopes.

As an application example of this methodology, I will implement the modeling in the PHENIX reactor to evaluate the performance of the DRG system. Through this modeling, I will derive the detected signal as the function of the crack size and estimate the minimum signal and the relevant minimum crack size detectable among the background signals.

With the description of the entire DRG system using the deduced methodology, I will propose the possible optimization of the gas detection system for the future design. I will also perform a deconvolution process on the detected signal to have a better understanding of the released gas at the fuel pin.

4.1 Introduction

The whole detection process in DRG system is proceeded as follows: during the reactor operating, the fission gases are produced and diffused in the fuel pin. Part of the fission gas will be released from the fuel pin and be accumulated in fission gas plenum, a gas expansion volume inside the cladding [45]. When there is a crack failure on the cladding, the fission gas accumulated in the gas plenum in the cladding will release through the crack, go through the sodium coolant, and finally will be transported into the cover gas. The transfer process is described as a transfer function which is studied in last chapter [33]. Then the activity in the cover gas will be increased due to the fission gas release. The DRG system makes the sampling in the cover gas and the gases are transported to the ionization chamber continuously, which will monitor the overall activity. In this chapter, the purpose is to evaluate the detection reliability, thus small leakages are focused on, for which the release is not instantaneous.

The aim of this chapter is to develop a general methodology to evaluate the performance of gas detection in DRG system and dedicate to the optimization of the early signal detection in future design. Since the whole detection system involves several processes, a generic model is devised from fission gas release to detection, including: fission gas quantity accumulated in the fuel gas plenum during the burn up; the gas leakage condition through different crack size; the transfer process in the reactor and detection system; detector sensibility to different isotopes; sources of background signal. The work is performed to have a theoretical database prior to the actual experiment of the future SFRs. This methodology is applied to PHENIX data as an illustration of its applicability and relevance. With the analysis of modeling results, it will be possible to optimize the early detection on the activities of released fission gas and develop a real time monitoring system of the cladding failure.

4.2 The developed methodology

4.2.1 The generic equation of detection process

A global measurement in DRG system aimed to assessing the fission gas release by continuously monitoring the total activity in the cover gas, which is carried out using circulating ionization chambers. The electric signal is induced by the β and γ particles released by the fission gas [49]. According to the scenario developed in Sec. 3.1, the equation of the current signal with all the processes described in the scenario is derived, by the rewritten of Eq. 2.1:

$$I_{signal}(t) = \sum_{i=FG} R_i(t) * F_i(t) \times E_i + \sum_{j=BI} Q_j(t) * T_j(t) \times E_j \tag{4.1}$$

with i the isotopes of fission gases (FG); R_i the fission gas flux released from the crack; $F_i(t)$ the transfer function, a mathematical description of the transportation through the sodium flow, cover gas and sampling pipes up to the detector; E_i the detection sensitivity for the fission gas; j the background isotopes (BI); Q_j the quantity of background isotopes in the cover gas; $T_j(t)$ the transfer function of background isotopes from cover gas to the detector; E_j the detection sensitivity for the background isotopes.

The main background sources in the DRG detection system include two isotopes: ^{23}Ne, with a half-life of 37.2 seconds, is produced by ^{23}Na (n, p) ^{23}Ne; ^{41}Ar, with a half-life of 110 minutes, is produced by ^{41}K (n,p) ^{41}Ar and ^{40}Ar (n, γ) ^{41}Ar.

The whole process can be divided into modules to derive the detected signal I_{signal} according to the developed scenario. Then all the modules can be combined to derive the detected signal related to the crack size, and to evaluate the early detection reliability. The modules includes: the fission gas quantity accumulated in the fuel gas plenum during the burn up and the gas leakage rate through the crack R_i, the transfer function F_i and the ionization chamber sensitivity E_i.

4.2.2 Fission gas accumulation and leakage R_i

During the SFR operation, the fission gases are produced and diffused in the fuel pin. In the rated operating conditions of the fast reactor pin, with the fuel being very hot on the average, a high amount of gaseous fission products (Xe and Kr) is released and accumulated in the gas plenum inside the cladding [104].

There are both long-lived and short-lived fission gases created in the fuel pin. During the burn up, the quantity of long-lived fission gas will increase continuously and the short-lived one will reach an equilibrium value sometime depending on the decay constant. Thus as the accumulation of the fission gas, the pressure in the gas plenum will increase.

The fission products evolution, the diffusion through the fuel pin and the gas quantity released to the gas plenum during the burn up under fast neutron flux can be performed by the fuel performance code, e.g. Germinal computation [81].

With the quantity of fission gas accumulated and the pressure in the gas plenum during the burn up, the gas flux release through the crack with different size can be deduced. For most conditions in SFR, when there is a crack on the cladding, the gaseous fission products in the gas plenum will be released instantaneously through the crack because of the pressure difference between the fuel and

the coolant. But the instantaneous release has to be mitigated for small leakage.

Gas flux q is calculated by Eq. 4.2 [50], which is the product of the volume of gas lost per unit of time by the pressure. For an ideal gas at constant temperature T, it is related to the number of atoms lost per unit of time.

$$q = k_b T \frac{dn}{dt} \tag{4.2}$$

with k_b the Boltzman constant. The expression of the gas flux q as a function of the pressure P of the gas differs according to the flux type, characterized by the Knudsen number K_n, where q is molecular flux when $K_n < 1$; laminar flux when $K_n > 200$; intermediate flux when $1 < K_n < 200$:

$$K_n = \frac{l}{df} \tag{4.3}$$

with df the hydraulic diameter of the crack, which is identical to a geometric diameter for cylinders and l the mean free path:

$$l = \frac{k_b T}{\sqrt{2}\pi d^2 P} \tag{4.4}$$

with d the atom diameter and P the gas pressure in the gas plenum. The evolution of the pressure P is calculated by:

$$V \frac{dP}{dt} = \Delta P V - q(P) \tag{4.5}$$

with V the volume of gas plenum and ΔP the increase rate of the pressure.

The fission gas release flux q is the sum of R_i in Eq. 4.1.

4.2.3 Transfer function F_i for different isotopes

The detected signal is the convolution of the released signal at the fuel pin and the transfer function of the detection system. After the simulation of gas leakage flux at the fuel pin, the transfer function of the detection system is needed to deduce the detected activity. The transfer function of DRG system is studied and validated in [33]:

$$F_i(t) = \frac{\alpha V_d}{\alpha V_c - V_d} \times [e^{-(\frac{Q}{V_c}+\lambda_i)t} - e^{-(\frac{\alpha Q}{V_d}+\lambda_i)t}] \tag{4.6}$$

with λ the decay constant of fission gas isotopes; Q the total gas flow rate in the cover gas; q the gas flow rate to the detector; V_c the volume of cover gas; V_d the volume of detector chamber; $\alpha = q/Q$ $(0 < \alpha < 1)$.

4.2.4 Detector sensitivity E_i

Using the computed gas leakage flux and the derived transfer function, the fission gas activity to the detector can be obtained with the convolution. Then it is necessary to study the detector sensitivity E_i for different isotopes. As mentioned above, the circulation ionization chamber is used in DRG system for the continuously monitoring in the cover gas, which provide an overall activity. E_i can be derived by the modeling of ionization chamber.

An ionization chamber is made of two electrodes and there is filling gas in the inter-electrode space. When a particle passes through the gas with enough energy, it can create electron-ions pairs along its path [79]. The electric current is calculated by [22]:

$$I = \varepsilon A \Delta E q_e W^{-1} \tag{4.7}$$

In Eq. 4.7, ε is the collection efficiency, which is assumed to 1; A is the activity of the sample in Bq; ΔE is the total energy deposition within the filling gas per source; q_e is the elementary charge; W is the average energy required to produce an ion pair. Eq. 4.7 is applied to our case in Eq. 4.1:

$$I_{signal}(t) = \sum_{i=FG} R_i(t) * F_i(t) \times \varepsilon \Delta E_i q_e W^{-1} + \sum_{j=BI} Q_j(t) * T_j(t) \times \varepsilon \Delta E_j q_e W^{-1} \tag{4.8}$$

$R_i(t)$ and $F_i(t)$ are already calculated in the above sections. It can be derived that the detector sensitivity E_i is proportional to the total energy deposition ΔE in the chamber. Therefore it is necessary to compare the energy deposition of different fission gases and argon in the ionization chamber, which depends on the detector design and the energy distribution of photon and electron from the sources. For example, the energy distribution of the particles from the background source ^{41}Ar is higher than the fission gas ^{133}Xe, as shown in Fig. 4.1 in JENDL-4.0.

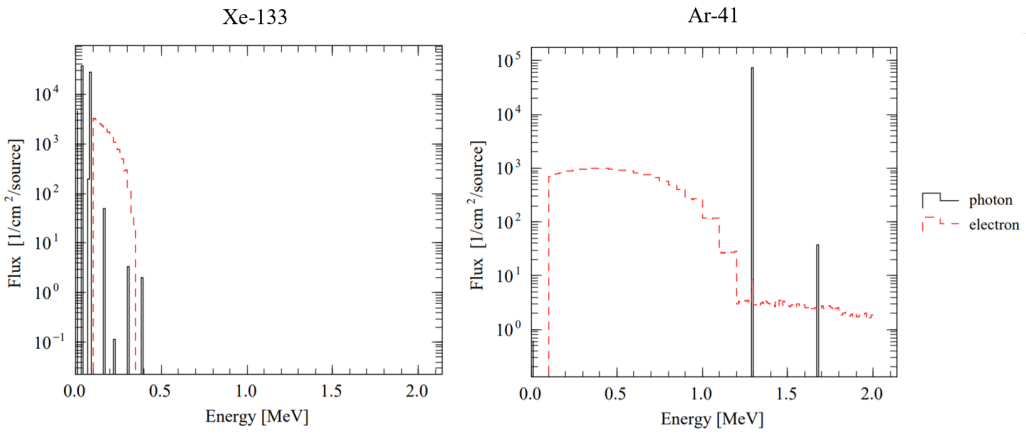

Figure 4.1: Energy distribution of photon and electron from source ^{133}Xe and ^{41}Ar in JENDL-4.0.

The energy deposition ΔE can be performed by the Monte Carlo particle transport simulation code, e.g. PHITS 3.22 [70, 110]. Then E_i can be deduced, combined with $R_i(t)$ and $F_i(t)$ studied in the above sections, I_{signal} in Eq. 4.1 can be derived. Thus the modeling taking into account the whole detection process can be implemented.

4.3 Application to PHENIX reactor

The developed equation and the methodology are applied to PHENIX reactor as an application example. Through the modeling, the whole process of early detection can be evaluated; the minimum signal and the relevant minimum crack size detectable among the background signal can be estimated; the significant parameter optimizable in the future design of SFR detection system can be determined.

4.3.1 Fission gas release flux R_i calculation

The accumulated fission gas quantity and the pressure in the gas plenum are computed in Germinal [81] with the calculation condition: MOX fuel; average linear power is around 380 W/cm; maximum burn up is 9.34 %; the gas temperature is around 400 °C.

The computed release rate of fission gas in a given fuel pin in PHENIX is shown in Fig. 4.2. It can be observed that the release rate rises rapidly during the beginning of life, reaches 30 - 50 % ; most of the fission gases are released and accumulated in the gas plenum when the burn up is larger than 4 %, the release fraction is around 80 - 90 % .

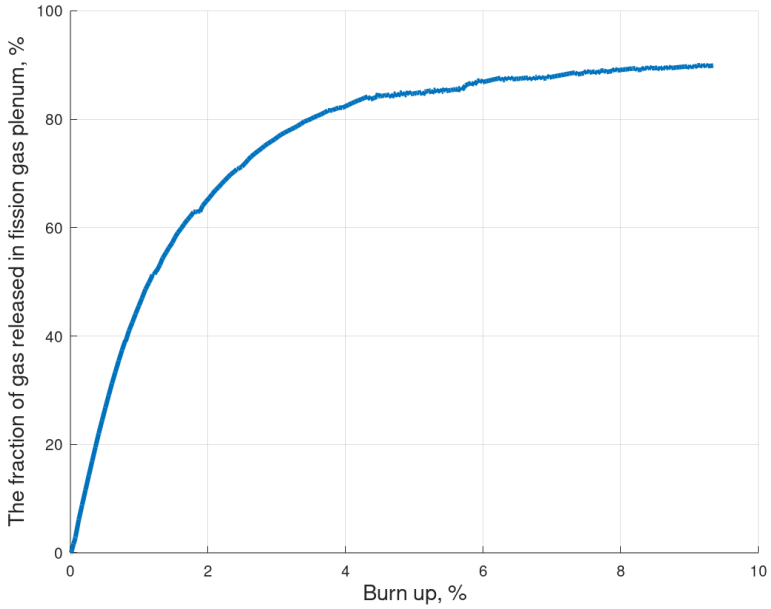

Figure 4.2: The fraction of gas released in fission gas plenum as computed by Germinal.

The calculated pressure in the gas plenum is presented in Fig. 4.3, from a few to dozens of atmosphere (the drops are due to the power change during the operation).

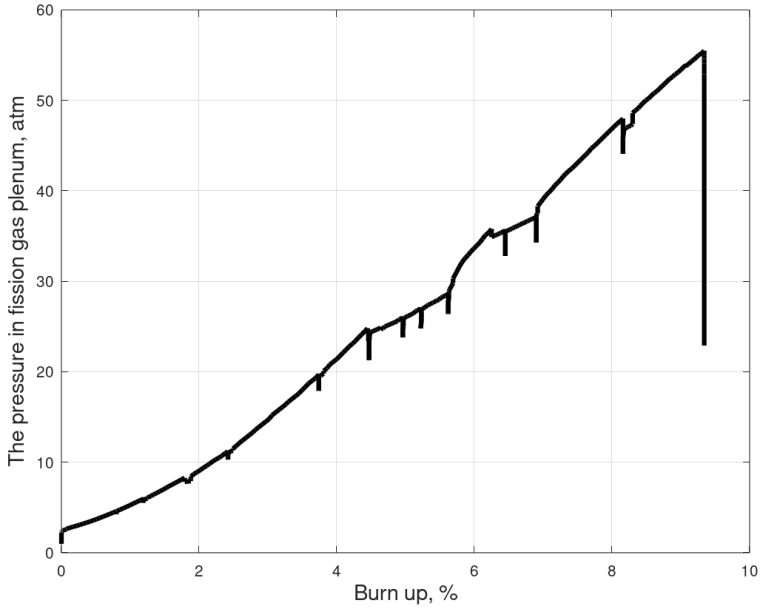

Figure 4.3: The pressure in fission gas plenum in operating condition.

The isotopes of interest among the fission gases for ionization chamber de-

tection are radioactive isotopes (the stable isotopes will be interested in mass spectrometry detection), which will reach an equilibrium value quickly and keep a stable amount in the gas plenum during the burn up. The activity of accumulated fission gas in gas plenum is shown in Fig. 4.4, mainly isotopes of Xenon and Krypton.

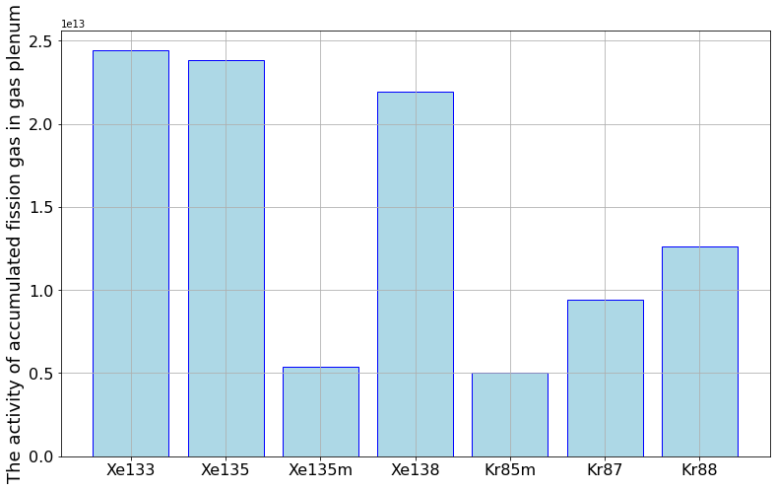

Figure 4.4: The activity of accumulated fission gas in gas plenum.

With the fission gas accumulation and the pressure calculated, the evolution of gas flux q is computed by Eq. 4.2. Due to the gas flux depends on the pressure in the gas plenum and the crack size, 2 examples are performed with P_0 (the initial pressure when the crack happens)=3 atm and 50 atm, df=10 μm, as shown in Fig. 4.5. The calculated gas flux q will be the term R_i in Eq. 4.1. The gas plenum is emptied in laminar regime and the speed is faster with higher pressure (larger burn up).

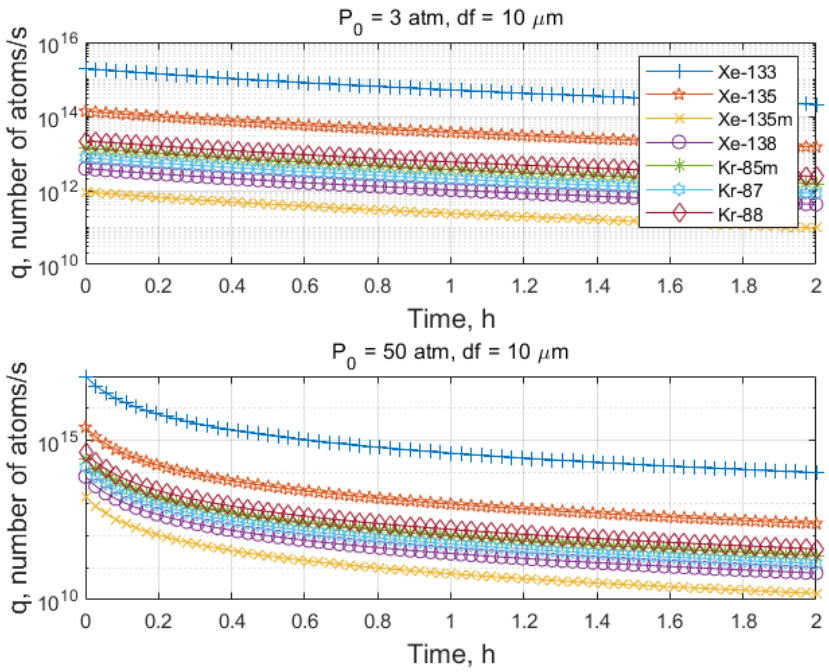

Figure 4.5: Gas flux with P_0 = 3 atm and 50 atm, with df=10 μm as example.

4.3.2 Transfer function F_i calculation

The modeling is under PHENIX reactor configuration according to Eq. 4.6. The transfer functions of isotopes with different half life are illustrated in Fig. 4.6, which will be the term $F_i(t)$ in Eq. 4.1.

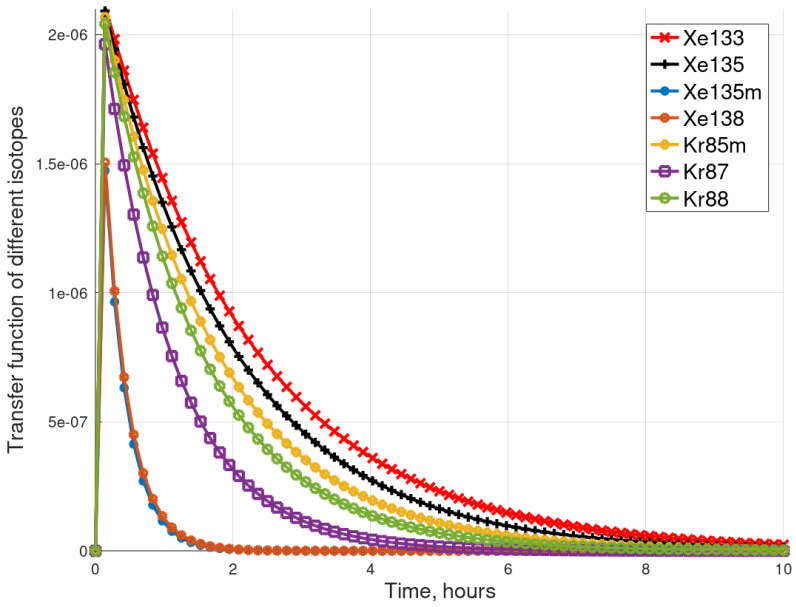

Figure 4.6: Transfer function of different isotopes.

4.3.3 Detector sensitivity E_i calculation

The modeling of ionization chamber is based on the configuration of MX 32 used in PHENIX reactor. The calculation is performed by a Monte Carlo particle transport simulation code, PHITS 3.22.

Particle and Heavy Ion Transport code System (PHITS)[1] is a general purpose Monte Carlo particle transport simulation code that is used in many studies in the fields of accelerator technology, radiotherapy, space radiation, etc. It can deal with the transport of nearly all particles, including neutrons, protons, heavy ions, photons, and electrons, over wide energy ranges using various nuclear reaction models and data libraries [121]. More information is introduced in Appendix B.

The energy deposition is simulated for isotopes interested (mainly fission gas isotopes Xenon and Krypton and the background sources): the ionization chamber is a 2 cm thick brass (67 % Cu and 33% Zn) cylindrical housing of approximately 30 cm diameter and 50 cm in length; the filling gas is air in atmosphere pressure; the source (the fission gases and Argon) is set as a surface source; the number of particles is 10^6 times 10 batches. The modeling result of energy deposition of ^{133}Xe in the detector per volume is presented in Fig. 4.7 as an example, with the statistical relative error around 10^{-2}.

[1] https://phits.jaea.go.jp

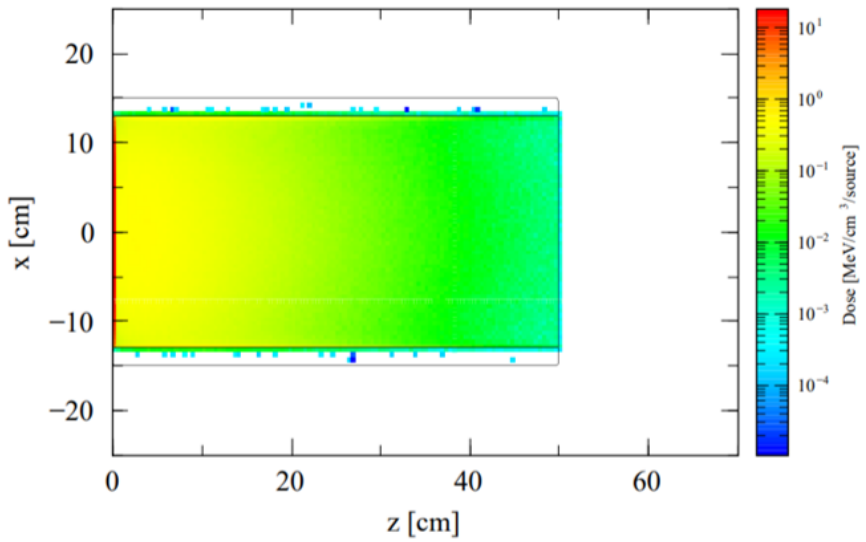

Figure 4.7: Energy deposition of ^{133}Xe in the detector per volume.

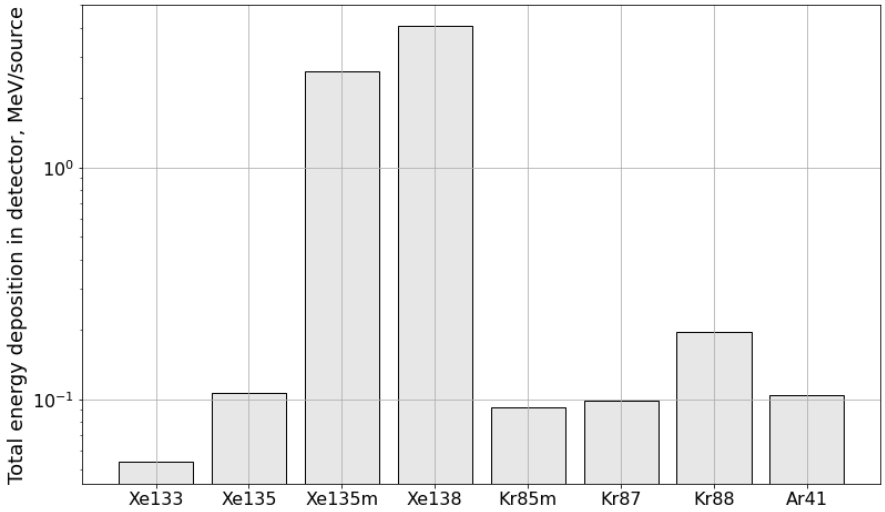

Figure 4.8: Total energy deposition ΔE of different isotopes per source.

The same modeling is implemented for all the isotopes interested. The total energy deposition ΔE of different isotopes per source is calculated, as shown in Fig. 4.8. It can be observed that ^{138}Xe and ^{135m}Xe have higher energy deposition than other isotopes and in contrast ^{133}Xe has the lowest energy deposition. Then with the calculation in the above sections, the total detector current can be derived using Eq. 4.8.

4.3.4 The detected current I_{signal} calculation

Then the detected current can be deduced by the combination of the calculations above and the background signal.

The main background sources are: the activity of ^{23}Ne is 5-7 TBq/m^3 (135-190 Ci/m^3) in the cover gas in PHENIX. Due to the short half-life of ^{23}Ne, the activity was reduced by a delay line in PHENIX. After the delay line (around 20 minutes), the background of ^{23}Ne is negligible. After the delay line, the main background noise is ^{41}Ar. The order of magnitude of background is 0.4-1.5 GBq/m^3 (0.01-0.04 Ci/m^3) in the cover gas in PHENIX.

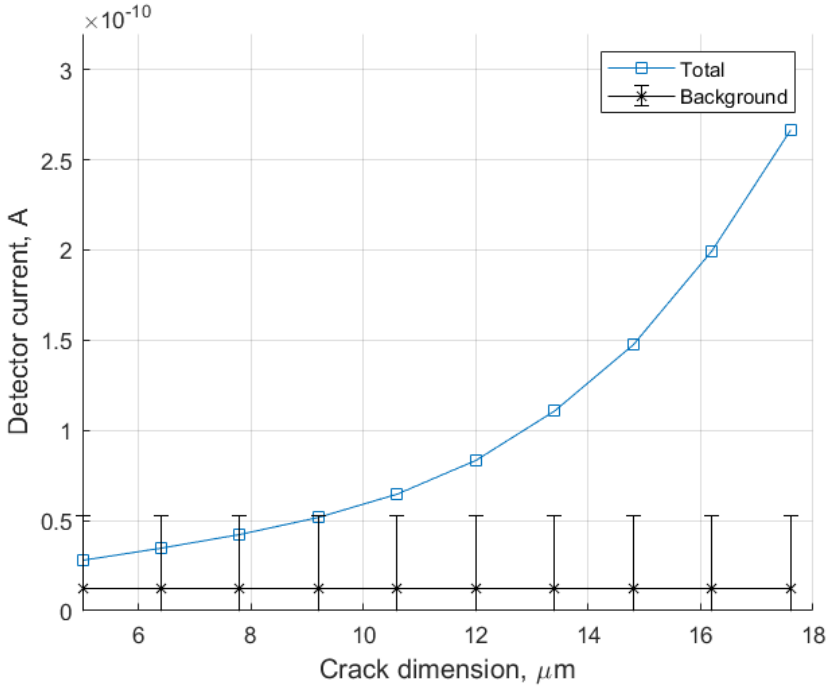

Figure 4.9: The total detector current as the function of crack dimension.

The total detector current calculated as the function of crack dimension is shown in Fig. 4.9, with $P_0 = 50$ atm as an example, for high burn up condition as shown in Fig. 4.3. By comparison with the background signal, the minimum signal detectable and the relevant crack size can be estimated, which is around 9-12 μm. The error bars around ^{41}Ar are obtained according to Poisson statistics, taking a 1-sigma criterion. The minimum crack size for $P_0 = 3$ atm and 20 atm is 25 μm and 15 μm respectively. The order of magnitude of the detectable crack size is dozens micrometers. It can be observed that the detectable size and leakage conditions are similar for both middle and end of life. Because the release rate of the fission gas is around 85 % after 4 % burn up and the pressure in the gas plenum is relatively high.

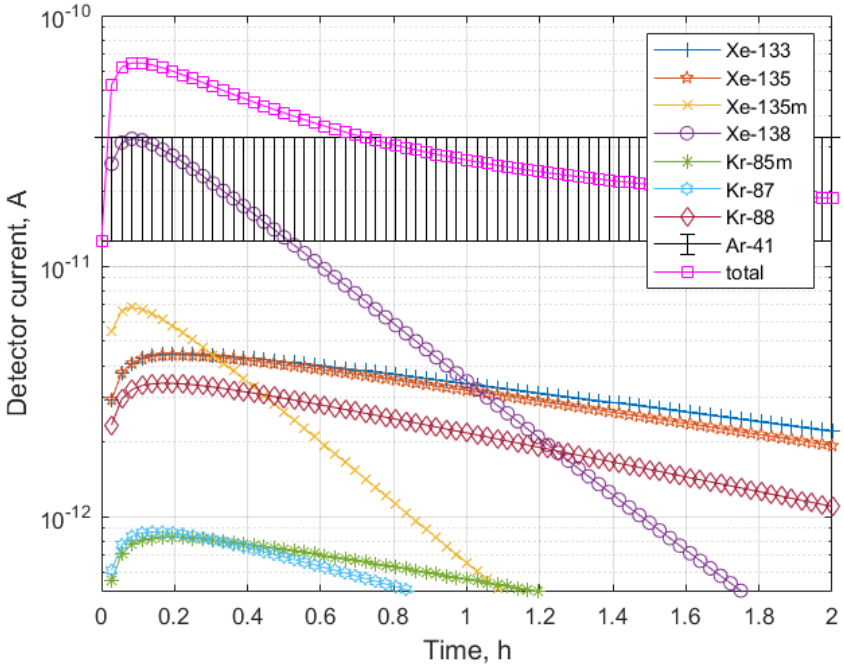

Figure 4.10: The detected current for different isotopes, with df=12 μm.

The modeling result of detected current signal for different fission gas isotopes is presented in Fig. 4.10, with the leakage condition: burn up=8.5 % (P_0=50 atm) and crack dimension df=12 μm. In the modeling, the influence of delay line on the activity of fission gases is taken into account, which is 20 minutes aimed at reducing the background activity in PHENIX. Except from the current quantity, the fission gas signal can also be identified from the width, which is around 40 minutes (0.6 h) in this case. From the modeling result, it can also be concluded that the predominant isotopes making the activity contributions are ^{138}Xe, ^{133}Xe and ^{135}Xe.

4.4 Discussions

With the proposed comprehensive model, the simulation of the whole system has been realized. I would like to discuss optimization of future designs and potential applications of transfer functions in gas detection systems.

4.4.1 Guidance for the future design

According to the methodology developed and the applied modeling results, the methodology can serve as a comprehensive toolbox to optimize detection systems aimed at monitoring fission gas release in SFRs. For each term of the equation,

several optimization directions are proposed:

- For background signal: the delay line is necessary due to the background signal, but after the fission gas release through the crack and the transfer process in the system, ^{138}Xe will be the predominant isotope detected in the first several minutes and then will be ^{133}Xe and ^{135}Xe. In order to have the maximum fission gas activity, the delay line time should be minimized, between 8-15 minutes, as shown in Fig. 4.11.

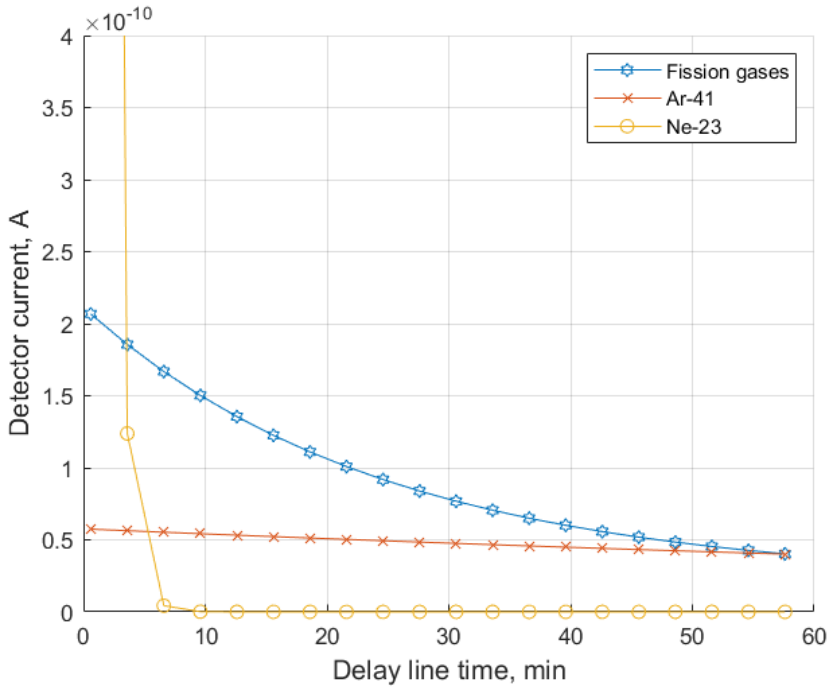

Figure 4.11: The detector current of fission gases and the background as a function of delay line time.

- For E_i: with regard to ionization chamber detection of the global activity monitoring, in order to minimize the difference of the energy deposition in future detector design, it is recommended to shorten the length of the ionization chamber (25 cm for example), due to the energy deposition of ^{133}Xe decreasing fast along the path, as shown in Fig. 4.12.

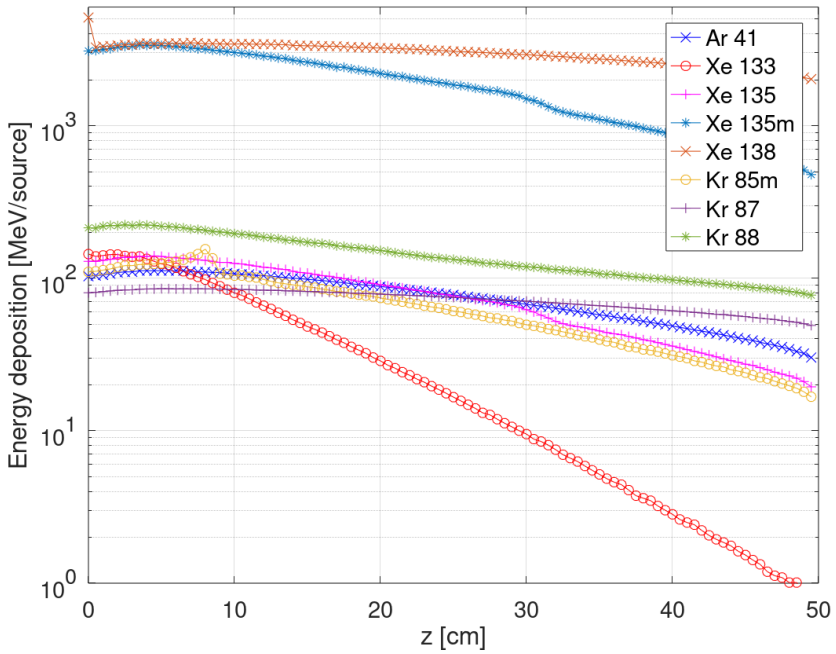

Figure 4.12: Energy deposition of different isotopes per detector chamber length.

- For $F_i(t)$: in the global activity detection, the shorter the transit time of the fission gas, the larger activity detected. The time broadening introduced by the transfer function will also affect the time resolution in gas detection. As shown in Fig. 4.13, different FGR entry signals are defined with different time patterns represented in blue curves. The purple curve is the transfer function with the PHENIX functional parameter; the orange curves represent the detected signals. It can be observed that when several gas bursts occur on a relatively short time scale, it is hard to distinguish them in the detected signals. To achieve a better resolution of the detection system, the time broadening needs to be decreased.

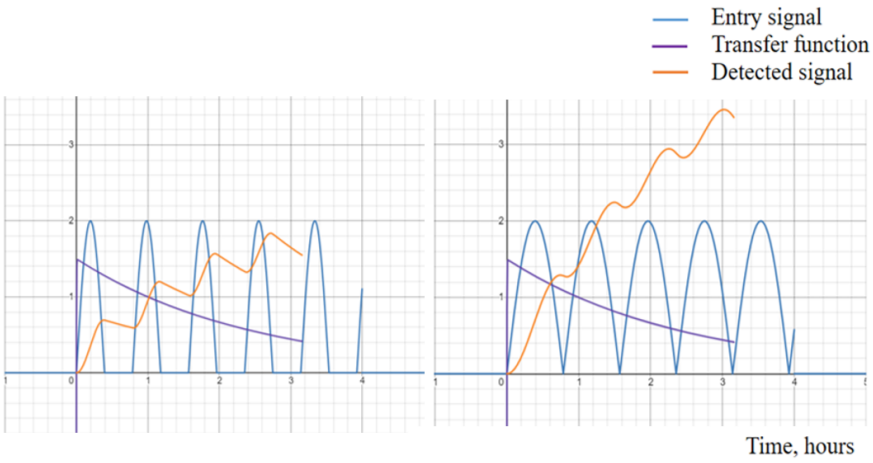

Figure 4.13: The detected signals with different time resolution and the entry signals with different frequencies.

Thus the transfer function becomes a critical factor in the gas detection, which depends on the reactor configuration and the detection system design. The transit time of the detection system should be shortened by optimizing the parameters of the transfer function. The variables in the equation which can be changed during the system design are interested, e.g. Q, V_c.

For example, with analysis of the results in Sec. 3.4.3, the volume of the cover gas is the main factor which can influence the time broadening. As shown in Fig. 4.14, the gas activity in MX 32 is calculated with different cover gas volumes in RG 14 with Q equal to 5.0 l/s. 40 m^3, 30 m^3 and 20 m^3 for V_c are chosen respectively. It can be observed that with smaller volume of the cover gas, there will be smaller time broadening and a larger maximum gas activity can be detected.

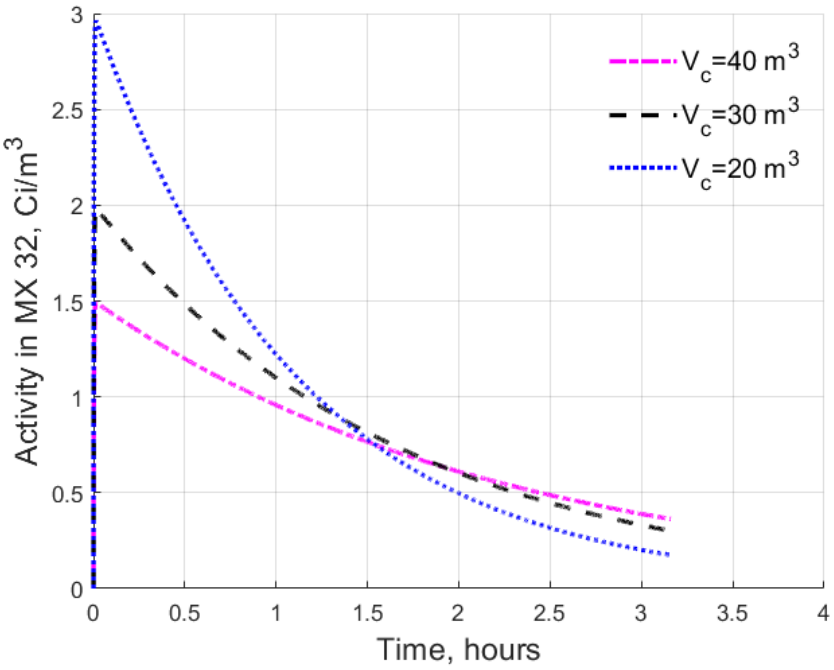

Figure 4.14: Activity in MX 32 modeled with different cover gas volumes in RG 14.

Similarly, the system can be optimized to determine the gas flow of the sipping system in the cover gas and the one to the detector. Through the analysis of the transfer function, a larger flow rate Q in the cover gas will introduce a smaller time broadening.

4.4.2 The deconvolution of the detected gas signal

A potential application of the transfer function is the deconvolution of the detected signal. Through the observation of the detected gas signals, in addition to instantaneous bursts, there are some gas signals that evolve over time, and the release mechanism is still unclear. With the determination of the transfer function of the DRG detection system, the deconvolution process can be applied to different gas signals in order to obtain the entry signal at the fuel pin and interpret the DRG signal in real time.

In mathematics, deconvolution is the operation inverse to convolution used in signal processing. For example, it may be possible to recover the original signal after a filter (convolution) by using a deconvolution method with a certain degree of accuracy [98]. There are several deconvolution methods. For example, six deconvolution techniques are compared in [89]. A method of blind deconvolution in spectroscopy is proposed in [99]. A method with an excellent signal-to-noise

ratio is developed in [47]. Some deconvolution methods are also discussed in [87], including analytical deconvolution and forward-fitting method. The deconvolution method used in this thesis is shown below.

To perform the deconvolution process, the relation between $R(t)$ and $N_d(t)$ should be derived. The equation Eq. 3.7 is reused:

$$R(t) = \frac{V_c}{\alpha Q}\frac{\mathrm{d}^2 N_d}{\mathrm{d}t^2}(t) + (\frac{V_c}{V_d} + \frac{1}{\alpha})\frac{\mathrm{d}N_d}{\mathrm{d}t}(t) + \frac{Q}{V_d}N_d(t) \tag{4.9}$$

As introduced in Sec. 3.3.2, $R(t)$ is the fission gas release from the fuel pin; $N_d(t)$ is the number of atoms in the detector; other values can be calculated with the detection system parameters. Then it can be obtained:

$$R(t) = 200000\frac{\mathrm{d}^2 N_d}{\mathrm{d}t^2}(t) + 444500\frac{\mathrm{d}N_d}{\mathrm{d}t}(t) + 56N_d(t) \tag{4.10}$$

In the experiment data, the activities per volume are detected. Thus $N_d(t)$ can be calculated, as well as its first and second derivative for each time interval. With Eq. 4.10, $R(t)$ can be computed quantitatively.

Although the signal data that can be retrieved is limited, several examples of the deconvolution process in the PHENIX reactor have been performed, as shown below.

Example 1 is RG 11 with a small gas release, which is different from the release condition of RG 14. The detected signal of fission gas release in RG 11 as well as the result of the deconvoluted entry signal is shown in Fig. 4.15. The gas signal was relatively stable at the beginning and then a sudden burst happened. It can be observed that it is a significant gas release during a certain time and then stopping quite abruptly, which is not an instantaneous release. It is an evidence that a new release mechanism needs to be studied.

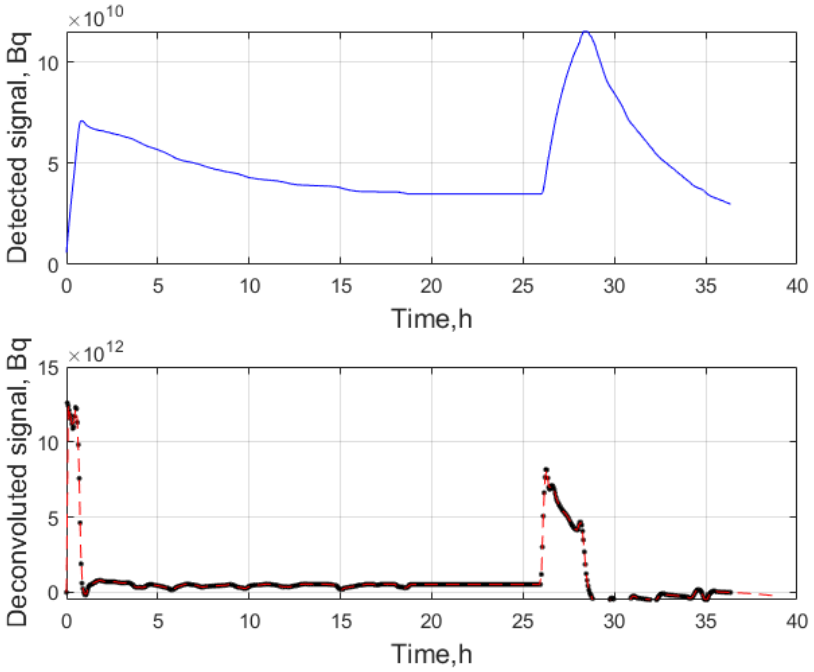

Figure 4.15: The deconvolution of the detected signal in RG 11.

Example 2 is RG 08, which has more than one failed pin. The deconvoluted gas signal in RG 08 is shown in 4.16. The interpretation of the release mechanism in this case is further complicated by the fact that the detected signal is from two failures. But it can be concluded from the deconvolved signal that the release is not continuous, but multiple bursts.

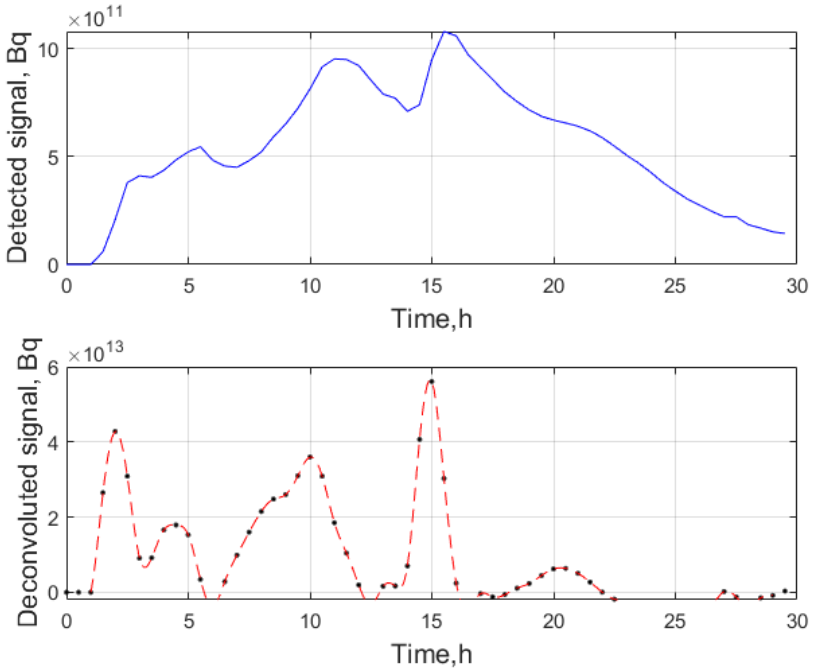

Figure 4.16: The deconvolution of the detected signal in RG 08.

Example 3 is the fluctuating small gas release in RG 14. After a significant release, the release mechanism of these small release can be investigated. Although accurate release data could not be retrieved due to the low quality of the experimental data, a burst at around 76 hours after the release can be observed. Compared to the neutron signal, as shown in Fig. 4.17, the gas burst is consistent with the first neutron signal detection, indicating possible crack growth. Thus the deconvolution result can make a link to neutron signals in DND detection system, which can help determine rupture propagation. The DND system will be studied in the next two chapters.

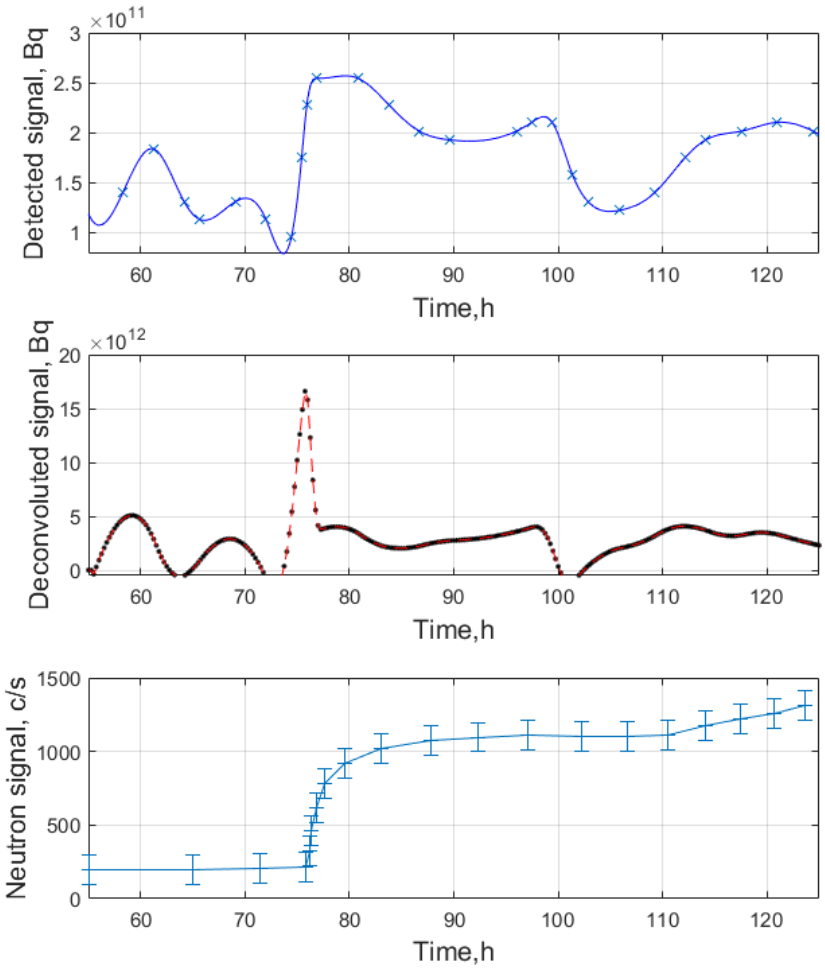

Figure 4.17: The deconvolution of the detected signal in RG 14, compared with the neutron signal.

4.5 Conclusion

In this chapter, a generic methodology has been developed to describe the whole gas detection system in SFR, including fission gas quantity accumulated in the fuel gas plenum, the gas leakage flux through the crack, the transportation from the fuel pin to the detector, the detector sensibility to different isotopes.

A safety assessment of small leakage for PHENIX using this methodology was performed in this study, reflecting its performance of early detection in the DRG system. With this methodology application, the detected current signal is derived as the function of crack size among the background signals and analyzed the importance of each isotope during the gas detection. The minimum crack detectable is estimated, and the possible optimizations for future design are proposed, ac-

cording to the modeling results. This methodology is applicable to arbitrary SFRs with different fuel and core designs.

For the future design of detection systems, the methodology can be used as a toolbox for comprehensive optimization by changing the variables in the general equation. The application of the transfer function can contribute to an improved understanding of fission gas transfer in SFR. The deconvolution of the detected signal could be used for the interpretation of DRG data in real-time.

In conclusion, thanks to the proposed methodology, I have achieved a comprehensive view of cladding failure detection for gas detection. In the following two chapters, I will study neutron detection with the same research strategy.

Chapter 5

Direct recoil release and neutron signal transfer process

After the study of gas detection system in chapter 3 and chapter 4, this chapter will be devoted to the general description of the neutron detection system, the DND system, which is dedicated to monitor the neutron signal during the rupture stage of cladding failure.

In this chapter, similar to the DRG study, I will apply the general equation Eq. 2.1 defined in chapter 2 to DND system in order to describe the whole detection process.

I will develop an overall scheme of the release of delayed neutron precursors (DNP) and its transfer process, according to which I will perform a modeling. The release of DNP involves several physico-chemical mechanisms, the comprehensive study of which is beyond the scope of this thesis. In this chapter the modeling will be implemented with only direct recoil release, which is an athermal mechanism with no time dependence. Other DNP release mechanisms will be studied in the next chapter.

5.1 Introduction

During the rupture stage of the cladding failure, the DND system (neutron detection system) monitors the delayed neutron signal continuously to avoid the fissile material release in the coolant, as introduced in Sec. 2.1.2. The delayed neutrons are emitted by some of the released fission products through the cladding rupture, which are called delayed neutron precursors (DNP). Briefly, the whole process is conducted as: first, DNPs are released from the breached area of fuel pin to the sodium coolant; then, sodium samples are continuously extracted from the outlet of fuel assemblies thanks to sample lines and transited out of the primary vessel; finally, DNPs are transited to neutron detection block and the emitted delayed neutrons are detected by the neutron detectors.

Similar to the method for deriving the comprehensive description of the gas detection system, a DND detection scenario is developed for the whole process of DNP release and delayed neutron detection, as shown in Fig. 5.1. The scenario can be mainly divided into 4 stages:

1. DNP release from the breached fuel pin to the sodium coolant;
2. Transfer process by sodium samples in sample lines;
3. Detector efficiency for delayed neutron;
4. Sources of background signal.

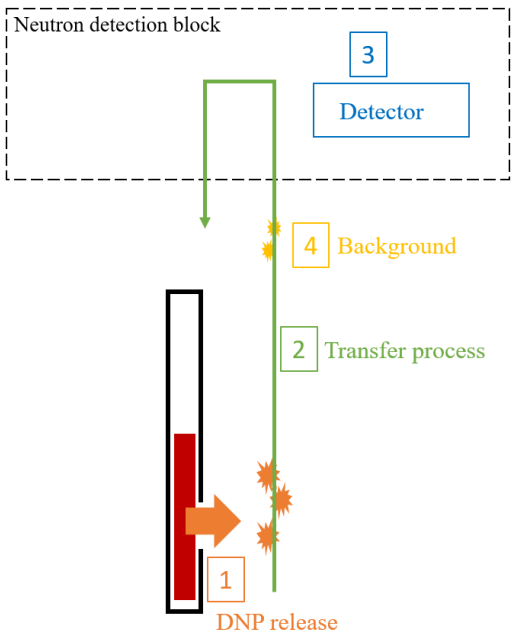

Figure 5.1: The scenario of DNP release and delayed neutron detection.

As introduced in Sec. 1.5.4, the athermal release mechanism of DNP is direct recoil, which is an apparent release and exists all the time during the cladding failure [83] [150]. Another release mechanism is thermal diffusion release, which is different from the recoil release and depends on the temperature and the fuel conditions.

Therefore, in this chapter, guided by the DND detection scenario and combined with the general equation Eq. 2.1, a modeling of the whole process of DND detection will be performed under the direct recoil only hypothesis. The diffusion release and the related fuel behaviours will be studied and discussed in the next chapter.

5.2 Isotopes of interest in DND system: DNP

Before the modeling, the characteristics of DNP should be clarified. DNP are searched by detection system because a neutron emission from a sodium sample is a specific signature of the presence of these fission products, e.g. [42], [137], [40], [74]. DNP include isotopes of ^{137}I, ^{88}Br, ^{87}Br, etc. DNP are mainly short-lived volatile fission products. Both iodine and bromine occur in sodium as halides. NaBr and NaI are both have low volatility. Also because their concentrations in nuclear grade sodium are very low, precipitation is unlikely to occur. After the rupture, DNP will be transported with the sodium flow to detection system.

Table 5.1: Delayed neutron fraction β and decay constant λ for DNP from JEFF 3.1.

Group	Precursor	β_i (pcm)	λ_i (s^{-1})
1	^{87}Br	5.8	0.0125
2	^{137}I	59.8	0.0283
3	^{88}Br	21.8	0.0425
4	^{138}I,^{93}Rb,^{89}Br	52.1	0.133
5	^{94}Rb,^{139}I,^{85}As,^{98m}Y	115.3	0.2925
6	^{93}Kr,^{144}Cs,^{140}I	47.2	0.6665
7	^{91}Br,^{95}Rb	42.0	1.6348
8	^{96}Rb,^{97}Rb	20.4	3.5546

It is a customary way to group the DNP in eight groups with different delayed neutron fraction β and decay constant λ in fast reactor [80] [136], listed in Tab. 5.1. The time evolution of delayed neutron fraction for each DNP group is shown in Fig. 5.2. The relevant time scale for comparisons is the transit time between the assembly and the detection device, which is 30 s in PHENIX reactor.

It can be observed that ^{137}I is the predominant DNP can be detected after the transit time, following with the isotopes ^{88}Br and ^{87}Br. Iodine and Bromine have the similar chemical behaviours. Thus ^{137}I, ^{88}Br and ^{87}Br are taken as the representative DNPs for the study.

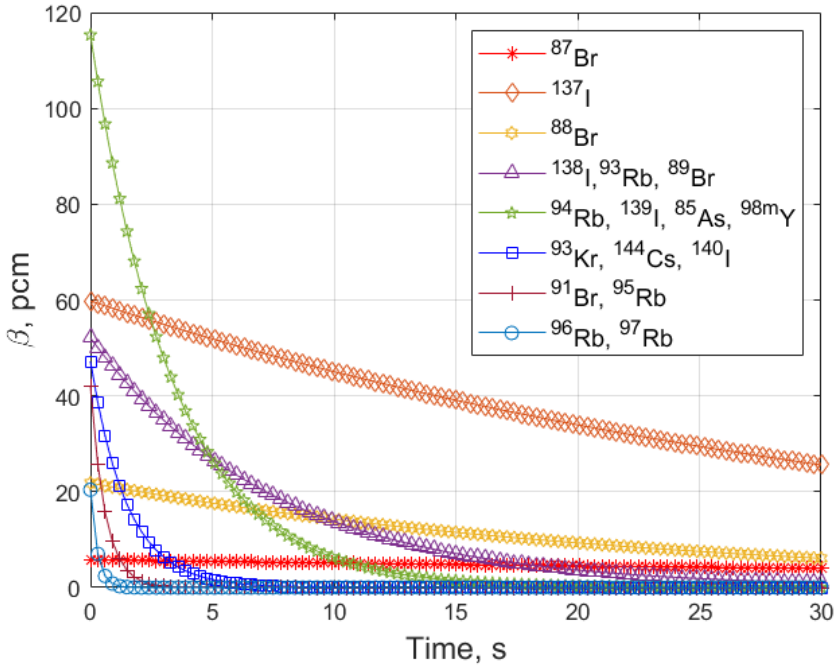

Figure 5.2: The time evolution of delayed neutron fraction for each DNP group.

5.3 DND detection modeling of direct recoil release

A modeling of the whole process of DND detection for DNP direct recoil release is performed in this section, through the simulation and analysis for each stage in the scenario.

5.3.1 Direct recoil release of DNP

Recoil mechanism happens when the kinetic energy given to the fission product by the fission event is sufficient for it to reach the sodium [84]. Practically, for a cladding rupture in a reactor, the fuel surface is licked by sodium (inside the cladding), and the fission products from the recoil can be carried away by the sodium flow.

Firstly, the balance equation is listed for the fission product concentration in the fuel pin and use recoil ratio to represent the term of DNPs going outside the

fuel pin. The scheme of recoil ratio is shown in Fig. 5.3.

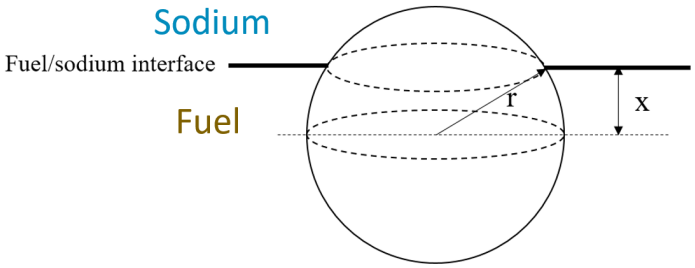

Figure 5.3: The scheme of recoil ratio.

$$R_{rec} = \begin{cases} \frac{2\pi r_i(r_i - x)}{2\pi r_i^2} = \frac{1}{2}(1 - \frac{x}{r_i}) & \text{if } 0 \leqslant x \leqslant r_i \\ 0 & \text{if } x > r_i \end{cases} \tag{5.1}$$

In Eq. 5.1, R_{rec} represents the ratio of DNP recoils out of the surface; F is fission rate per unit volume; r_i is the range of $\mathrm{DNP_i}$, which is calculated by SRIM[1], e.g. the result for the ^{137}I recoil range is 6.25 μm, computed with an initial kinetic energy of 65 MeV in uranium oxide with a density of 10.95 g/cm^3.

$$\frac{\mathrm{d}C_i}{\mathrm{d}t} = \begin{cases} \frac{1}{2}y_i F(1 + \frac{x}{r_i}) - \lambda_i C_i & \text{if } 0 \leqslant x \leqslant r_i \\ y_i F - \lambda_i C_i & \text{if } x > r_i \end{cases} \tag{5.2}$$

The concentration in the fuel pin is calculated in Eq. 5.2. C_i is the concentration of $\mathrm{DNP_i}$ at distance x near the surface in a unit volume of fuel; y_i is the fission yield of $\mathrm{DNP_i}$; λ_i is the decay constant of $\mathrm{DNP_i}$. The solution of Eq. 5.2 is computed and it is obtained that:

$$C_{i\infty} = \frac{y_i F}{\lambda_i}(1 - e^{-\lambda_i t}) \tag{5.3}$$

$$\frac{C_i(x,t)}{C_{i\infty}} = \frac{1}{2}(1 + \frac{x}{r_i}) \qquad \text{if } 0 \leqslant x \leqslant r_i \tag{5.4}$$

The scheme of concentration of DNP in the fuel is shown in Fig. 5.4. In Eq. 5.3, $C_{i\infty}$ represents C_i in the fuel where x is larger than r_i. $C_{i\infty}$ is constant for short-lived fission products, thus $C_{i\infty}$ of DNP will be constant. For this calculation, the hypothesis is made that fission density is homogeneous near the fuel surface. Then the recoil current out of the fuel pin through the failure surface can be deduced.

$$I_i = S_{\mathrm{rec}} \int_0^{r_i} y_i F R_{rec} \mathrm{d}x = S_{\mathrm{rec}} y_i F \frac{r_i}{4} \tag{5.5}$$

[1] http://www.srim.org/

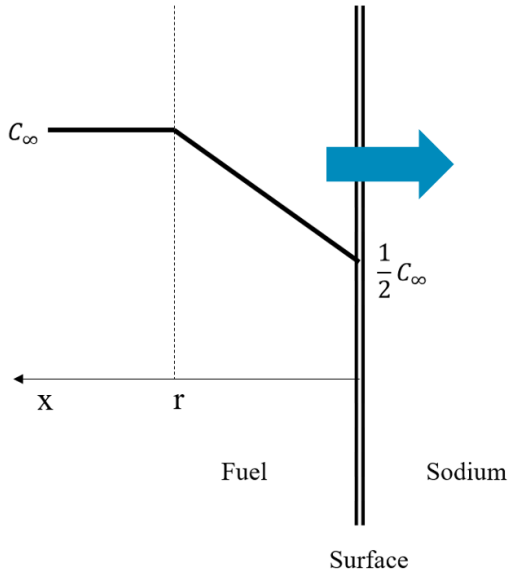

Figure 5.4: The scheme of DNP isotopes concentration in the fuel.

In Eq. 5.5, I_i is the recoil current of $\mathrm{DNP_i}$ cross the geometric surface S_{rec}, number of atoms per second. If S_{rec} remains the same size, I_i will be constant as the time evolution.

Thus the DNP direct recoil release I_i has been derived, which represents R_i in Eq. 2.1.

5.3.2 The transfer process

To identify the parameters during the transfer process, a scheme of DNP release from the fuel pin to neutron detection system has been developed, as shown in Fig. 5.5.

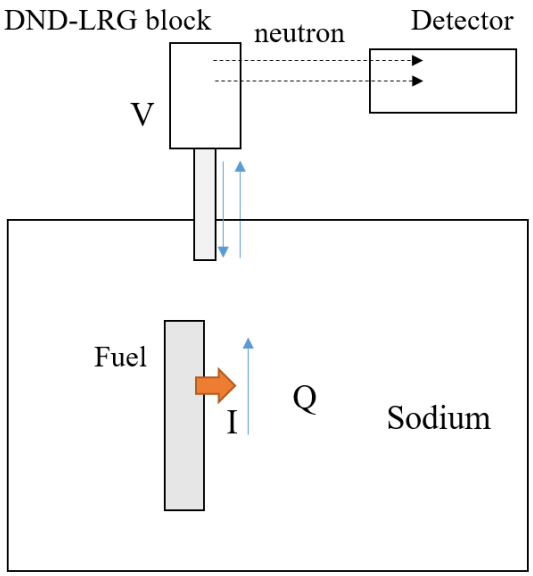

Figure 5.5: The scheme of DNP release from the fuel pin to neutron detection system.

The diffusion of the DNP within the sodium and the gravity are negligible with respect to the convection force under the sodium flow rate, thus it is considered that all the DNP released are taken out by sodium flow. The sipping system samples the sodium to the DND-LRG block. Then the delayed neutron emitted by DNP in DND-LRG block can be detected by the neutron detector. The concentration of DNP collected in DND-LRG block has been calculated:

$$C_{d_i}(t) = \varepsilon \int_{T_r}^{T_d+T_r} \frac{I_i}{Q} e^{-\lambda_i t} dt \tag{5.6}$$

In Eq. 5.6, C_{d_i} is the concentration of $\mathrm{DNP_i}$ collected in DND-LRG block, transported by the sodium coolant; ε is efficiency of sipping system; Q is flow rate of sodium through the assembly; T_r is the transit time from the fuel pin to the detector, which is 30 s in PHENIX reactor; T_d is average transit duration in DND-LRG block.

Thus in this section, DNP transported to the detector sector has been deduced, which represents $R_i * F_i$ in Eq. 2.1.

5.3.3 The detector efficiency

Then the count rate of neutron in the detector can be obtained:

$$Count_{\mathrm{DN}}(t) = \sum_{i=DNP} \lambda_i C_{d_i}(t) V f_{n_i} E_i \tag{5.7}$$

In Eq. 5.7, $Count_{\mathrm{DN}}$ is detector count rate of the delayed neutron emitted by DNPs; V is the volume of sodium contained in the DND-LRG block; f_{n_i} is the branching ratio of decay path for neutron of DNP; E_i is the efficiency of the detector.

It can be observed that, to calculate the detected signal $Count_{\mathrm{DN}}$, the term E_i needs to be derived.

Because plenty of research has been made in regard to the neutron detector efficiency, and because a comprehensive optimization study of the detector is beyond the scope of this thesis, the detector modeling will not be implemented in this chapter and the value E_i will be derived from the literature study. A bibliographical synthesis will be stated here:

Several solutions for optimizing the detector design, in order to detect potentially harmful failures in hard gamma-rays fluxes and low-neutron activity levels, have been investigated in e.g. [26], [27], [114], [115], [42].

The detector part has several requirements: it should be isolated from the hot sodium since partial discharges are an issue for gaseous detectors [48]; a gamma-ray shield should be set to limit the production of photon pile-up pulses and photoneutron events; a moderator should be used to thermalize neutron since the cross section of usual neutron absorbers (^{3}He, ^{235}U) is higher by several orders of magnitude for thermalized neutrons (the delayed neutrons are slightly less energetic than fission neutrons, with a mean energy of about few hundreds of keV) [26]. Thus the conception options have to be identified, including detector technology, gamma-ray shielding, and moderator. The privileged ways of DND detector design have been summarised:

- Detector technology: ^{3}He proportional counters are selected as the best available technology for neutron detection. They can be replaced by ^{10}B proportional counters with 3 times lower sensitivity and by fission chambers with 30 times lower sensitivity [26].

- Gamma-ray shielding: gamma-ray shielding is usually based on lead or tungsten, both having high atomic number and high density. Tungsten provides a better gamma-ray stopping power than lead, but the slight gamma shielding gain achieved with tungsten will then penalize neutron sensitivity [26].

- Moderator: graphite can be the best alternative due to its high moderation power and its elevated photoneutron reaction energy threshold. It offers a complete suppression of photoneutron noise while maintaining suitable neutron sensitivity compared to polyethylene [115].

5.3.4 Background signal

The background signal in DND detection is mainly from a slight fissile material deposit on the cladding at the weld plug places during the manufacture of fuel rods, which is unavoidable. This pollution is responsible for a residual fission product production, providing a constant neutron signal: the order of magnitude of background signal is 150-200 c/s in PHENIX reactor; the order of 1 count per second as registered in SUPERPHENIX, with a standard ^{3}He counter plus lead and polyethylene configuration.

Since the background signal is a constant value associated with the reactor and cannot be eliminated by detection system design, it will not be added to the modeling results.

5.3.5 Results

With the combination of the above modeling and analysis, for a given rupture size, the DNP recoil release and the detected neutron signal can be calculated. Thus the count rate for an assumed rupture size ($S_{\text{rec}} = 0.5$ cm^2) has been computed, for the DNP isotopes ^{137}I, ^{88}Br and ^{87}Br.

The calculation is performed with the following parameters: $Q = 3.6.10^{-2}$ m^3/s; $T_r = 30$ s; $T_d = 19$ s; $V = 3$ l; $\varepsilon = 0.5$; $E_i = 7.4.10^{-3}$. As shown in Fig. 5.6, the upper plot is the DNP recoil current I_i, and the lower plot is the count rate $Count_{\text{DN}}$ of delayed neutron from recoil release. X-axis represents the time after breach.

It can be observed that the transfer function is only time shift of the release signal, which is straight forward compared to the transfer function in gas detection. Indeed, the flow transportation towards the detector is mainly done by pipes, without passing by the cover gas as for the DRG system. It should be noted that the circulation of the sodium between the head of the assemblies and the sipping pipe is more complex that what implied by the model of Fig. 5.5 (e.g. interference with other assembly flows, global sodium circulation in the primary vessel). However, while a detailed modeling of this could be beneficial from the quantitative point of view, it would be very specific to a reactor design, and should not alter qualitatively the present result. Therefore, the transfer function will not be the research emphasis in neutron detection system.

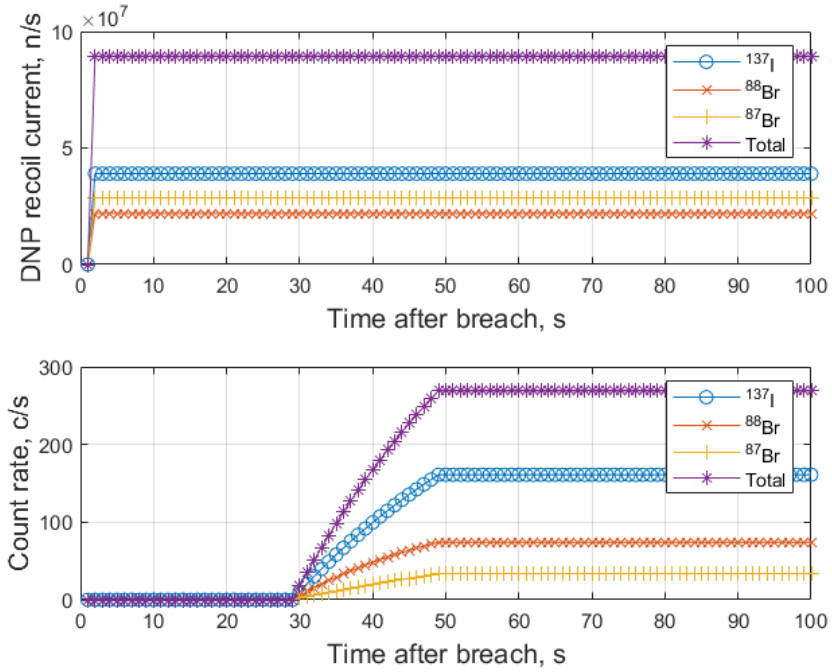

Figure 5.6: The DNP recoil current and the count rate of neutron signal after the transfer process of recoil release.

The experimental data from PHENIX cases RG 11 and RG 14 has been chosen, as shown in Fig. 5.7, from which the neutron signal evolution at the beginning can be observed. With the comparison, it is observed that part of the experimental curve is consistent with the modeling result: the signal from 0 to 8 h of RG 11 and from 75 to 100 h of RG 14; part of which is not: after 10 h of RG 11 and after 110 h of RG 14. It can be concluded that the signal of recoil release mechanism is consistent with the detected signal at the beginning. But for the neutron signal with the time evolution, additional release mechanisms need to be investigated.

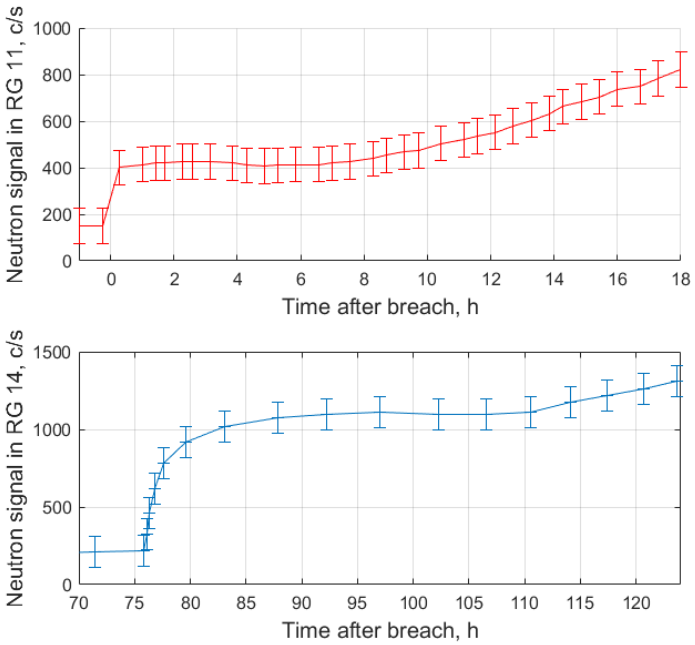

Figure 5.7: Experiment data of neutron signal at the beginning.

5.4 Conclusion

In this chapter, an overall scheme of the whole process of neutron detection has been developed for the direct recoil release of DNP, and modeling of the neutron signal transfer has been performed.

In the modeling, the neutron signal for a given rupture size has been predicted and compared with experimental data. As a result, the transfer function of DND is found to be a time shift. The signal of recoil release is consistent with the detected signal at the beginning.

However, the release mechanism of DNP during the time evolution of the cladding rupture is still not clear. Therefore, in order to have a better determination of the geometrical area of damage, the diffusion release and related fuel behaviors will be studied and discussed in the next chapter.

In conclusion, a global view of the neutron signal transfer process has been derived. The recoil release is sufficient to explain the neutron signal at the beginning, but further studies are needed for the time-evolving signal.

Chapter 6

Enhanced diffusion release during corrosion layer formation

During DND detection, the monitoring of the neutron signal evolution, which reflects the breached size of cladding, is important to avoid the fissile material release into the coolant. After the modeling of DND detection for the DNP direct recoil release in chapter 5, I will focus on the potential enhanced release mechanism during the time evolution of neutron signal.

The release mechanisms of DNP is related to the fuel pin evolution. In this chapter, in order to interpret the neutron signal time evolution and to have a better prediction to the breached fuel area, I will perform a modeling to study the enhanced thermal diffusion release due to corrosion layer formation. As an experimental benchmark, I will also study an experiment case RG 11 in PHENIX reactor.

6.1 Introduction

This chapter will focus on the neutron signal with the time evolution. The detected neutron signal comes from the released DNP through the cladding failure, hence the evolution of the neutron signal can be used to monitor the breached fuel area exposed to the coolant. As far as the breach and fission rate remain constants, recoil release is inherently a time-independent mechanism. Thus a possible, obvious explanation of a neutron signal increase is that the rupture becomes more severe. However, the change of fuel condition can also cause the time evolution of neutron signal. In other words, even if the breached surface remains constant, the neutron signal may still evolve due to the physical and chemical condition change at the fuel pin [143].

The calibration for the detected rupture size in detection system is based on the recoil only assumption, which is conservative and sufficient from the engineering scenario. However, through the comparison between the equivalent rupture surface according to the detected neutron signal and the actual rupture size discovered during the fuel pin wash, direct recoil cannot explain all the signal evolution. Although much experience with DND failures has been gathered all over the world, the determination of the geometric area of damage on the basis of the DND signals is still very inaccurate. In general, the accuracy is within plus/minus one order of magnitude [72]. The cause for this relatively high inaccuracy is related to the fuel condition, which are not well known at the time of occurrence of the cladding failure.

Because thermal diffusion release depends on the temperature and the fuel conditions, an important phenomenon during the fuel evolution which may change the diffusion behaviour is the corrosion layer formation. When there is a rupture on the cladding, sodium will penetrate inside the the fuel pin through the rupture followed by exchange of sodium between inside and outside the fuel pin. $(\mathrm{U,Pu})\mathrm{O}_2$ reacts with sodium to form sodium urano-plutonate, which is the corrosion layer. The reaction of corrosion layer formation takes place at the periphery of the fuel pin and is stopped when the oxygen potential is low enough to reach equilibrium [59]. Then the corrosion layer will be stable. Because the thermal conductivity of corrosion layer is lower than the oxide fuel [130], it will change the fuel temperature condition during the process of formation.

The goal of this chapter is to study the relation between DNP release mechanism and the neutron signal evolution, by the means of a physical modeling and with a comparison with PHENIX experimental data. In order to explain neutron signal going beyond recoil mechanism and to have a better understanding of DND signal, a specific experiment case RG 11 in PHENIX reactor is studied.

6.2 Experiment case RG 11

In this section, the general information of experiment case RG 11 is outlined, including the rupture size of cladding failure and the detected neutron signal.

There have been 15 open-pin failures in PHENIX reactor in total. RG 11 is chosen as the study case for several reasons: RG 11 had a good monitoring of the neutron signal for 36 hours after the rupture happened; RG 11 is at the beginning of life with burn up of 0.35 % and with small rupture size, which makes the analysis easier.

6.2.1 RG 11 rupture size

The rupture is approximately 20 mm long and located on the fissile column 310 mm from the top of the fuel pin. The rupture size discovered in the fuel pin wash is around 0.2 cm^2 while the maximum detected surface S_{DND} according to the neutron signal in RG 11 is 2.5 cm^2. The surface detected S_{DND} is much larger (around 10 times) than the surfaces discovered S_{dis}.

The calibration of the detected signal in DND system and the breached surface is based on the recoil only assumption. Thus the inconsistency of S_{DND} and S_{dis} indicates that the DNP release from the recoil mechanism is not sufficient to explain the detected neutron signal.

6.2.2 RG 11 neutron signal

Through the observation of experiment data, neutron signals have different behaviours including slow or rapid increase. In RG 11, there are mainly three different steps of neutron emissions, as shown in Fig. 6.1: a first stable emission lasted about 10 hours; then the neutron signal increased corresponding to a small emission surface; several hours later, a rapid neutron evolution was observed.

It can be observed that a stable and continuous release at the beginning of the neutron detection and it is known that recoil is an athermal mechanism and with no time dependence, thus it is an apparent release mechanism existing all the time. Thus there is no reason to suppose that the first stable signal is due to something else than direct recoil release.

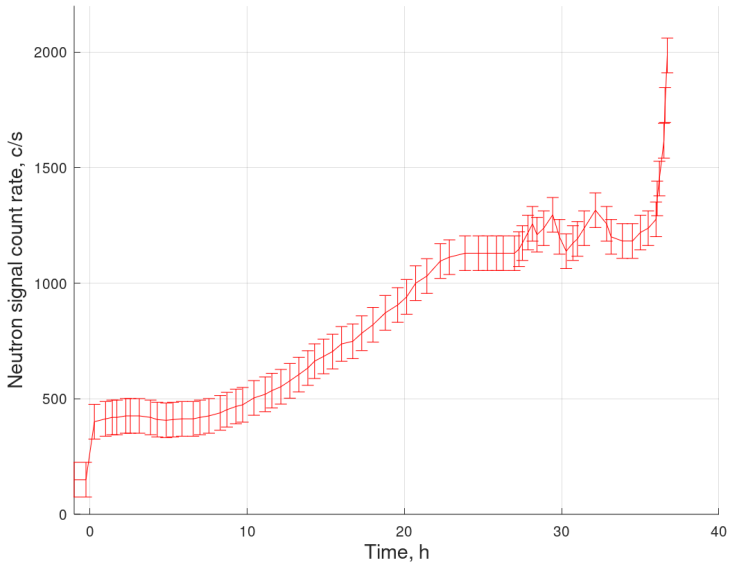

Figure 6.1: Neutron signal in RG 11.

For the following increase of neutron signal, there are two possibilities: the increase of rupture size and the change of the fuel condition. RG 11 is at the beginning of life with burn up of 0.35 %. The gap between the fuel and cladding was not closed and the JOG (Joint Oxyde Gaine) was not formed, so the gas accumulated in the fission gas plenum will be emptied when the rupture is formed and the relative pressure between gap and sodium will be zero. RG 11 has the standard cladding material 15-15 Ti, thus the rupture propagation requires a mechanical loading, which means high stress is needed to have wider rupture. Due to the fission gas release, there is no gas pressure and the cladding is stress free after the rupture happened. So the rupture scenario of RG 11 is supposed to be stable after the rupture happened and the rupture is likely to be the fabrication defect. Thus it is reasonable to consider that the increase of the neutron signal is due to the change of the fuel condition and the release mechanism.

6.3 Enhanced thermal diffusion modeling

As analyzed above, it is found that: the direct recoil is not enough to explain the neutron signal during the time evolution; it is unlikely to have the rupture enlargement without pressure change for the rupture. Thus the DNP release will be evaluated under the hypothesis of enhanced thermal diffusion caused by fuel condition change in this section. ^{137}I is taken as the representative DNP for the modeling, because ^{137}I is the predominant DNP can be detected, and Iodine and Bromine have the similar chemical behaviours.

6.3.1 Model rationale

In contrast with direct recoil, diffusion release mechanism is influenced by temperature. The corrosion layer formation will increase the temperature at the fuel periphery because the thermal conductivity of sodium urano-plutonate layer is lower than the oxide fuel [130]. Thus an equivalent diffusion modeling will be made which includes both direct recoil and diffusion to study how the fuel condition changes the temperature at the fuel pin periphery and then consequently changes the DNP release.

A scheme of the corrosion layer formation is proposed, as shown in Fig. 6.2. The fuel evolution process is supposed to be: the rupture happened and the fission gas is released through the rupture, the pressure inside the cladding decreased; the rupture remained the same; the sodium flowed in through the rupture and the corrosion layer formed; its thickness was increased until it reached the maximum length; the corrosion layer kept stable afterwards.

I propose a scheme for the corrosion layer formation, as shown in Fig. 6.2, which is a simplified model because we cannot know the actual surface covered by the corrosion layer. I propose an assumption of a global surface, including the crack size and surrounding areas. Since the gap still exists between the fuel and cladding at the beginning of life, I do not consider the interaction with cladding in our model.

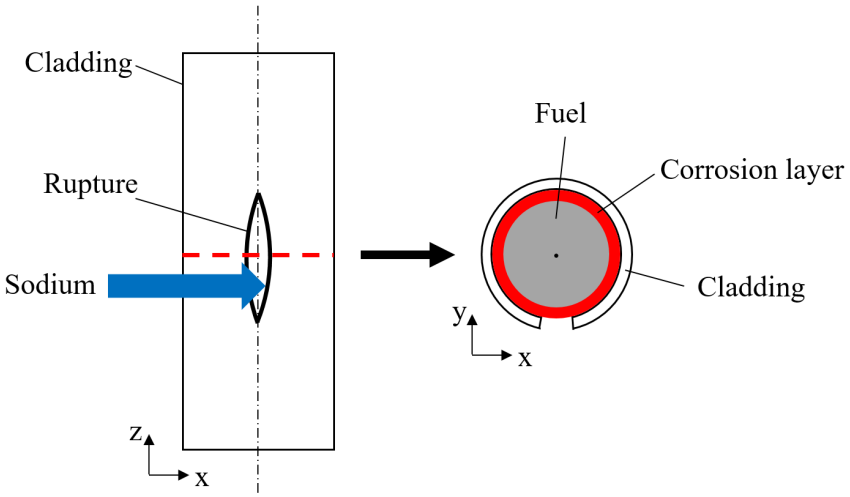

Figure 6.2: Scheme of corrosion layer formation.

6.3.2 The heat transfer computation

To study the temperature change at the fuel pin periphery due to the corrosion layer formation, the computation for the temperature distribution in the fuel pin

is performed by COMSOL Multiphysics® version 5.5[1].

COMSOL Multiphysics is a commercial software suite for numerical simulation based on the finite element method. It includes a certain number of modules (optional) corresponding to as many models of physical phenomena, with possibilities of coupling, within a multi-platform graphic interface (Linux, Windows, Mac), making it possible to define and solve a problem by a series of mouse clicks. More information is introduced in Appendix C.

The average thickness of the corrosion layer in SFR is between 0.15 and 0.20 mm [130]. Thus, we define the geometric conditions with the corrosion layer width growing from 0.01 mm to 0.21 mm. The modeled geometry is 2d axisymmetric. The length of the fuel pin is 2 cm with the assumption that the corrosion layer is formed all around the fuel pin. The dimensions and material data set in COMSOL are listed in Tab. 6.1. The boundary conditions are set to simulate those found in the PHENIX reactor: the fuel is a heat source with a linear power density of 409 W/cm, the convective heat flux condition is set as external forced convection flowing over the fuel pin cylinder (with a diameter of 5.42 mm) with a sodium flow rate of 2 m/s, the external temperature is 823 K and the pressure is 1 atm (sodium density 825.02 kg/m^3, thermal conductivity 62 W/(m $\cdot$ K), heat capacity 1.26 J/(kg $\cdot$ K), and dynamic viscosity 0.2264 Pa $\cdot$ s).

Table 6.1: The dimensions and material data set in COMSOL.

Region	Radius, cm	Density, g/cm^3	Thermal conductivity, W/(m $\cdot$ K)
Central void (Helium)	$0 - 0.045$	5.4e^{-4}	k(T)
Fuel (Equiaxed grain)	$0.045 - 0.18$	10.67	2.4
External fuel (Fabricated)	$0.18 - 0.271$	11	2.6
Corrosion layer	Changed thickness	5.6	1.2

[1]https://www.comsol.fr/

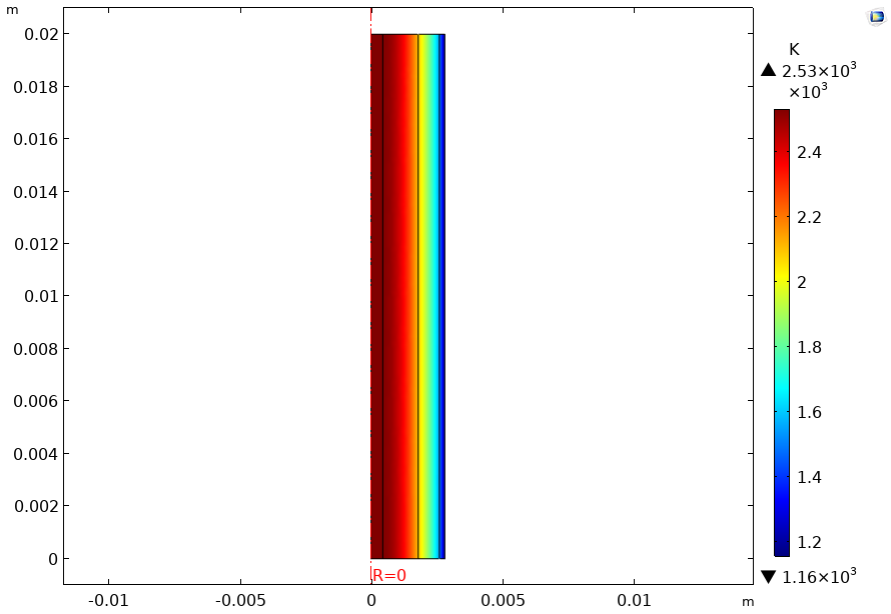

Figure 6.3: The temperature distribution in the fuel pin and the corrosion layer.

The temperature distribution in the fuel pin and the corrosion layer is illustrated in Fig. 6.3. The computation results for the radial temperature distribution of the fuel pin with different thicknesses of the corrosion layer are shown in Fig. 6.4, and the part at the fuel pin periphery is inset. The curves represent the temperature in the fuel and the corrosion layer, and the kinks in the curves indicate the boundary between them. The result shows that the temperature increased around 350 K at the fuel periphery (at the positions of the kinks) as the corrosion layer formed.

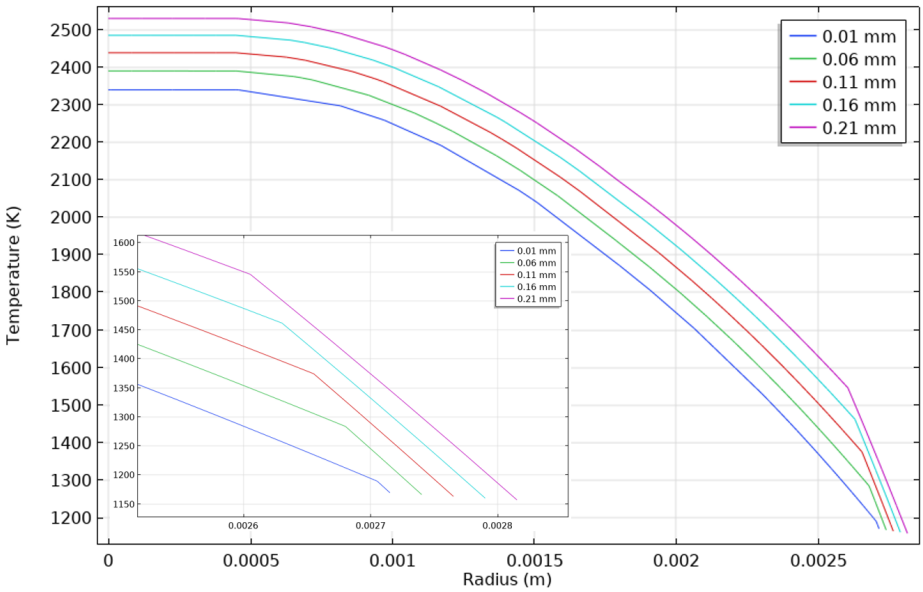

Figure 6.4: Radial temperature distribution with different thicknesses of corrosion layer.

6.3.3 Thermal diffusion calculation

To evaluate the thermal diffusion change, the thermal diffusion release fraction as the function of temperature is calculated. Diffusion coefficient D is used to calculate the diffusion release fraction. Diffusion coefficient in the fuel under irradiation is usually described with three terms representing the temperature contribution, the nonthermal mechanisms (recoil and knockout) and the influence of the vacancies creation under irradiation (mixed term) [14]:

$$D = D_{th} + D_{ath} + D_{mix} \tag{6.1}$$

$$D_{th} = 7.6 \times 10^{-10} \exp[-\frac{35225}{\mathrm{T}}] \tag{6.2}$$

$$D_{ath} = 6 \times 10^{-40} \mathrm{F} \tag{6.3}$$

$$D_{mix} = 1.39 \times 10^{-24} \frac{\sqrt{\mathrm{F}}}{2} \exp[-\frac{13870}{\mathrm{T}}] \tag{6.4}$$

In Eq. 6.1−Eq. 6.4, T is the temperature; F is the fission rate density (fission $\mathrm{m}^{-3}\mathrm{s}^{-1}$); the coefficients are according to the data of xenon due to its diffusion behaviour is similar to iodine [142].

The equation for the fraction of fission gases released gives [63] [111]:

$$f = 3(\frac{D}{\lambda a^2})^{1/2} \tag{6.5}$$

In Eq. 6.5, f is the fraction of fission gases released; D is the diffusion coefficient; λ is the decay constant; a is the radius of the Booth sphere (m). The calculation result for the fraction of ^{137}I released as a function of temperature is shown in Fig. 6.5. It is noticed that when the temperature is lower than 800 K, the release fraction is mainly due to recoil contribution but when temperature is higher than 1000 K, the diffusion release starts to increase rapidly.

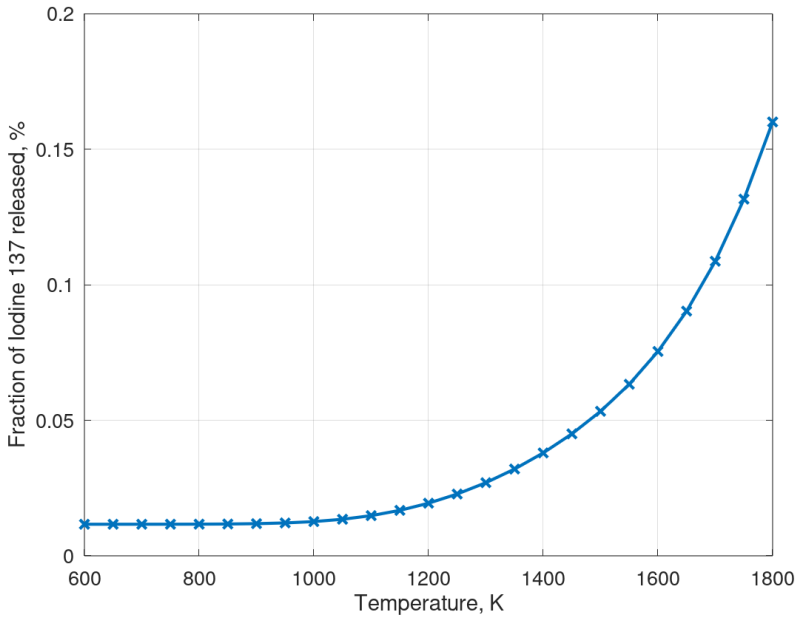

Figure 6.5: The fraction of ^{137}I released as a function of temperature.

6.3.4 Corrosion layer kinetics calculation

Then we also calculated the corrosion layer formation as a function of time. The corrosion layer thickness was found to grow approximately parabolically in the initial time frame, and the rate slows down for a longer time frame [95]. The corresponding law for MOX fuel, in the initial time frame of interaction, can be approximated to [6]:

$$\mathrm{y} = 0.65\mathrm{t}^{0.5} \tag{6.6}$$

In Eq. 6.6, t is the time, and y is the thickness of the corrosion layer in μm. The corrosion layer formation as a function of time is shown in Fig. 6.6. It is noteworthy that the different materials (dense single crystal in [6] and ceramic with cracks in PHENIX) make the reaction areas different, but the rate of corrosion

stays the same, so the rate of volume of the corrosion layer formation should be more extensive in the PHENIX case. Therefore, we made a normalization procedure: the corrosion layer thickness shown in Fig. 6.6 is multiplied by a coefficient to achieve the average thickness of the corrosion layer in SFR. The reaction stops when the oxygen potential is low enough to reach equilibrium, and the corrosion layer will reach a maximum width and remain stable.

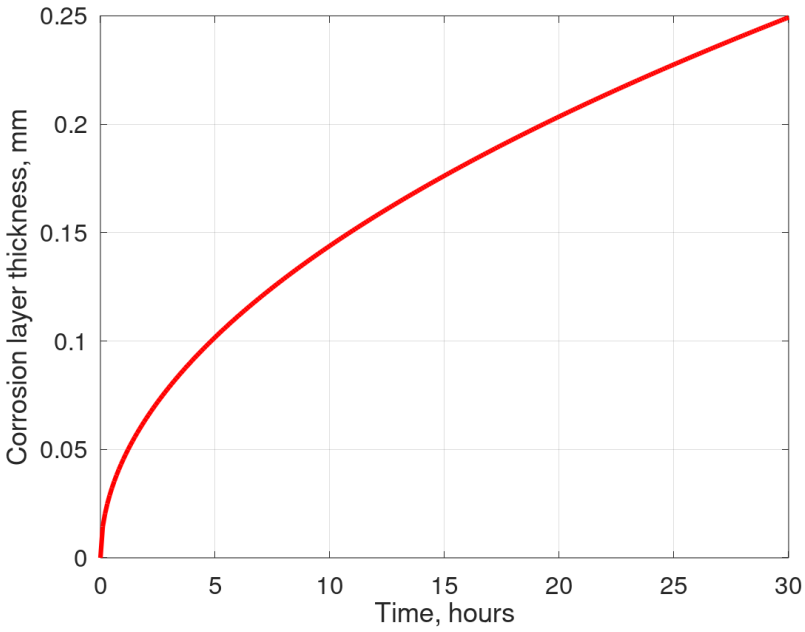

Figure 6.6: Corrosion layer formation as a function of time.

6.3.5 Results

By combining the heat transfer model with the thermal diffusion calculations and corrosion layer formation, we can derive the diffusion release fraction as a function of time. The results of the combined model for the diffusion mechanism are shown in Fig. 6.7: the first diagram is the corrosion thickness as a function of time, the second diagram is the temperature at the pin's periphery (at the boundary of the fuel pin and corrosion layer) as a function of corrosion thickness, the third diagram is the fraction of ^{137}I released as a function of temperature, and the last diagram is the combined result of the time evolution of the ^{137}I release fraction during corrosion layer formation.

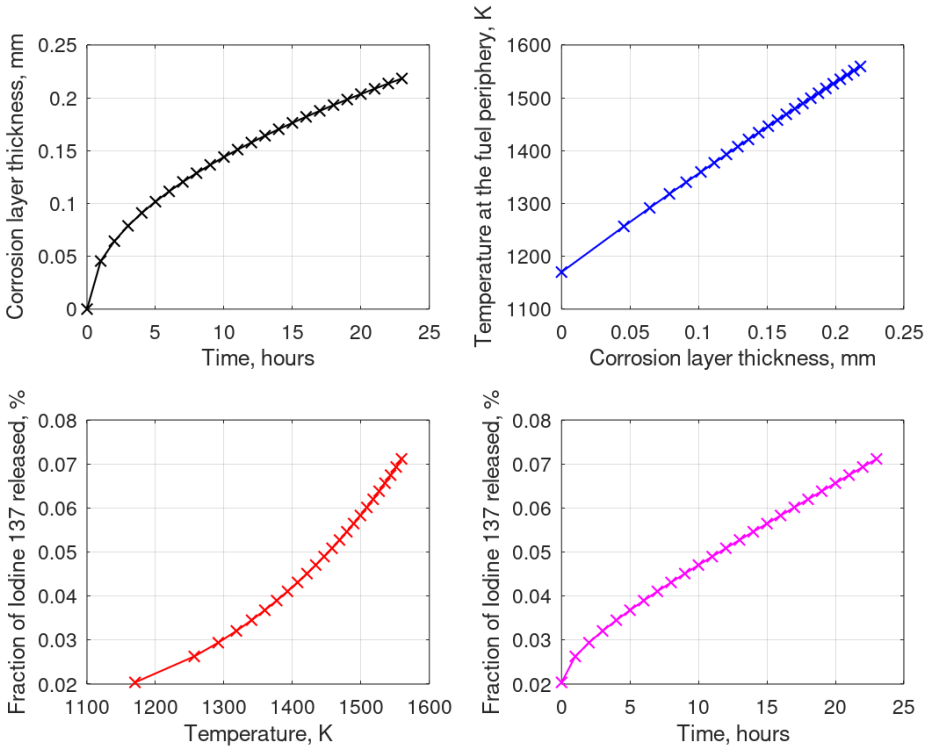

Figure 6.7: The combined modeling for the diffusion release during corrosion layer formation.

Based on the modeled result of enhanced diffusion release during the corrosion layer formation, we can infer the characteristic of the diffusion release increase: the DNP release increases rapidly at the beginning and then grows slowly, then, after the corrosion layer is formed, the release fraction will stay stable. The model's result is consistent with the experiment data: the neutron count rate increases gradually and subsequently approaches an equilibrium level. Although the model result is a release fraction and the experimental data is a count rate, the relation of these two variables is proportional. To make the comparison, we multiplied by a coefficient to make the starting point of the diffusion release the same value as the first stable release, as shown in Fig. 6.8.

We can observe that the model result matches well with the growth characteristic of the neutron signal, and the diffusion mechanism could be one reasonable interpretation for the delayed neutron signal's time evolution. We can conclude that the DNP release is consistent with the temperature-influenced diffusion mechanism due to the corrosion layer formation. The diffusion enhanced release is likely to explain the neutron signal, but further experiments to quantify the influence are required.

However, one shortcoming can be noticed: the curvature is not perfectly

matched, which differs from the experimental data, indicating that the model needs improvement. But more detailed modeling requires specific conditions at the rupture, such as how the sodium contacts the fuel rod, rupture shape, fuel structure, etc., which are difficult to obtain.

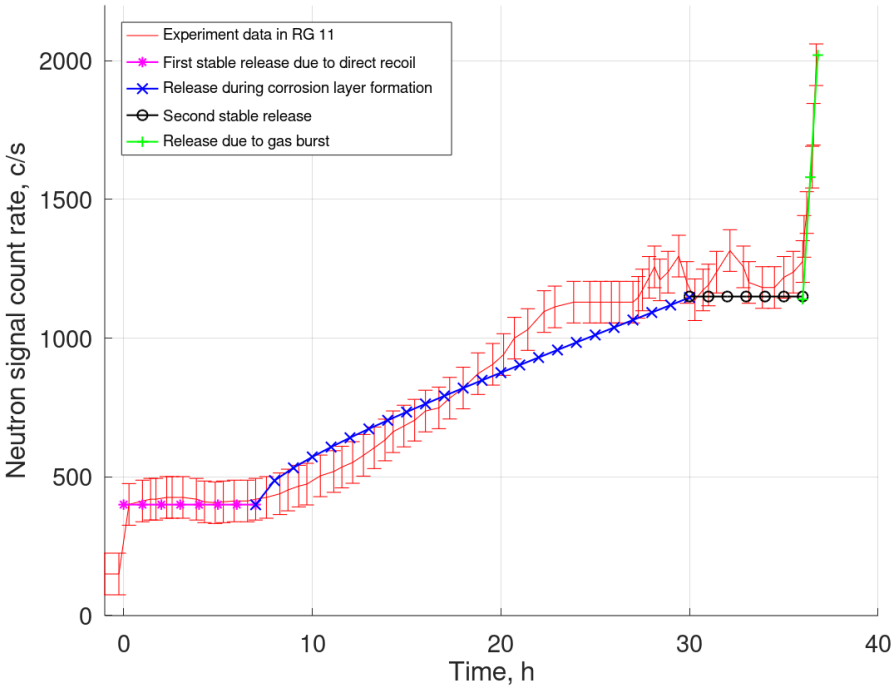

Figure 6.8: Analysis of DND signal in different periods according to the model results, with the comparison of experiment data in RG 11.

Summarising the above model, we propose a possible interpretation of the delayed neutron signal's time evolution. The illustration is compared to the data from a DND signal experiment (RG 11), as shown in Fig. 6.8. At the very beginning of the rupture, DNP are released by direct recoil, which is the first stable release period. Then, with the formation of the corrosion layer, the temperature rises and the thermal diffusion accelerates the DNP release. As the corrosion layer reaches the maximum and stable thickness, the delayed neutron signal gradually reaches the second stable release level.

6.4 Discussions of other release phenomena

In addition to the diffusion release induced by corrosion layer, I will also discuss other signal release phenomena related to the corrosion layer formation.

6.4.1 Gas burst during neutron emission

Apart from direct recoil and thermal diffusion which is modeled above, another phenomenon may accelerate the DNP release is the gas burst. After the neutron signal reached the second stable level in RG 11, a pulsed gas burst was observed, as shown in Fig. 6.9. The gas release was monitored by DRG system. The accumulated fission gas was emptied at the beginning of the rupture formed, thus the pulsed gas is supposed to be released from the gas bubbles in the fuel pin [12].

An evidence is shown in MERARG experiment (a heat treatment test of the fuel to study the release of fission gas during the thermal transients at high temperature): there will be some significant pulsed gas bursts at certain temperature (e.g. around 1000 °C) [107]. When the situation in RG 11 is considered, the corrosion layer formation caused the fuel temperature increase, then the pulsed gas burst from the bubbles happened at one certain temperature. Because DNP (i.e.^{137}I) are volatile isotopes, which are parts of the gas in the bubbles, then the neutron signal will also be increased. The observation in MERARG experiment is consistent with the signal detected in RG 11. Thus it can be proposed that the DNP release from the fuel gas bubbles due to the gas burst is likely to be the reason for the rapid increase of neutron signal afterwards, as shown in Fig. 6.8.

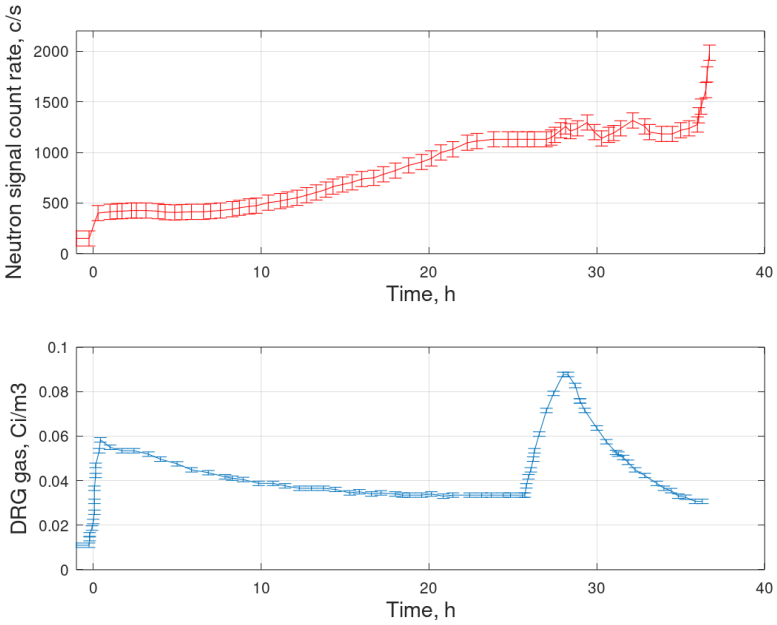

Figure 6.9: Neutron history (above) and DRG gas history (below) of RG 11.

6.4.2 Large gas release after reactor shut down

Another phenomenon has been noticed during the release: there was large gas release after the reactor shut down in several cases in PHENIX reactor. One example of RG 11 is shown in Fig. 6.10: a significant release with a maximum activity about 8 Ci/m^3 is observed after the reactor shut down.

For this phenomenon, an explanation with a scheme illustration is proposed, as shown in Fig. 6.11. During the reactor operation, the corrosion layer was formed at the rupture place. As the width of corrosion layer growing, it blocked the rupture and the fission gas accumulated in the gas plenum cannot be released out. After the reactor shut down, the power is reduced to zero and the size of the fuel pin as well as the corrosion layer shrinks, thus the gap reopens and an important gas release occurs consequently.

A suggestion may be proposed on the fuel management according to this phenomenon: due to the large amount of fission gas are released due to the reopened gap, which means the fission gas plenum is emptied, the defective fuel pin is not recommended to be reloaded to avoid the sodium flow into the cladding.

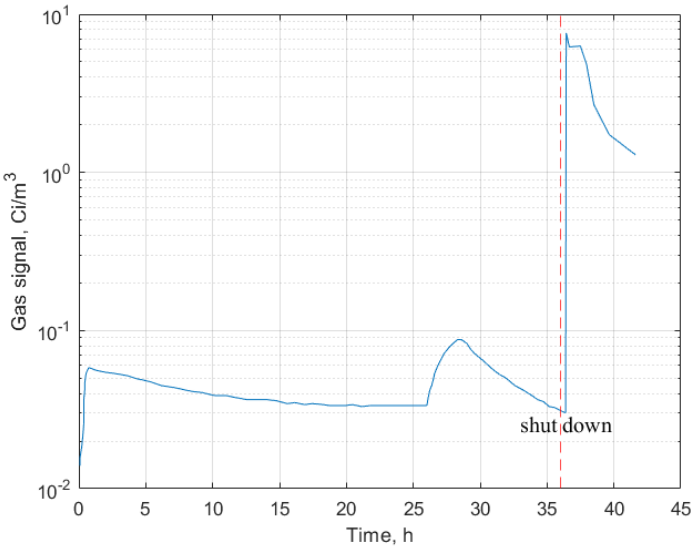

Figure 6.10: The significant gas emission of RG 11 after shut down.

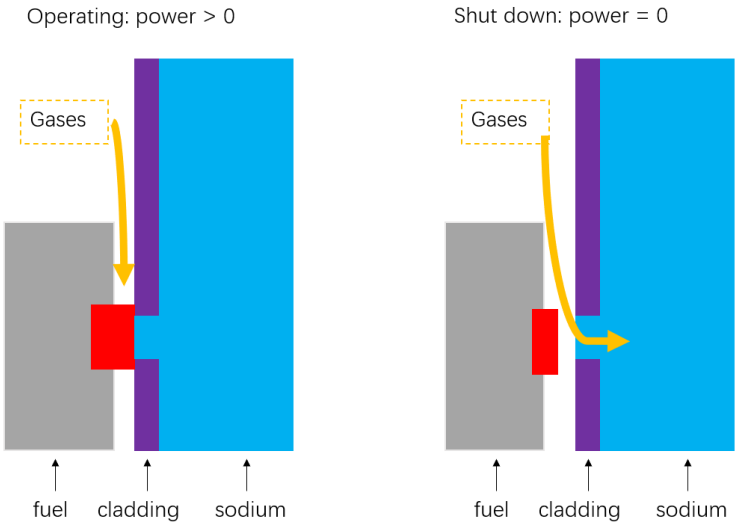

Figure 6.11: The scheme of fission gas release after the power change.

6.5 Conclusion

In this chapter, physical modeling is presented to study the fuel corrosion layer's influence on the delayed neutron signal time evolution in SFR. The DNP diffusion release during the corrosion layer formation is modeled and compared with the experiment data in RG 11 in the PHENIX reactor. It can be concluded that a temperature change influences the diffusion mechanism at the fuel pin periphery due to corrosion layer formation; the enhanced diffusion release is consistent with the neutron signal evolution. Thus diffusion enhanced release is likely to explain neutron signal evolution but will require further experiments to be quantified.

In addition, other fuel phenomena during the DNP release have been discussed: the temperature rise due to the corrosion layer can generate a pulsed gas burst from the gas bubbles in the fuel, which can also lead to an increase in the neutron signal; due to the re-opening of the gap, the gas release after shutdown is significant, so it is not recommended to reload defective fuel rods.

In conclusion, the neutron signal evolution in the DND detection system is not only because of the enlarged rupture size for direct recoil but also related to the enhanced diffusion release due to the corrosion layer formation. Further development of this work could be to devise a corrective model to tell apart a genuine worsening of the cladding failure from corrosion layer formation effects, which would increase the dependability of the reactor. This part of the work has been published in [32].

Chapter 7

Discussions of methodology applications and improvements

In this chapter, I will discuss the application of this methodology to future design, since the design is a problem of multivariate optimization. I will also propose where the model needs to be improved, and what experiments can be done in future work.

7.1 Application to future reactor designs

One of the progress areas of the french R&D SFR program is oriented towards: reactor design options to make inspection and maintenance more accessible and, more generally, to improve the availability, the performance, and the general economic characteristics of the facility [53] [35] [144] [61].

However, an installation inside the reactor vessel severely constraints the detector design to ensure the detector dependability, that is, its reliability and maintainability [41]. The rarity of cladding failures demands the high efficiency of the detector to prevent reactor safety threats such as channel blockages. Still, at the same time, alarms should be raised only when necessary.

Therefore, the functions of the detection system should include two parts: 1) the reliability of the reactor: to prevent the potential channel blockage; 2) the inner component contamination monitoring: to detect and locate the crack with the low-level release, to monitor the crack evolution and propagation state, and to change the failed pin during the regular shut down. According to different demands of the detection system functions, different ways to realize the detector performance should be identified. Enough time countenance of the detectors should be guaranteed for the early detection to prevent the core incidents/accidents, e.g., the detection time in the PHENIX reactor is in hours, which is too late. The strategies of the reactor operation in different scenarios should be clarified. In addition, the diversification of detectors should be noticed. Ideally, a detection system should include several sub-systems, with two strong ones. The sub-systems should be independent, i.e., without common failure modes.

Since the reactor is a multi-parameter system, the optimization of the conceptual design needs to be carried out as a whole under many constraints, including performances, safety and economic points of view, such as the reactor neutronic requirements and thermal-hydraulic limitations. As part of the reactor, the instrumentation system and detector design should be considered together from the beginning of the design to select reactor parameters.

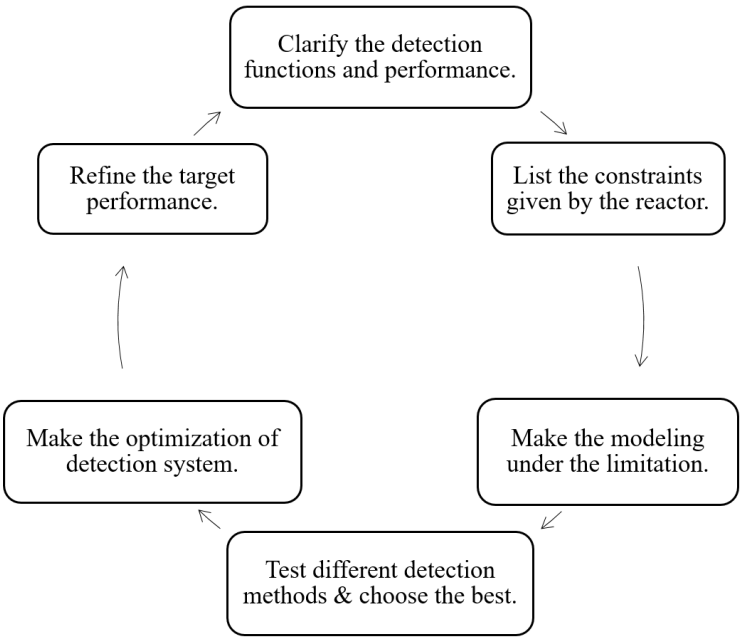

Figure 7.1: An optimization loop.

Therefore, an optimization loop can be considered in a design procedure for future reactors, as illustrated in the sketch of a feedback loop, as shown in Fig. 7.1. The general methodology using the equation Eq. 2.1 can be applied in this loop to help the conception design: for each item $R_i(t)$, $F_i(t)$ and E_i, the variables should be specified as two types, one that is constraint-dependent, and one that can be modified to improve detection performance; after the variables of interest are identified, they can be optimized through modeling.

Some examples are proposed:

- the volume of cover gas: as described in Sec. 4.4, it is recommended to use a smaller volume of cover gas in the detection system. However, the presence of a cover gas above the hot sodium pool is an essential design feature of SFR to prevent chemical reaction at the free surface of sodium and allow for coolant volume change when the operating temperature varies [5] [67]. The cover gas volume should first be determined under the design criteria of the primary system surrounding the core, according to the technique reports, e.g. [100], [66], [119], [90]. Thus it should be optimized under the reactor constraints.

- delay line: the delay line time should be minimized as described in Sec. 4.4, but it depends on the amount of background signal, which is related to the reactor design. Optimization can therefore be achieved by simulating varying reactor parameters (e.g., the vessel size, cover gas volume, sodium coolant

content, and the flow rate of the sipping system). Another way to reduce the delay line is to improve detection techniques, such as gamma spectrometry.

- new detectors technology: historical gamma spectrometry systems have been compromised by the presence of Compton scattering noise related to the activated sodium coolant and the cover gas. Delay lines are necessary to overcome the noise but will increase the measurement response time and lead to the deactivation of short-lived isotopes of interest. The spectrometry detector technology has been improved by the implementation of a Compton suppression system in the thesis work of Sara Garti [49], which shortens the response time and enriches the available isotopic information (short-lived fission products). Thus the cladding rupture of fuel in contact with sodium can also be detected from the gamma signal of short-lived isotopes, which means the signal of whether the crack has worsened can be achieved before reaching the undesirable rupture. A better detection method can be selected by comparing it with neutron detector technology. If it is necessary to use both ways, the breached fuel size can be better monitored.

This general methodology can also be applied to other reactor types, such as PWR, lead-cooled fast reactor (LFR), etc. For example, the general function Eq. 2.1 can be applied to LFR, for both fission products and delayed neutron detection. Each term of the function can then be investigated separately under the guidance of LFR reactor characteristics and lead properties [4] [39]. The general process should be similar, including the release of fission products, the transfer process in the coolant and cover gas, and the detector efficiency. Differences will include chemical reactions and corrosion between fuel and lead coolant, fission gas dissolution in lead coolant, etc. In this systematic way, experience between SFR and LFR can be learned, and the most efficient way of monitoring the cladding failure can be determined [34].

7.2 Improvement of the modeling

7.2.1 Detection methods

Future SFR may include new technical devices, such as optical methods (laser measurements [101]), ultrasonic technology [9] [127] [91], different types of neutron detectors and spectrometry detectors, etc.

Regarding optical methods, laser-induced breakdown spectroscopy (LIBS) has already been applied to measure trace elements, such as Xenon or Krypton, for the onset of fuel failure in gas-cooled fast reactors (GCFR) [93] [38]. Preliminary

results show that trace Xe detection using LIBS is possible, but LIBS must demonstrate its adequate sensitivity to competing with well-established techniques for trace noble gas detection such as gas chromatography or laser absorption spectrometry [19].

Acoustic monitoring systems can operate in a hostile environment, such as the liquid metal at high temperatures with high neutron and gamma fluxes [85]. The ultrasonic viewing system tailored for periodic reactor core in-service monitoring and maintenance inspections has been studied [58]. Ultrasonic inspection is applied in the prototype fast breeder reactor (PFBR) for defects of hexcan seal welds in fuel subassemblies [31] [133]. Acoustic techniques have been developed to meet the system protection and monitoring requirements in SFR [76]. Under-sodium imaging has been studied to detect and characterize potentially hazardous damage [88]. It has been shown that the basic Non-Destructive Testing (NDT) of a structure immersed under liquid sodium using conventional immersion ultrasonic techniques can be performed sufficiently [117].

With the development of new instrumentation technologies, it is possible to improve the modeling by applying new detection methods to the general methodology, which corresponds to the improvement of E_i in the equation Eq. 2.1. According to the characteristic of each approach, the detection scenario and the functions can be clarified; then the detector performance and target signal can be identified; the modeling can be performed for each step, including the release, transfer, and detection.

7.2.2 Signal real time interpretation

There are many detection systems in a reactor, devoted to neutron, gamma, acoustic, pressure, temperature measurements. All signals should be analyzed together, including gas, neutrons and signals from other methods. Combinatorial modeling can be done using all approaches for better real-time interpretation of the signal. For example, gamma spectroscopy signals from very short-lived fission gases and neutron signals from DNPs can be analyzed together to understand the propagation of ruptures, allowing for more rational and reliable decisions about whether to shut down the reactor or not.

The experience can be learned from the signal analysis of the SARA database of the PHENIX reactor, which is a comprehensive recording of all the measurements performed for the last ten years of operation, and the signals of multiple neutron detectors are recorded. Thus it is possible to complete some cross-analysis with other measurements (accelerometers, sonar, thermocouples) to get more insight into the nature and the amplitude of the supposed vibration phenomenon

observed with neutron detectors [152]. However, it was shown that the data storage and formatting make the exploitation very unpractical from the SARA data [153]. Thus data acquisition should be thought of with data processing/online information treatment in the future reactor, with new technology, e.g., artificial intelligence (AI) and massive computation.

7.2.3 Fuel element behavior

The knowledge of fuel phenomena should be improved and the fuel element behaviors should be more precise in the modeling, which corresponds to the improvement of $R_i(t)$ in the equation Eq. 2.1. Thus some research directions are mentioned:

- how does sodium penetrate the cladding: this is a coupled problem of hydraulic and chemical reactions that can be partially studied. For hydraulic studies, simplified modeling is possible using codes such as Comsol, but the description can be tricky: the geometric description of the fracture is complex (clean open parallelogram or something porous, depending on the cause of the rupture, e.g., fabrication defects or mechanical stress); space of the fuel and cladding is small enough for surface forces to dominate volumetric forces, which is addressed by microfluidics; where cladding rupture occurs is random, making the condition (fuel type, power, temperature, etc.) different. The study in an experimental way should be added.

- the chemistry of sodium in contact with fuel (different types): another Ph.D. student, Tristan Bossert, is working on the kinetics of MOX corrosion layer by sodium (how does irradiation affect the kinetics of the reaction between sodium and MOX fuel) in CINNA project of CEA. The reaction of MOX with sodium will be performed in airtight steel containers. The oxygen level in the container is kept at a level similar to that expected in SFR cores by an oxygen buffer material (Na_3NbO_4 or $NaCrO_2$) that releases oxygen as the reaction progress. The phase created in the reaction is analyzed by X-ray diffraction (XRD) analysis, and the reaction progress is determined by measuring the thickness of the reaction layer after the reaction with sodium. The same experiments on irradiated fuel (45% Pu) will also be performed [7].

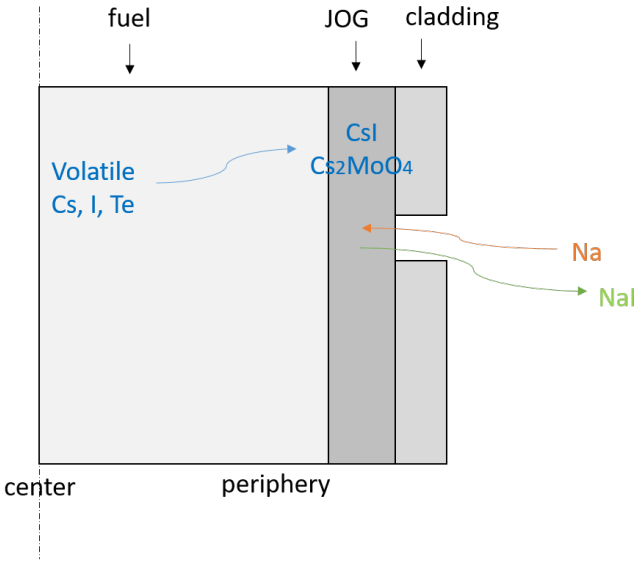

Figure 7.2: Scheme of chemical behavior of volatile FPs with sodium.

- the JOG formation effect to DNP release is still unclear: the thermochemical equilibrium calculations carried out with the SAGE software have confirmed that the JOG does not protect its integrity following the penetration of sodium (from CEA technical report): iodine reacts with sodium to form sodium iodides NaI and Na_2I_2. These compounds could have been expelled from the fuel pin in the primary sodium circuit through the cladding rupture. A scheme is developed to illustrate the chemical behavior of volatile FPs in the fuel and the reaction of JOG and sodium, as shown in Fig. 7.2. It can be derived that there are some iodine isotopes released to the sodium coolant through the cladding failure. However, only the release of short-lived iodine isotopes (e.g. ^{137}I) can have an influence on the DND detection. Unfortunately, the present calculation (e.g. Germinal) of the released quantity of iodine in the JOG only includes long-lived isotopes. The short-lived isotopes proportion among the released iodine is unclear, thus it is hard to do the modeling of DNP release in JOG formation. Further investigation of the impact of JOG on DND detection requires a larger inventory of isotopes of interest in the fuel performance code calculation.

7.3 Dedicated experiments

Dedicated experiments can be designed in the future for better modeling and methodological applications. I will propose a few examples:

- Some tests can be done in the water mock-up. For example, the transfer

function test: the hydraulic properties of water (density, viscosity) are very close to those of sodium. Due to the transparency of the water, the behavior of the fission products can be observed with a visual tracer. The experience can be learned from the DONALD mock-up, which is a hydraulic mock-up representing the hot plenum vessel of the SUPERPHENIX. It is supplied with cold water at its base under the plate simulating the subassemblies. The emission of fission products after cladding failure is simulated by the injection of a tracer of either colored or salt water in the subassembly. Finally, the transfer functions give the temporal evolution of the ratio between the concentration at the measurement point and the concentration injected into the subassembly [138] [44]. Another water mock-up test example can be the hydraulic properties of sodium penetration in the rupture (without the fuel chemical reaction part): the water flows with the tracer penetrating the cladding ruptures of different types and shapes can be observed.

- Some experiment loops can be installed in the material test reactor, such as Jules Horowitz Reactor (JHR) [17]. For example, the loops for detector capability tests of fission products: the experience can be learned from the CARAMEL test, which is a rig containing naked uranium (in contact with the sodium) set up in the assembly placed in the core [60] [62], and the loops to test the innovative detectors (laser, ultrasonic, etc.). The design of the JHR facility allows large flexibility in order to comply with a large range of experimental needs, regarding the type of samples (fuels or materials), neutron flux and spectrum, type of coolants, and thermal-hydraulics conditions (LWR, Gen IV), in accordance with the scientific objectives of the programs [57]. The test devices dedicated to GEN IV fuels in JHR are under conceptual design. SFR experimentations, such as fuel irradiation within the framework of GEN IV, can be implemented in the CALIPSO device (in-Core Advanced Loop for Irradiation in Potassium SOdium), which could be used to test fuel under nominal conditions in experimental locations within the core, and to test incidental/accidental conditions in the reflector [23] [131] [132].

- Computer programs can be designed using the digital twin technology to create simulations for each piece of the detection process [37]. Multiphysics simulation associated with the digital twin allows advanced interpretation of experiments with online measurement. The simplified models at a fine-scale on a reduced spatial or temporal domain can be set for parameter study. The experience can be learned from an example of using digital twin in the design of a secondary circuit for the NUWARD project [28].

General conclusion

The main objective of this thesis was to develop a general methodology describing the whole detection process of cladding failure for comprehensive optimization for future designs. The research covers the theoretical models for identifying the fission products release, predicting the signal transfer function, modeling the detector efficiency, evaluating the fuel-sodium corrosion effect, etc. The main steps of the work can be summarized as follows.

In the first part of the work, the DRG detection process has been emphatically described. Fission products of interest were identified, and the whole scenario of gas detection was developed and divided into different stages. A transfer function model was proposed to predict the time broadening of the observed signal. The general formula of transfer function was deduced by establishing the fission gas transfer scheme and the fission gas conservation equation. A transfer function modeling was performed using PHENIX reactor parameters and compared with the experiment data of a chosen case RG 14. The results showed a good agreement, with the same order of magnitude of the time broadening and the exact shape of exponential decreasing. As a result, the transfer function of the DRG system has been validated, which is necessary for the global modeling of the DRG system. This part of the work has been published in [33].

In the second part of the work, based on the transfer function, a generic methodology has been developed to describe the whole gas detection system in SFR. The global detection process has been modeled with the simulation of each module: 1) In the absence of a cladding crack, the production and inventory of the fission gas were calculated. The fuel performance code Germinal performed the accumulated fission gas in the gas plenum; 2) In the case of a crack, the gas leakage modeling has simulated the fission gas release; 3) The fission gas activity in the detector was obtained with the convolution of gas leakage flux and the transfer function; 4) The detector sensitivity was modeled by the Monte Carlo particle transport simulation code PHITS. With this methodology application, the detected current signal has been derived as the crack size function and a safety assessment of small leakage for PHENIX has been performed.

In the third part of the work, the detection process of the DND system was

described. The isotopes of interest in the rupture stage were clarified, which are DNPs (iodine, bromine). An overall scheme of the entire detection process was formulated. The neutron signal transfer from direct recoil release was simulated: 1) The recoil current from the failure surface was derived using the release ratio and recoil range calculated by SRIM; 2) A scheme of DNP release through the sodium was established, and the concentration of DNP collected in the DND block was obtained; 3) The detector efficiency was derived from literature studies; 4) The count rate of delayed neutrons in the detector for a given rupture size was computed, and the modeling results were compared with the experimental data. It was found that the transfer function of DND is a time shift, and the recoil release signal is consistent with the detected signal at the beginning.

In the fourth part of the work, the enhanced release of DNP from thermal diffusion was mainly studied. An experiment case RG 11 with a small size rupture was chosen, and the characteristics of the rupture and signal were analyzed. Physical modeling was presented to evaluate the fuel corrosion layer effect on the neutron signal: 1) A scheme of corrosion layer formation was proposed; 2) The temperature distribution at the fuel pin periphery was computed in COMSOL; 3) The thermal diffusion release as the function of temperature was calculated, as well as the corrosion layer kinetics; 4) The enhanced diffusion release during the corrosion layer formation was deduced. The modeling result was compared with the experiment data in RG 11, and the possible interpretation of the neutron evolution was proposed. It can be concluded that a temperature change influences the diffusion mechanism at the fuel pin periphery due to corrosion layer formation, and the enhanced diffusion release is consistent with the neutron signal evolution. This part of the work has been published in [32].

It can be generally concluded that a comprehensive view of cladding failure detection has been achieved with the proposed methodology. Thus, I have formulated the following conclusions:

- For the DRG system, the methodology that has been developed is applicable to arbitrary SFRs with different fuel and core designs. A model for the transfer function of the gas detection process was proposed and validated by a comparison between the modeling result and the experimental data, which realized the prediction of the time broadening of the observed signal. Based on this determined transfer function, a general methodology to describe the whole gas detection system has been developed, including fission gas quantity accumulated in the fuel gas plenum, the gas leakage flux through the crack, the transportation from the fuel pin to the detector, the detector sensibility to different isotopes. A safety assessment of small leakage for PHENIX using

this methodology was performed, reflecting its performance of early detection in the DRG system. With this methodology application, the detected current signal is derived as the function of crack size among the background signals and analyzed the importance of each isotope during the gas detection. For the future design of the detection system, the general formula developed can be applied to guide the conception choice. The methodology can be used as a toolbox for comprehensive optimization by changing the variables in the general equation. Moreover, applying the transfer function can contribute to an improved understanding of fission gas transfer in SFR. The deconvolution of the detected signal could be used to interpret DRG data in real-time.

- For the DND system, a global view of the neutron signal transfer process has been derived. The direct recoil release of DNPs was modeled, and the neutron signal for a given rupture size was predicted. The transfer function of DND is found to be a time shift. The signal of recoil release is consistent with the experiment data at the beginning. For the neutron signal during the time evolution, it was studied by physical modeling of DNP diffusion release during the corrosion layer formation. It was found that a temperature change influences the diffusion mechanism at the fuel pin periphery due to corrosion layer formation. The enhanced diffusion release is consistent with the neutron signal evolution in the experiment data. It can be concluded that the enhanced diffusion release due to the corrosion layer is likely to explain neutron signal evolution but will require further experiments quantified. For more accurate monitoring of rupture size, the DNP release mechanism and the fuel behaviors at the rupture should be the focus of future research.

Due to its promising results and applications, I hope that the general methodology developed in this thesis will be a valuable contribution to researchers and engineers working on cladding failure detection in SFR.

As a result of this thesis work, perspectives in two directions are open:

- For future reactors:

  Since the reactor is a multi-parameter system, the optimization of the conceptual design needs to be carried out as a whole under many constraints, including performance, safety, and economic points of view. As part of the reactor, the instrumentation system and detector design should be considered together from the beginning of the design to select reactor parameters. An optimization loop can be considered in a design procedure for future reactors. The general methodology can be applied in this loop to help the conception design: the variables should be specified as two types, one that

is constraint-dependent, and one that can be modified to improve detection performance; after the variables of interest are identified, they can be optimized through modeling. For example, a comprehensive instrumentation design software can be developed, taking into account the different choices of detection system parameters, detector methods, and the configuration of future reactors.

For the DRG system, a real-time deconvolution algorithm for the detected numerical data can be developed: deconvoluting the experiment signal and transfer function to derive the fission gas release at the fuel pin for better gas leakage monitoring. For the DND system, a corrective model could be devised, in order to tell apart a genuine worsening of the cladding failure from corrosion layer formation effects, which would increase the dependability of the reactor.

- For the future work:

  The collaboration between the fuel and the detection research should be enhanced. The discussions between these two research domains have already taken place for my thesis and were beneficial for the work. For example, organizing multidisciplinary meetings between fuel and detection teams; adding the short-lived isotopes inventory, which is interested in detection, to fuel performance code computation; planning experimental tests to study the fuel structure at the rupture to provide more details for signal evolution study.

  The modeling should be improved in several directions: with the development of new instrumentation technologies, it is possible to enhance the modeling by applying new detection methods to the general methodology, such as optical methods, ultrasonic technology, different types of neutron detectors, and spectrometry detectors; there are many detection systems in a reactor, devoted to neutron, gamma, acoustic, pressure, temperature measurements, the signals in which should be analyzed together and combinatorial modeling can be done for better real-time interpretation of the signal; the knowledge of fuel phenomena should be improved, and the fuel element behaviors should be more precise in the modeling, such as how does sodium penetrate the cladding, the chemistry of sodium in contact with fuel and the JOG formation effect to DNP release.

  Dedicated experiments can be designed in the future for better modeling and methodological applications: some tests can be done in the water mock-up, such as the transfer function test because the hydraulic proper-

ties of water (density, viscosity) are very close to those of sodium, and the hydraulic properties of sodium penetration in the rupture (without the fuel chemical reaction part); some experiment loops can be installed in the material test reactor, such as the loops for detector capability tests of fission products, and the loops to test the innovative detectors (laser, ultrasonic); computer programs can be designed using the digital twin technology to create simulations for each piece of the detection process, and the simplified models at a fine-scale on a reduced spatial or temporal domain can be set for parameter study.

Appendix A: Isotopes of interest

In the process of transportation and detection of radioactive fission products, it is necessary to clarify the characteristics of isotopes, such as decay paths, decay constants, parent isotopes, daughter isotopes, emitted particles, etc.

For the convenience of research, the decay path of the main isotopes of interest are shown (from JANIS database) in Fig. A.1 - Fig. A.7:

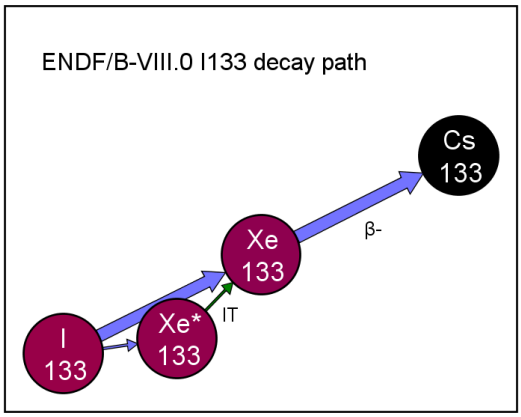

Figure A.1: The decay path of ^{133}Xe.

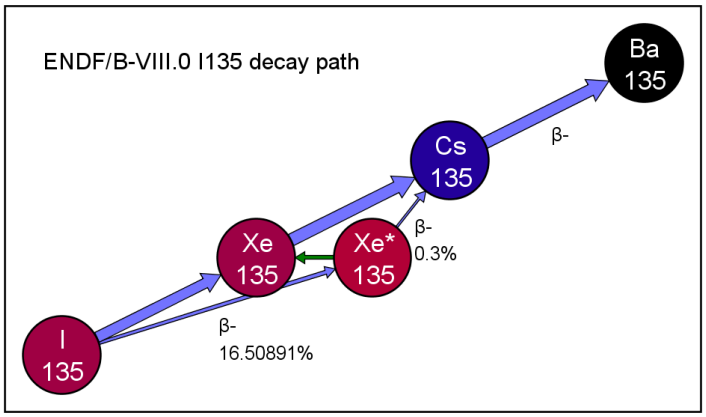

Figure A.2: The decay path of ^{135}Xe and ^{135m}Xe.

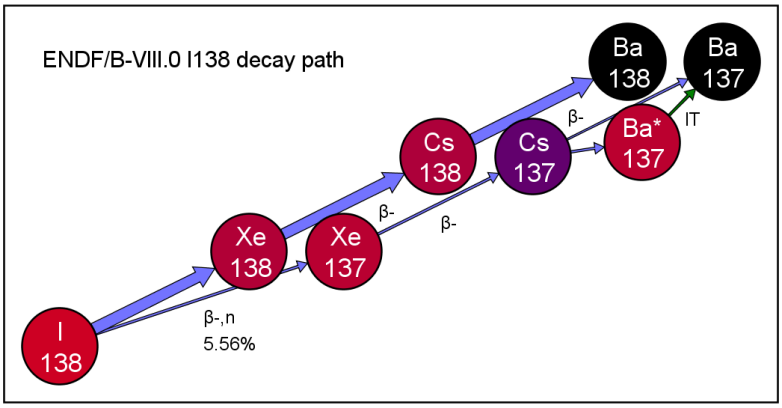

Figure A.3: The decay path of ^{138}Xe.

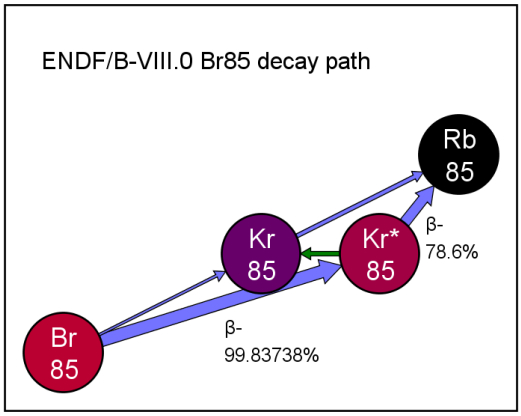

Figure A.4: The decay path of ^{85m}Kr.

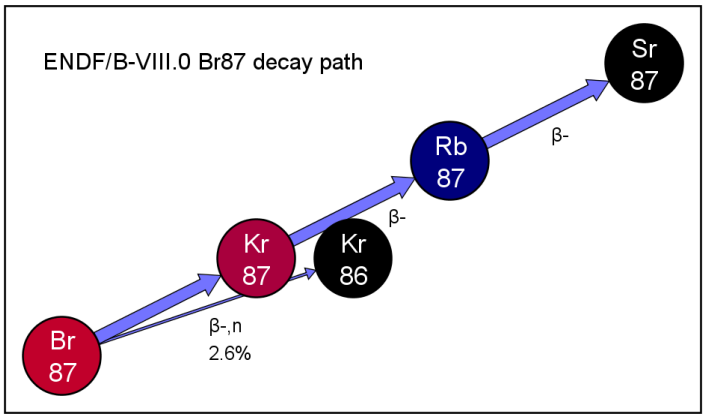

Figure A.5: The decay path of ^{87}Kr and ^{87}Br.

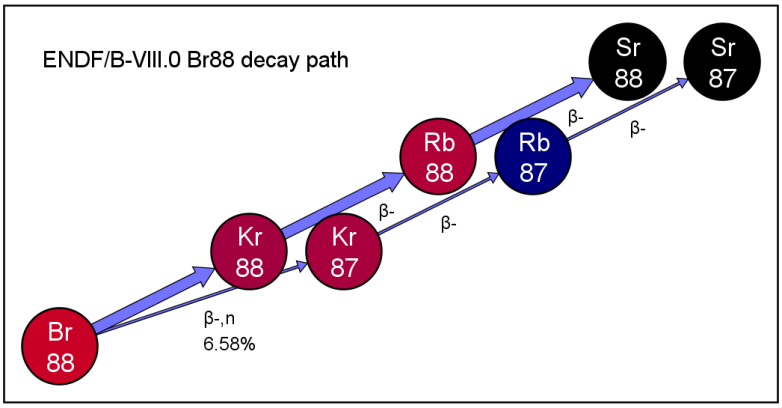

Figure A.6: The decay path of ^{88}Kr and ^{88}Br.

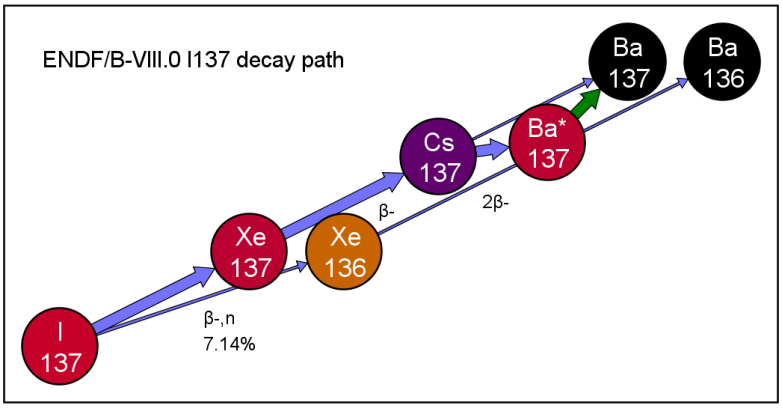

Figure A.7: The decay path of ^{137}I.

Appendix B: Simulation with PHITS software

Particle and Heavy Ion Transport code System (PHITS)[1] is a general purpose Monte Carlo particle transport simulation code that is used in many studies in the fields of accelerator technology, radiotherapy, space radiation, etc. It can deal with the transport of nearly all particles, including neutrons, protons, heavy ions, photons, and electrons, over wide energy ranges using various nuclear reaction models and data libraries [121]. PHITS is a fortran-based code; it can be executed on Windows, Mac, Linux, and Unix operating systems.

PHITS is an all-in-one-package type code, i.e. all components of the code such as its source, executable and data-library files are included in one package. The conditions of PHITS simulation can be specified by preparing an input file written in free-format ASCII text. Variables and mathematical equations can be used in the PHITS input files. The main components of a PHITS input file are "Geometry", "Source" and "Tally", statistical uncertainties of PHITS simulation depend on the history number:

- "Geometry" is defined by material, surface and cell sections, and various 3D geometrical components can be defined;
- "Source" is defined by shape, species, energy and direction of the particles;
- "Tally" is used to calculate the quantities in PHITS radiation transport calculation, and a variety of information can be deduced.

An example of the PHITS input file in this thesis work is shown in Fig. B.1 and Fig. B.2.

[1] https://phits.jaea.go.jp

```
[ P a r a m e t e r s ]
 icntl    =           0     # (D=0) 3:ECH 5:NOR 6:SRC 7,8:GSH 11:DSH 12:DUMP
 maxcas   =        1000000     # (D=10) number of particles per one batch
 maxbch   =          10     # (D=10) number of batches
 file(1)  = c:/phits        # (D=c:/phits) PHITS install folder name
 file(6)  = phits.out       # (D=phits.out) general output file name
 negs     =           1     # (D=-1) =-1:original, =0:No, =1:EGS
  ikermap = 0
  e-mode = 2

[ S o u r c e ]
  totfact =   2.0           # (D=1.0) global factor
 <Source> =   1.0000        # weight of this sub-source
   s-type =   26             # axial source with energy spectrum
     proj =  photon          # kind of incident particle
    suf = 15
        cut = -11
      dir =   1           # z-direction of beam [cosine]
   e-type =  28             # RI source
       ni =   1             # number of registered nuclide
                            #  data = ( nuclide(i), activity(i), i = 1, ni )
    Xe-135    7.4E+4         # (Bq)
                            # ->  1.00000E+00 (Bq), half life:  1.66354E+08 (sec)
     norm =   0             # (D=0) normalization factor =0:(/sec) =1:(/source)
  <Source> =   1.0000        # weight of this sub-source
      s-type =   26            # axial source with energy spectrum
     proj =  electron        # kind of incident particle
     suf = 15
        cut = -11
      dir =   1          # z-direction of beam [cosine]
   e-type =  28             # RI source
       ni =   1             # number of registered nuclide
                            #  data = ( nuclide(i), activity(i), i = 1, ni )
    Xe-135    7.4E+4     # (Bq)
                            # ->  2.00000E+02 (Bq), half life:  9.52027E+08 (sec)
     norm =   0             # (D=0) normalization factor =0:(/sec) =1:(/source)
    dtime = -10             # (D=-10.0) cooling time: sec(+) or half_life(-)

[ M a t e r i a l ]
mat[1]    N 8  O 2
mat[2]    Cu 7  Zn 3

[ Mat Name Color ]
    mat   name      color
     1    Air     pastelblue
     2    Cu       orangeyellow

[ S u r f a c e ]
  10  so     500.
  11  cz      13.
  12  pz       0.
  13  pz      50.
  14  cz      15.
  15  pz       -0.1

[ C e l l ]
 100    -1           10                 $ outer region
 101     1 -0.0012   -11  12  -13        $ air
 102     2 -8.93        -14 11 12 -13
 110     0          -10  #102  #101         $ void
```

Figure B.1: An example of the PHITS input file (1).

```
[ delta ray ]
reg   del
101   0.001

[ T - T r a c k ]
    title = Track Detection in xyz mesh
     mesh =  xyz            # mesh type is xyz scoring mesh
   x-type =    2            # x-mesh is linear given by xmin, xmax and nx
       nx =  100            # number of x-mesh points
     xmin =  -25.           # minimum value of x-mesh points
     xmax =   25.           # maximum value of x-mesh points
   y-type =    1            # y-mesh is given by the below data
       ny =    1            # number of y-mesh points
           -15.0  15.0
   z-type =    2            # z-mesh is linear given by zmin, zmax and nz
       nz =  160            # number of z-mesh points
     zmin =  -0.1           # minimum value of z-mesh points
     zmax =   70.           # maximum value of z-mesh points
   e-type =    1            # e-mesh is given by the below data
       ne =    1            # number of e-mesh points
            0.0  5000.0
     unit =    1            # unit is [1/cm^2/source]
     axis =   xz            # axis of output
     file = track_xz.out    # file name of output for the above axis
     part =  photon electron
    gshow =    1            # 0: no 1:bnd, 2:bnd+mat, 3:bnd+reg 4:bnd+lat
   epsout =    1            # (D=0) generate eps file by ANGEL

   [ T - Deposit ]
    title = Energy deposition in xyz mesh
     mesh =  xyz            # mesh type is xyz scoring mesh
   x-type =    2            # x-mesh is linear given by xmin, xmax and nx
     xmin =  -25.           # minimum value of x-mesh points
     xmax =   25.           # maximum value of x-mesh points
       nx =  100            # number of x-mesh points
   y-type =    1            # y-mesh is given by the below data
       ny =    1            # number of y-mesh points
           -15.0  15.0
   z-type =    2            # z-mesh is linear given by zmin, zmax and nz
       nz =  160            # number of z-mesh points
     zmin =  -0.1           # minimum value of z-mesh points
     zmax =   70.           # maximum value of z-mesh points
     unit =    1            # unit is [MeV/cm^3/source]
 material =  all            # (D=all) number of specific material
 dedxfnc = 1
   output =  dose           # total deposit energy
     axis =    xz           # axis of output
     file = deposit.out     # file name of output for the above axis
     part =   all
    gshow =    1            # 0: no 1:bnd, 2:bnd+mat, 3:bnd+reg 4:bnd+lat
   epsout =    1            # (D=0) generate eps file by ANGEL
```

Figure B.2: An example of the PHITS input file (2).

Appendix C: Simulation with Comsol software

COMSOL Multiphysics® is a commercial software suite[2] for numerical simulation based on the finite element method. It includes a certain number of modules (optional) corresponding to as many models of physical phenomena, with possibilities of coupling, within a multi-platform graphic interface (Linux, Windows, Mac), making it possible to define and solve a problem by a series of mouse clicks.

The main steps in setting up a model are:

1. definition of the component to be studied:
   (a) definition of the geometry by taking advantage of the symmetries of the problem (1D, 2D, axisymmetric 2D, 3D). To do this, you can combine simple shapes (circles, cylinders, cubes, etc.), modify them as needed (chamfers, fillets, etc.), or, for the most complex geometries, import from software CAD, Solidworks®.
   (b) definition of materials, through the properties necessary for the study (e.g. density, specific heat capacity, thermal conductivity) possibly a function of calculated quantities such as temperature or pressure. There is a library of predefined materials, which the user can extend.
   (c) choose one or more "physics", that is to say a model for a physical phenomenon. Each physics is described by a set of partial differential equations to which the user must add boundary conditions corresponding to the elements of the geometry.
   (d) possibly choose a coupling between different physics, for example between a flow and a heat transfer.
   (e) define a mesh.
   (f) it is possible to define several components, and to couple them by indicating how for example via a change of coordinates a geometrical entity of one corresponds to a geometrical entity of the other.

[2] http://www.comsol.fr

2. define one or more "studies". A study is characterized by the physics and the couplings that it must solve by finite element method and by its stationary character or not.

3. the study is launched by a "compute" button. A convergence graph is displayed, until a convergence criterion (or a maximum number of iterations) is reached.

4. definition and exploitation of results, for example:

   - possibility to define cuts, profiles.
   - tables of quantities calculated by studies, or derived from calculations, such as the temperature value at a point.
   - 1D or 2D graphics, animations, exports.

The interface obeys an object-oriented programming logic: for example, each component can be seen as a class instance possessing data (materials, geometry) and methods (physical models). An example of the Comsol computation in this thesis work is shown in Fig. C.1 and Fig. C.2.

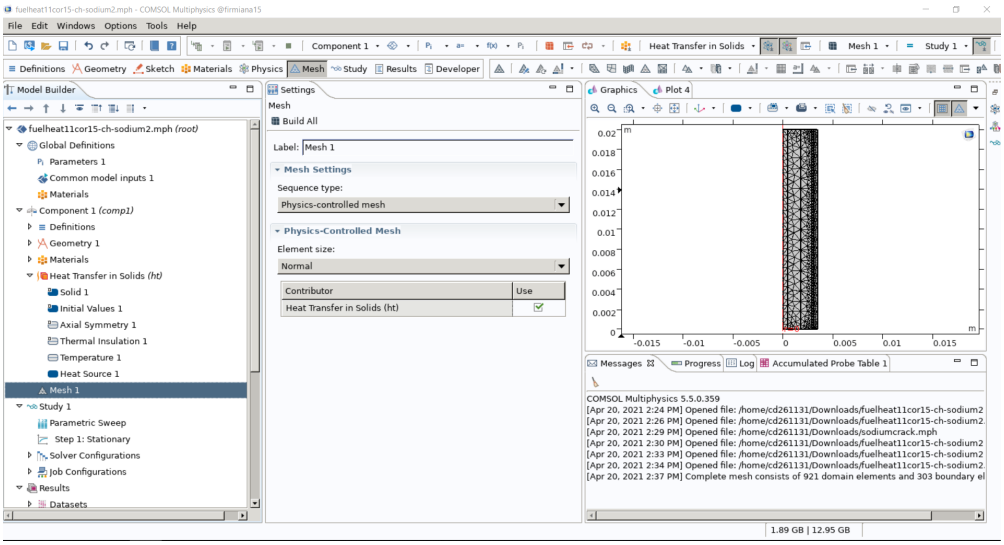

Figure C.1: An example of the Comsol computation (1).

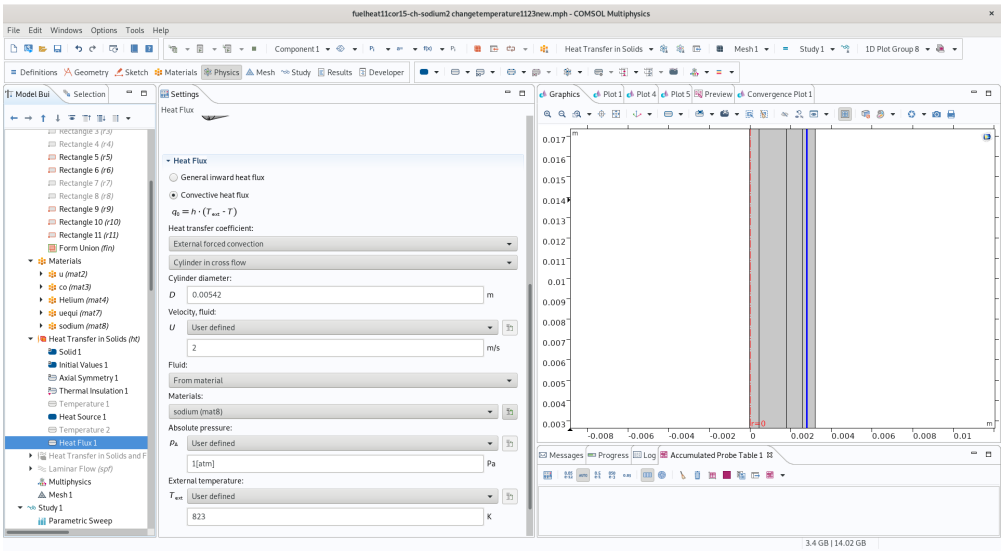

Figure C.2: An example of the Comsol computation (2).

Bibliography

[1] K. Aizawa and Y. Chikazawa. Tagging-gas failed fuel detection and location system for sodium-cooled reactors. *Nuclear Technology*, 189(2):143–151, 2015.

[2] K. Aizawa, K. Fujita, H. Kamide, and N. Kasahara. Selector-valve failed fuel detection and location system for japan sodium-cooled fast reactor. *Nuclear Technology*, 189(2):111–121, 2015.

[3] O. Albutova and A. Lukyanov. Investigation of dependence of BN-600 reactor sector fuel cladding leak detection system responses on the operation parameters. *Nuclear Energy and Technology*, 1, Mar. 2016. doi: 10.1016/j.nucet.2016.02.011.

[4] A. Alemberti, M. Frogheri, S. Hermsmeyer, L. Ammirabile, V. Smirnov, M. Takahashi, C. Smith, Y. Wu, and I. Hwang. Lead-cooled fast reactor (lfr) risk and safety assessment white paper. GEN IV International Forum, 2014.

[5] K. Allen, G. Meadows, and W. Schuck. Liquid metal reactor cover gas purification and analysis in the usa. Technical report, Argonne National Lab., Idaho Falls, ID (USA); Hanford Engineering ..., 1986.

[6] C. Andrello. *Mechanism and kinetics of the reaction between liquid sodium and nuclear fuel of future fast neutron reactors*. PhD thesis, Université de Lyon, 2020.

[7] C. Andrello, L. Favergeon, D. Freis, and L. Desgranges. UO2 corrosion by liquid sodium. In *NuFuel-MMNSF 2019 Workshop*, Zurich, Switzerland, Nov. 2019. PSI - Paul Scherrer Institut (Suisse) and ENEA - Italian National Agency for New Technologies, Energy and Sustainable Economic Development (Italie) and INL - Idaho National Laboratory INL (Etat-Unis). URL https://hal-emse.ccsd.cnrs.fr/emse-02904095.

[8] K. Aoto, P. Dufour, Y. Hongyi, J. P. Glatz, Y.-i. Kim, Y. Ashurko, R. Hill, and N. Uto. A summary of sodium-cooled fast reactor development. *Progress in Nuclear Energy*, 77:247–265, Nov. 2014. ISSN 0149-1970. doi: 10.1016/j.pnucene.2014.05.008. URL http://www.sciencedirect.com/science/article/pii/S0149197014001279.

[9] M. Attaar. State-of-the-art ultrasonic detection of failed fuel. *Transactions of the American Nuclear Society*, 61, 1990.

[10] E. Avrorina and A. Chebeskovb. Fast reactors and nuclear nonproliferation. 2013.

[11] A. Bachchan, K. Devan, K. Yernamma, M. Alagan, K. Natesan, D. Naga Sivayya, and P. Mohanakrishnan. Simulation of delayed neutron precursor release due to wet rupture in a fuel pin and its detection methodology in PFBR. *Nuclear Engineering and Design*, 382:111372, Oct. 2021. ISSN 0029-5493. doi: 10.1016/j.nucengdes.2021.111372. URL https://www.sciencedirect.com/science/article/pii/S0029549321003241.

[12] C. Baker. The fission gas bubble distribution in a mixed oxide fast reactor fuel pin. *Journal of Nuclear Materials*, 75(1):105–109, July 1978. ISSN 0022-3115. doi: 10.1016/0022-3115(78)90033-8. URL https://www.sciencedirect.com/science/article/pii/0022311578900338.

[13] B. Barkia, J. L. Courouau, E. Perrin, V. Lorentz, M. Rivollier, R. Robin, L. Nicolas, C. Cabet, and T. Auger. Investigation of crack propagation resistance of 304L, 316L and 316L(N) austenitic steels in liquid sodium. *Journal of Nuclear Materials*, 507:15–23, Aug. 2018. ISSN 0022-3115. doi: 10.1016/j.jnucmat.2018.04.036. URL http://www.sciencedirect.com/science/article/pii/S0022311518302228.

[14] D. D. Baron and L. Hallstadius. 2.19 - Fuel Performance of Light Water Reactors (Uranium Oxide and MOX). In R. J. M. Konings, editor, *Comprehensive Nuclear Materials*, pages 481–514. Elsevier, Oxford, Jan. 2012. ISBN 978-0-08-056033-5. doi: 10.1016/B978-0-08-056033-5.00040-9. URL https://www.sciencedirect.com/science/article/pii/B9780080560335000409.

[15] C. Behar et al. Technology roadmap update for generation iv nuclear energy systems. In *In OECD Nuclear Energy Agency for the Generation IV International Forum*, volume 17, pages 2014–03, 2014.

[16] M. Benfarah, M. Zouiter, T. Jobert, F. Dacquait, M. Bultot, and J.-B. Genin. Pwr circuit contamination assessment tool. use of oscar code for engineering studies at edf. *EPJ Nuclear Sciences & Technologies*, 2:15, 2016.

[17] G. Bignan and J. Estrade. The jules horowitz reactor: a new high performances european mtr (material testing reactor) with modern experimental capacities: toward an international user facility. *energy*, 1009:1, 2013.

[18] G. Bignan, J.-F. Villard, C. Destouches, P. Baeten, L. Vermeeren, and S. Michiels. The key-role of instrumentation for the new generation of research reactors. In *2011 2nd International Conference on Advancements in Nuclear Instrumentation, Measurement Methods and their Applications*, pages 1–8, 2011. doi: 10.1109/ANIMMA.2011.6172882.

[19] M. Burger, L. A. Finney, L. Garrett, S. S. Harilal, K. C. Hartig, J. Nees, P. J. Skrodzki, X. Xiao, and I. Jovanovic. Laser ablation spectrometry for studies of uranium plasmas, reactor monitoring, and spent fuel safety. *Spectrochimica Acta Part B: Atomic Spectroscopy*, 179:106095, 2021.

[20] M. Chantot, A. Paziaud, A. Rulleau, et al. Phenix reactor equipment for fuel failure detection and location. Technical report, 1975.

[21] M. Chenaud, N. Devictor, G. Mignot, F. Varaine, C. Venard, L. Martin, M. Phelip, D. Lorenzo, F. Serre, F. Bertrand, et al. Status of the astrid core at the end of the pre-conceptual design phase 1. *Nuclear Engineering and Technology*, 45(6):721–730, 2013.

[22] G. Choppin, J. Liljenzin, and J. Rydberg. Chapter 8-detection and measurement techniques. *Radiochemistry and Nuclear Chemistry; Choppin, GR, Liljenzin, J.-O., Rydberg, J., Eds*, pages 192–238, 2002.

[23] C. Colin, J. Pierre, C. Blandin, C. Gonnier, M. Auclair, and F. Rozenblum. Test devices in jules horowitz reactor dedicated to the material studies in support to the current and future nuclear power plants. In *Fontevraud 8– Contribution of Materials Investigations and Operating Experience to LWRs' Safety, Performance and Reliability*. 2014.

[24] D.-T. Costin, L. Desgranges, T. Retegan, and C. Ekberg. Storage of defective fuel pins in sfr core. *Procedia Chemistry*, 21:378–385, 2016.

[25] R. Coulon, S. Normand, G. Ban, E. Barat, T. Montagu, T. Dautremer, H.-P. Brau, V. Dumarcher, J.-L. Portier, M. Michel, L. Barbot, T. Domenech,

K. Boudergui, V. Kondrasovs, A.-M. Frelin, J.-M. Bourbotte, and P. Jousset. Sodium fast reactor power monitoring and clad failure detection using ADONIS system. In *2009 IEEE Nuclear Science Symposium Conference Record (NSS/MIC)*, pages 1378–1386, Oct. 2009. doi: 10.1109/NSSMIC.2009.5402341. ISSN: 1082-3654.

[26] R. Coulon, E. Rohée, J. Dumazert, S. Garti, P. Filliatre, and C. Jammes. Design of a delayed neutron detection system for the astrid sodium-cooled fast reactor. In *EPJ Web of Conferences*, volume 170, page 04006. EDP Sciences, 2018.

[27] R. Coulon, E. Rohée, J. Dumazert, S. Garti, P. Filliatre, and C. Jammes. Ex-Vessel Delayed Neutron Detection Systems for the ASTRID Sodium-Cooled Fast Reactor. *IEEE Transactions on Nuclear Science*, 65(9):2502–2509, Sept. 2018. ISSN 1558-1578. doi: 10.1109/TNS.2018.2832987. Conference Name: IEEE Transactions on Nuclear Science.

[28] C. Crampon and G. Le Gros. Nuward, the future french smr. the french smr nuward tm in the spotlight. 2019.

[29] F. Dacquait, J.-B. Genin, J. Francescatto, G. Benier, G. Galassi, F. Broutin, M. Gherrab, E. Tevissen, D. You, T. Jobert, et al. The oscar code: a simulation tool to assess the pwr contamination for decommissioning. In *DEM 2021–International Conference on Decommissioning Challenges:*, pages Oral–T04, 2021.

[30] J. Deutch, E. Moniz, S. Ansolabehere, M. Driscoll, P. Gray, J. Holdren, P. Joskow, R. Lester, and N. Todreas. The future of nuclear power. *an MIT Interdisciplinary Study, http://web. mit. edu/nuclearpower*, 2003.

[31] R. Dhayalan, A. Kumar, K. Rajkumar, and C. Mukhopadhyay. Ultrasonic high frequency guided wave for detection and identification of defect location in seal welds of sodium cooled fast reactor fuel subassemblies. *Annals of Nuclear Energy*, 133:795–804, 2019.

[32] C. Ding, P. Filliatre, L. Desgranges, and D. Friant. How could fuel corrosion influence the delayed neutron signal time evolution in sodium cooled fast reactors? *Nuclear Engineering and Design*, 398:111977, 2022. ISSN 0029-5493. doi: https://doi.org/10.1016/j.nucengdes.2022.111977. URL https://www.sciencedirect.com/science/article/pii/S0029549322003284.

[33] Ding, C., Filliatre, P., and Desgranges, L. Gas detection in sodium cooled fast reactors: determination of a transfer function. *EPJ Web Conf.*, 253:

05002, 2021. doi: 10.1051/epjconf/202125305002. URL https://doi.org/10.1051/epjconf/202125305002.

[34] A. V. Dragunova, M. S. Morkin, and V. V. Perevezentsev. Features of methods for monitoring the fuel cladding tightness in lead-cooled fast breeder reactors. *Nuclear Energy and Technology*, 7:319, 2021.

[35] P. Dufour. Status of the astrid project. 2015.

[36] T. Dujardin. Generation iv and the nea. *NEA News*, (20.1), 2002.

[37] A. El Saddik. Digital twins: The convergence of multimedia technologies. *IEEE multimedia*, 25(2):87–92, 2018.

[38] K. E. Eseller, F.-Y. Yueh, and J. P. Singh. Non-intrusive, on-line, simultaneous multi-species impurity monitoring in hydrogen using libs. *Applied Physics B*, 102(4):963–969, 2011.

[39] C. Fazio, V. Sobolev, A. Aerts, S. Gavrilov, K. Lambrinou, P. Schuurmans, A. Gessi, P. Agostini, A. Ciampichetti, L. Martinelli, et al. Handbook on lead-bismuth eutectic alloy and lead properties, materials compatibility, thermal-hydraulics and technologies-2015 edition. Technical report, Organisation for Economic Co-Operation and Development, 2015.

[40] P. Filliatre, C. Jammes, J. P. Jeannot, and F. Jadot. In vessel detection of delayed neutron emitters from clad failure in sodium cooled nuclear reactors: Information treatment. *Annals of Nuclear Energy*, 65:385–389, Mar. 2014. ISSN 0306-4549. doi: 10.1016/j.anucene.2013.11.046. URL http://www.sciencedirect.com/science/article/pii/S0306454913006439.

[41] P. Filliatre, C. Jammes, Z. Elter, G. de Izarra, H. Hamrita, M. Bakkali, G. Galli, B. Cantonnet, and J. Nappé. Dependability of the fission chambers for the neutron flux monitoring system of the french gen-iv sfr. In *IAEA-International Conference on Fast Reactors and Related Fuel Cycles Next Generation Nuclear Systems for Sustainable Development (FR17)*. IAEA-International Conference on Fast Reactors and Related Fuel Cycles Next . . . , 2017.

[42] P. Filliatre, C. Jammes, C. Ding, L. Desgranges, and R. Coulon. Conception of delayed neutron detector blocks in a sodium cooled fast reactor. *Nuclear Engineering and Design*, 371:110933, Jan. 2021. ISSN 0029-5493. doi: 10.1016/j.nucengdes.2020.110933. URL http://www.sciencedirect.com/science/article/pii/S0029549320304271.

[43] G. Flanagan, T. Fanning, and T. Sofu. Sodium-cooled fast reactor (sfr) technology and safety overview. In *Department of Energy Seminar, Washington, DC, February*, volume 18, 2015.

[44] G. Francois, G. Azarian, J. Astegiano, C. Lacroix, and G. Poet. Assessment of thermal-hydraulic characteristics of the primary circuit. *Nuclear science and engineering*, 106(1):55–63, 1990.

[45] C. Friskney and J. Turnbull. The characteristics of fission gas release from uranium dioxide during irradiation. *Journal of Nuclear Materials*, 79(1):184–198, Jan. 1979. ISSN 00223115. doi: 10.1016/0022-3115(79)90446-X. URL https://linkinghub.elsevier.com/retrieve/pii/002231157990446X.

[46] Y. Fukano. Development of safety assessment methodology on fuel element failure propagation in SFR and its application to Monju. *Journal of Nuclear Science and Technology*, 52(2):178–192, Feb. 2015. ISSN 0022-3131. doi: 10.1080/00223131.2014.939117. URL https://doi.org/10.1080/00223131.2014.939117. Publisher: Taylor & Francis _eprint: https://doi.org/10.1080/00223131.2014.939117.

[47] S. Gadomski, G. Hall, T. Høgh, P. Jalocha, E. Nygård, and P. Weilhammer. The deconvolution method of fast pulse shaping at hadron colliders. *Nuclear Instruments and Methods in Physics Research Section A: Accelerators, Spectrometers, Detectors and Associated Equipment*, 320(1-2):217–227, 1992.

[48] G. Galli, H. Hamrita, C. Jammes, M. J. Kirkpatrick, E. Odic, P. Dessante, and P. Molinié. Paschen's law in extreme pressure and temperature conditions. *IEEE Transactions on Plasma Science*, 47(3):1641–1647, 2019.

[49] S. Garti. *Spectrométrie gamma haute résolution et bas bruit Compton pour la détection des ruptures de gaine dans les réacteurs rapides refroidis au sodium*. PhD thesis, Université Grenoble Alpes [2020-....], 2020.

[50] S. Garti, J. Dumazert, R. Coulon, P. Filliatre, and C. Jammes. A new model to predict fission product diffusion & release in (pu, u) o 2 matrix for sfr clad failure detection. In *2018 IEEE Nuclear Science Symposium and Medical Imaging Conference Proceedings (NSS/MIC)*, pages 1–5. IEEE, 2018.

[51] S. Garti, J. Dumazert, R. Coulon, Q. Lecomte, F. Carrel, G. Corre, M. Imbault, C. Theroine, and C. Jammes. Characterizing low-activity waste containers: A case study for compton suppression systems under challenging

signal-to-noise ratio. *Nuclear Instruments and Methods in Physics Research Section A: Accelerators, Spectrometers, Detectors and Associated Equipment*, 949:162806, 2020.

[52] F. Gauche. Astrid, technological demonstrator of the 4 generation nuclear systems. *REE Revue de l'Electricite et de l'Electronique*, (5):46–53, 2013. ISSN 1265-6534. Place: France INIS Reference Number: 45052422.

[53] F. Gauche, J. Rouault, D. Verwaerde, J. Sauvagem, and J. Serpantie. Rnr sodium, the sfr program and the astrid prototype; rnr sodium-le programme sfr et le prototype astrid. 2010.

[54] J. Genin, T. Jobert, and N. Engler. The oscar-fp v1. 4 code simulation of fission product and alpha emitter contamination in pwr circuits. In *The 21st international conference on water chemistry in nuclear reactor systems (NPC 2018)*. EPRI, 2018.

[55] J.-B. Genin, M. Benfarah, C. Dinse, and M. Corbineau. Simulation of alpha contamination in pwr with the oscar code. 2014.

[56] M. Giot, L. Vermeeren, A. Lyoussi, C. Reynard-Carette, C. Lhuillier, P. Mégret, F. Deconinck, and B. Goncalves. Nuclear instrumentation and measurement: a review based on the animma conferences. *EPJ N-Nuclear Sciences & Technologies*, 3:33, 2017.

[57] C. Gonnier, J. Estrade, G. Bignan, and B. Maugard. Experimental devices in jules horowitz reactor and first orientations for the experimental programs. 2017.

[58] J. W. Griffin, T. J. Peters, G. J. Posakony, H.-T. Chien, L. J. Bond, K. M. Denslow, S.-H. Sheen, and P. Raptis. Under-sodium viewing: a review of ultrasonic imaging technology for liquid metal fast reactors. 2009.

[59] Y. Guerin. 2.21 - Fuel Performance of Fast Spectrum Oxide Fuel. In R. J. M. Konings, editor, *Comprehensive Nuclear Materials*, pages 547–578. Elsevier, Oxford, Jan. 2012. ISBN 978-0-08-056033-5. doi: 10.1016/B978-0-08-056033-5.00043-4. URL http://www.sciencedirect.com/science/article/pii/B9780080560335000434.

[60] J. Guidez and G. Prêle. *Superphenix: technical and scientific achievements*. Springer, 2017.

[61] J. Guidez, J. Bodi, K. Mikityuk, E. Girardi, and B. Carluec. New reactor safety measures for the european sodium fast reactor—part i: Conceptual design. *Journal of Nuclear Engineering and Radiation Science*, 8(1), 2022.

[62] P. Hammer. Report of activity-1997. Technical report, Direction chargee de la Gestion des Dechets, 1999.

[63] J. H. Harding and D. G. Martin. A recommendation for the thermal conductivity of UO2. *Journal of Nuclear Materials*, 166(3):223–226, Aug. 1989. ISSN 0022-3115. doi: 10.1016/0022-3115(89)90218-3. URL https://www.sciencedirect.com/science/article/pii/0022311589902183.

[64] H. Hayafune, J.-P. Glatz, Yang Hongyi, J.-M. Ruggieri, Y.-I. Kim, Y. Ashurko, and R. Hill. Current status of GIF collaborations on sodium-cooled fast reactor system. page v, International Atomic Energy Agency (IAEA), 2017. INIS Reference Number: 49085660.

[65] K. Herbreteau, N. Marie, F. Bertrand, J.-M. Seiler, and P. Rubiolo. Sodium-cooled fast reactor pin model for predicting pin failure during a power excursion. *Nuclear Engineering and Design*, 335:279–290, Aug. 2018. ISSN 00295493. doi: 10.1016/j.nucengdes.2018.05.023. URL https://linkinghub.elsevier.com/retrieve/pii/S0029549318302280.

[66] M. Holbrook and J. Kinsey. Guidance for developing principal design criteria for advanced (non-light water) reactors. Technical report, Idaho National Lab.(INL), Idaho Falls, ID (United States), 2015.

[67] X. Huang and S. He. Numerical modelling of cover gas thermal hydraulics in sodium-cooled fast reactors. *Nuclear Engineering and Design*, 355:110347, 2019.

[68] IRSN. Review of generation iv nuclear energy systems. 2015.

[69] C. Ito, I. Yoshihiro, H. Harano, T. Iguchi, and A. Takafumi. High sensitive and reliable ffdl technique for sfr using laser resonance ionization mass spectrometry. *Transactions of the American Nuclear Society*, 102:416–417, 2010.

[70] Y. Iwamoto, S.-i. Meigo, and S. Hashimoto. Estimation of reliable displacements-per-atom based on athermal-recombination-corrected model in radiation environments at nuclear fission, fusion, and accelerator facilities. *Journal of Nuclear Materials*, 538:152261, 2020.

[71] Y. Iwata, C. Ito, and H. Harano. Reliability evaluation for failed fuel identification using resonance ionization mass spectrometry. *Hyperfine Interactions*, 216(1):15–19, 2013.

[72] S. Jacobi. Fuel failure detection and location in lmfbrs. Technical report, Kernforschungszentrum Karlsruhe GmbH (Germany, 1982.

[73] C. Jammes, P. Filliatre, B. Geslot, L. Oriol, F. Berhouet, J.-F. Villard, and L. Vermeeren. Research activities in fission chamber modeling in support of the nuclear energy industry. *IEEE Transactions on Nuclear Science*, 57(6): 3678–3682, 2010.

[74] C. Jammes, P. Filliatre, B. Geslot, T. Domenech, and S. Normand. Assessment of the high temperature fission chamber technology for the french fast reactor program. *IEEE Transactions on Nuclear Science*, 59(4):1351–1359, 2012.

[75] C. Jammes, P. Filliatre, P. Loiseau, and B. Geslot. On the impact of the fissile coating on the fission chamber signal. *Nuclear Instruments and Methods in Physics Research Section A: Accelerators, Spectrometers, Detectors and Associated Equipment*, 681:101–109, 2012.

[76] J.-P. Jeannot, F. Baque, M. Cavaro, O. Gastaldi, C. Lhuilier, N. Massacret, J. Moriot, K. Paumel, M. Vandergaegen, and G. Rodriguez. Acoustic waves: A route to enhance sodium fast reactor safety. 2013.

[77] T. Julien. Méthodes acoustiques et vibratoires pour l'étude phénoménologique d'une rupture de gaine de combustible dans un réacteur nucléaire. 2022.

[78] T. Julien, V. Faucher, L. Pantera, G. Ricciardi, and E. Sarrouy. Numerical study of coupled fluid and solid wave propagation related to the cladding failure of a nuclear fuel rod. *Applied Sciences*, 12(4):1784, 2022.

[79] G. F. Knoll and F. Glein. Radiation detection and measurement, wiley. *New York*, 1989.

[80] A. Koning and OECD Nuclear Energy Agency. *The JEFF-3.1 nuclear data library: JEFF report 21*. 2006. ISBN 978-92-64-02314-7. OCLC: 1039431841.

[81] M. Lainet, B. Michel, J.-C. Dumas, M. Pelletier, and I. Ramière. Germinal, a fuel performance code of the pleiades platform to simulate the in-pile behaviour of mixed oxide fuel pins for sodium-cooled fast reactors. *Journal of Nuclear Materials*, 516:30–53, 2019.

[82] J. Lambert, R. Mikaili, K. Gross, R. Strain, T. Aoyama, S. Ukai, S. Nomura, and N. Nakae. Failed fuel monitoring and surveillance techniques for liquid metal cooled fast reactors. Technical report, Argonne National Lab., 1995.

[83] B. Lewis, P. Chan, A. El-Jaby, F. Iglesias, and A. Fitchett. Fission product release modelling for application of fuel-failure monitoring and detection - An overview. *Journal of Nuclear Materials*, 489:64–83, June 2017. ISSN 00223115. doi: 10.1016/j.jnucmat.2017.03.037. URL https://linkinghub.elsevier.com/retrieve/pii/S0022311517302362.

[84] B. J. Lewis and H. E. Sills. Fission-product transport and the diffusion approximation. *Journal of Nuclear Materials*, 184(2):107–112, Sept. 1991. ISSN 0022-3115. doi: 10.1016/0022-3115(91)90500-7. URL https://www.sciencedirect.com/science/article/pii/0022311591905007.

[85] M. Lions, R. Berger, A. Bret, H. Buis, and J. Barton. Apparatus for ultrasonic visualization in sodium (visus) and acoustic detection in the phenix reactor. Technical report, Societe des Electriciens, des Electroniciens et des Radioelectriciens, 92 . . . , 1973.

[86] Y. Liu and C. Qiu. The design and calculation of the delayed neutron detection system for pwr and cefr. *Engineering Sciences*, 7(4):61–67, 2009.

[87] J. Losfeld, L. Desgranges, S. Clement, and Y. Pontillon. Merarg experimental loop: A forward fitting method for fission gas release analysis. *IEEE Transactions on Nuclear Science*, 69(4):786–791, 2022. doi: 10.1109/TNS.2022.3151942.

[88] E. Lubeigt, S. Mensah, J.-F. Chaix, S. Rakotonarivo, G. Gobillot, and F. Baqué. Ultrasonic imaging in liquid sodium: A differential method for damages detection. *Physics Procedia*, 70:550–553, 2015.

[89] F. N. Madden, K. R. Godfrey, M. J. Chappell, R. Hovorka, and R. A. Bates. A comparison of six deconvolution techniques. *Journal of pharmacokinetics and biopharmaceutics*, 24(3):283–299, 1996.

[90] I. K. Madni. Containment and sodium-specific sfr design criteria in rg 1.232. 2018.

[91] M. Mala and M. Miklos. Nondestructive testing of nuclear reactor components integrity. 2011.

[92] J. Matthews and T. Preusser. On the failure of fast reactor fuel pins. *Nuclear Engineering and Design*, 101(3):281–303, May 1987. ISSN 00295493.

doi: 10.1016/0029-5493(87)90056-2. URL https://linkinghub.elsevier.com/retrieve/pii/0029549387900562.

[93] E. McNaghten, A. Parkes, B. Griffiths, A. Whitehouse, and S. Palanco. Detection of trace concentrations of helium and argon in gas mixtures by laser-induced breakdown spectroscopy. *Spectrochimica Acta Part B: Atomic Spectroscopy*, 64(10):1111–1118, 2009.

[94] P. Menegon, L. Desgranges, Y. Pontillon, and A. Poulesquen. Evidence of two gas release kinetics during the oxidation of an irradiated PWR UO2 fuel. *Journal of Nuclear Materials*, 378(1):1–8, Aug. 2008. ISSN 00223115. doi: 10.1016/j.jnucmat.2008.04.008. URL https://linkinghub.elsevier.com/retrieve/pii/S0022311508002110.

[95] M. A. Mignanelli and P. E. Potter. The reactions between sodium and plutonia, urania-plutonia and urania-plutonia containing fission product simulants. *Journal of Nuclear Materials*, 125(2):182–201, July 1984. ISSN 0022-3115. doi: 10.1016/0022-3115(84)90545-2. URL https://www.sciencedirect.com/science/article/pii/0022311584905452.

[96] A. Mitra, R. Sarangapani, S. Chandrasekaran, and M. Jose. Estimation of activity concentrations of radioactive gases inside containment building of fast breeder reactor fbtr: Leakage of active cover gas. *Progress in Nuclear Energy*, 124:103368, 2020.

[97] H. Mochizuki, N. Kikuchi, and S. Li. Computation of natural convection test at phenix reactor using the netflow++ code. *Nuclear Engineering and Design*, 262:1–11, 2013.

[98] P. O. Mogbolu, O. Akinola, and C. Uguru. Application of genetic algorithm in deconvolution of logs. In *Nigeria Annual International Conference and Exhibition*. OnePetro, 2011.

[99] Z. Mou-Yan and R. Unbehauen. A deconvolution method for spectroscopy. *Measurement Science and Technology*, 6(5):482, 1995.

[100] R. Nakai. Safety design criteria (sdc) for gen-iv sodium-cooled fast reactor. 2013.

[101] J. Namitha, U. Maity, T. Selvalakshmi, P. Manoravi, G. A. Kumar, M. Joseph, and N. Sivaraman. Feasibility study on application of laser induced breakdown spectroscopy for detection & identification of failed fuel pins and sodium–water reaction in fast reactors. *Journal of Analytical Atomic Spectrometry*, 35(7):1412–1422, 2020.

[102] H. Ohshima and S. Kubo. 5 - Sodium-cooled fast reactor. In I. L. Pioro, editor, *Handbook of Generation IV Nuclear Reactors*, Woodhead Publishing Series in Energy, pages 97–118. Woodhead Publishing, Jan. 2016. ISBN 978-0-08-100149-3. doi: 10.1016/B978-0-08-100149-3.00005-7. URL https://www.sciencedirect.com/science/article/pii/B9780081001493000057.

[103] D. R. Olander. Fundamental aspects of nuclear reactor fuel elements: solutions to problems. Technical report, California Univ., Berkeley (USA). Dept. of Nuclear Engineering, 1976.

[104] J. Parisot. *Sodium-cooled Nuclear Reactors*. DEN monographs. Editions Le Moniteur, 2016. ISBN 9782281140552. URL https://books.google.fr/books?id=wG_dnQAACAAJ.

[105] J.-F. Parisot and France, editors. *Sodium-cooled nuclear reactors*. DEN monograph. Editions Le Moniteur : CEA, Paris, 2016. ISBN 978-2-281-14055-2. OCLC: ocn957531942.

[106] M. Philippe et al. *Caracterisation et modelisation du comportement thermodynamique du combustible RNR-Na sous irradiation*. PhD thesis, Aix-Marseille, 2014.

[107] Y. Pontillon, I. Moysan, S. Bernard, and M. Ledieu. NEW INSIGHT ON VOLATILE FISSION PRODUCTS (I AND Cs) RELEASE FROM HIGH BURNUP UO2 FUEL UNDER LOCA TYPE CONDITIONS. page 10.

[108] H. O. Portner, D. C. Roberts, H. Adams, C. Adler, P. Aldunce, E. Ali, R. A. Begum, R. Betts, R. B. Kerr, R. Biesbroek, et al. Climate change 2022: impacts, adaptation and vulnerability. 2022.

[109] N. Ramanathan, M. Bootharajan, G. A. Kumar, K. Sundararajan, A. S. R. Murthy, S. Chandra, and V. Jayaraman. Interaction of krypton and xenon with sodium and activated charcoal: Identification and modeling using gas chromatography and density functional theory. *Journal of Nuclear Materials*, 558:153326, 2022.

[110] H. N. Ratliff, N. Matsuda, S.-i. Abe, T. Miura, T. Furuta, Y. Iwamoto, and T. Sato. Modernization of the dchain-phits activation code with new features and updated data libraries. *Nuclear Instruments and Methods in Physics Research Section B: Beam Interactions with Materials and Atoms*, 484:29–41, 2020.

[111] J. Rest and G. L. Hofman. Kinetics of Recrystallization and Fission-Gas-Induced Swelling in High Burnup UO2 and U3Si2 Nuclear Fuels. In S. E. Donnelly and J. H. Evans, editors, *Fundamental Aspects of Inert Gases in Solids*, NATO ASI Series, pages 443–456. Springer US, Boston, MA, 1991. ISBN 978-1-4899-3680-6. doi: 10.1007/978-1-4899-3680-6_38. URL https://doi.org/10.1007/978-1-4899-3680-6_38.

[112] S. Rogozhkin, S. Osipov, A. Salyaev, S. Usynina, V. Pokhilko, and M. Sazonova. Numerical modeling of delayed-neutron precursor transport in a sodium-cooled fast reactor. *Atomic Energy*, 128(4):245–250, 2020.

[113] E. Rohée. *Détection des ruptures de gaines sur RNR-Na par spectrométrie gamma hauts taux de comptage*. PhD thesis, Normandie Université, Université Caen Normandie, 2016.

[114] E. Rohée, R. Coulon, C. Jammes, S. Normand, F. Carrel, F. Lainé, H. Hamrita, and P. Filliatre. Clad failure detection system based on Delayed Neutron Detection without photoneutron noise for Sodium-cooled fast reactors. In *2014 IEEE Nuclear Science Symposium and Medical Imaging Conference (NSS/MIC)*, pages 1–7, Nov. 2014. doi: 10.1109/NSSMIC.2014.7431098.

[115] E. Rohée, R. Coulon, C. Jammes, P. Filliatre, S. Normand, F. Carrel, F. Lainé, and H. Hamrita. Delayed Neutron Detection with graphite moderator for clad failure detection in Sodium-Cooled Fast Reactors. *Annals of Nuclear Energy*, 92:440–446, June 2016. ISSN 0306-4549. doi: 10.1016/j.anucene.2016.02.003. URL http://www.sciencedirect.com/science/article/pii/S0306454916300639.

[116] H. Rui and C. Shu-ming. Sodium-cooled fast breed reactor fuel failure detection based on cover gas monitoring. In *International Confernece Pacific Basin Nuclear Conference*, pages 881–892. Springer, 2016.

[117] J.-F. Saillant, R. Marlier, and F. Baque. First results of non-destructive testing under liquid sodium at 200° c. In *2016 IEEE International Ultrasonics Symposium (IUS)*, pages 1–4. IEEE, 2016.

[118] Y. Sakamoto, J.-C. Garnier, J. Rouault, C. Grandy, T. Fanning, R. Hill, Y. Chikazawa, and S. Kotake. Selection of sodium coolant for fast reactors in the us, france and japan. *Nuclear Engineering and Design*, 254:194–217, 2013.

[119] P. Samanta, D. Diamond, and W. Horak. Nrc regulatory history of non-light water reactors (1950-2019). Technical report, Brookhaven National Lab.(BNL), Upton, NY (United States), 2019.

[120] K. Samuelsson, J.-C. Dumas, B. Sundman, and M. Lainet. An improved method to evaluate the "joint oxyde-gaine" formation in (u, pu) o2 irradiated fuels using the germinal v2 code coupled to calphad thermodynamic computations. *EPJ Nuclear Sciences & Technologies*, 6:47, 2020.

[121] T. Sato, K. Niita, N. Matsuda, S. Hashimoto, Y. Iwamoto, T. Furuta, S. Noda, T. Ogawa, H. Iwase, H. Nakashima, et al. Overview of particle and heavy ion transport code system phits. *Annals of Nuclear Energy*, 82: 110–115, 2015.

[122] J. Serp, C. Poinssot, and S. Bourg. Assessment of the anticipated environmental footprint of future nuclear energy systems. evidence of the beneficial effect of extensive recycling. *Energies*, 10(9):1445, 2017.

[123] E. Shpil'Rain, S. N. Skovorod'ko, and A. G. Mozgovoi. New data on the solubility of inert gases in liquid alkali metals at high temperature. *High temperature*, 40(6):825–831, 2002.

[124] E. E. Shpil'rain, S. N. Skovorod'ko, and A. G. Mozgovoi. The solubility of inert gases in liquid-metal heat-transfer agents. *High Temperature*, 38(3): 384–388, May 2000. ISSN 0018-151X, 1608-3156. doi: 10.1007/BF02755996. URL http://link.springer.com/10.1007/BF02755996.

[125] R. Smith and C. Doe. Cladding failure simulation tests in ebr-ii. Technical report, Argonne National Lab., Ill., 1966.

[126] R. Smith, E. Ebersole, R. Fryer, and P. Henault. Origin of fission-product releases in ebr-ii, november 23, 1967–may 6, 1968. Technical report, Argonne National Lab., Ill., 1970.

[127] B. J. Snyder and H. Foerch. Advanced ultrasonic failed fuel rod detection system. *Trans. Am. Nucl. Soc.;(United States)*, 52(CONF-860610-Summs.), 1986.

[128] T. Sofu. A review of inherent safety characteristics of metal alloy sodium-cooled fast reactor fuel against postulated accidents. *Nuclear Engineering and Technology*, 47(3):227–239, Apr. 2015. ISSN 1738-5733. doi: 10.1016/j.net.2015.03.004. URL http://www.sciencedirect.com/science/article/pii/S1738573315000753.

[129] G. Srinivasan, R. Keshavamurthy, D. Subramanian, A. Haridas, C. Reddy, V. Sathiyamoorthy, S. Varadarajan, and K. Suresh Kumar. Delayed neutron measurements with a natural uranium fission product source in Fast Breeder Test Reactor. *Annals of Nuclear Energy*, 65:314–319, Mar. 2014. ISSN 03064549. doi: 10.1016/j.anucene.2013.11.015. URL https://linkinghub.elsevier.com/retrieve/pii/S0306454913005999.

[130] R. V. Strain, J. H. Bottcher, S. Ukai, and Y. Arii. Fuel-sodium reaction product and its influence on breached mixed-oxide fuel pins. *Journal of Nuclear Materials*, 204:252–260, Sept. 1993. ISSN 0022-3115. doi: 10.1016/0022-3115(93)90224-M. URL http://www.sciencedirect.com/science/article/pii/002231159390224M.

[131] T. Stummer, Y. Peneliau, and C. Gonnier. Neutronic study regarding transmutation fuel research at jules horowitz reactor. Technical report, 2009.

[132] T. Stummer, M. Blanc, and B. Pouchin. Approximation of fast reactor spectra at the jhr. Technical report, 2011.

[133] K. Swaminathan, A. Rajendran, and G. Elumalai. The development and deployment of an ultrasonic under-sodium viewing system in the fast breeder test reactor. *IEEE Transactions on nuclear science*, 37(5):1571–1577, 1990.

[134] D. Tenchine. Some thermal hydraulic challenges in sodium cooled fast reactors. *Nuclear Engineering and Design*, 240(5):1195–1217, May 2010. ISSN 0029-5493. doi: 10.1016/j.nucengdes.2010.01.006. URL https://www.sciencedirect.com/science/article/pii/S0029549310000300.

[135] D. Tenchine, D. Pialla, T. H. Fanning, J. W. Thomas, P. Chellapandi, Y. Shvetsov, L. Maas, H. Y. Jeong, K. Mikityuk, A. Chenu, H. Mochizuki, and S. Monti. International benchmark on the natural convection test in Phenix reactor. *Nuclear Engineering and Design*, 258:189–198, May 2013. ISSN 0029-5493. doi: 10.1016/j.nucengdes.2013.02.010. URL https://www.sciencedirect.com/science/article/pii/S0029549313000599.

[136] J. Tommasi, J. M. Ruggieri, J. F. Lebrat, D. Plisson-Rieunier, and J. C. Sublet. Present status of jeff-3.1 validation for fast reactors using the eranos-2.1 code system. 7 2006. URL https://www.osti.gov/biblio/22039727.

[137] J. Trapp, C. Berlin, J. Gourdon, J. Perrigueur, and M. Vanbenepe. Clad failures detection using integrated detectors-validation at super-phenix. In *In core instrumentation and reactor assessment*. 1989.

[138] J. Trapp, M. Moro, M. D. Garreton, M. Vanbenepe, and P. Renaud. Comparison of failed fuel detection mock-up with superphenix measurements. *Nuclear science and engineering*, 106(1):88–93, 1990.

[139] B. S. Triplett, E. P. Loewen, and B. J. Dooies. Prism: a competitive small modular sodium-cooled reactor. *Nuclear Technology*, 178(2):186–200, 2012.

[140] A. Tsikunov, A. Zhilkin, A. Lastov, L. Mamaev, E. Lisitsin, and S. Osipov. Fuel release into primary sodium of the bn-600 and br-10 reactors through natural and artificial defects in fuel pin claddings. 1996.

[141] P. Tsvetkov. 9 - Generation IV: USA. In I. L. Pioro, editor, *Handbook of Generation IV Nuclear Reactors*, Woodhead Publishing Series in Energy, pages 223–239. Woodhead Publishing, Jan. 2016. ISBN 978-0-08-100149-3. doi: 10.1016/B978-0-08-100149-3.00009-4. URL https://www.sciencedirect.com/science/article/pii/B9780081001493000094.

[142] J. A. Turnbull, C. A. Friskney, J. R. Findlay, F. A. Johnson, and A. J. Walter. The diffusion coefficients of gaseous and volatile species during the irradiation of uranium dioxide. *Journal of Nuclear Materials*, 107 (2):168–184, June 1982. ISSN 0022-3115. doi: 10.1016/0022-3115(82)90419-6. URL http://www.sciencedirect.com/science/article/pii/0022311582904196.

[143] S. UKAI, I. SHIBAHARA, and Y. ENOKIDO. Release Characterization of Delayed Neutron Precursors from Breached FBR Fuel Element. *Journal of Nuclear Science and Technology*, 26(10):931–938, Oct. 1989. ISSN 0022-3131. doi: 10.1080/18811248.1989.9734408. URL https://doi.org/10.1080/18811248.1989.9734408. Publisher: Taylor & Francis _eprint: https://doi.org/10.1080/18811248.1989.9734408.

[144] F. Varaine, G. Rodriguez, J. Hamy, H. Hayafune, T. Iitsuka, and H. Mochida. The collaboration of japan and france on the design of astrid sodium fast reactor. In *International Congress on Advances in Nuclear Power Plants (ICAPP-2017)*. International Congress on Advances in Nuclear Power Plants (ICAPP-2017), 2017.

[145] D. Verwaerde, J.-P. Serpantié, and J. Rouault. French sfr program and the astrid prototype. Technical report, 2009.

[146] J.-F. Vidal, P. Archier, B. Faure, V. Jouault, J.-M. Palau, V. Pascal, G. Rimpault, F. Auffret, L. Graziano, E. Masiello, et al. Apollo3 homogenization

techniques for transport core calculations—application to the astrid cfv core. *Nuclear Engineering and Technology*, 49(7):1379–1387, 2017.

[147] S. S. P. Wahnon, L. Ammirabile, J. Kloosterman, and D. Lathouwers. Multi-physics models for design basis accident analysis of sodium fast reactors. part i: Validation of three-dimensional trace thermal-hydraulics model using phenix end-of-life experiments. *Nuclear Engineering and Design*, 331:331–341, 2018.

[148] A. E. Waltar, D. R. Todd, and P. V. Tsvetkov. *Fast spectrum reactors*. Springer, 2011.

[149] R. J. White and M. O. Tucker. A new fission-gas release model. *Journal of Nuclear Materials*, 118(1):1–38, Aug. 1983. ISSN 0022-3115. doi: 10.1016/0022-3115(83)90176-9. URL https://www.sciencedirect.com/science/article/pii/0022311583901769.

[150] C. Wise. Recoil release of fission products from nuclear fuel. *Journal of Nuclear Materials*, 136(1):30–47, Oct. 1985. ISSN 0022-3115. doi: 10.1016/0022-3115(85)90028-5. URL http://www.sciencedirect.com/science/article/pii/0022311585900285.

[151] B. Yewang, Z. Donghui, X. Wenbin, L. Huwei, W. Mingyu, and W. Xinzhe. Discussion of tag gas method using in china experimental fast reactor for failed fuel assembly location. *Journal of Nuclear Engineering and Radiation Science*, 4(4), 2018.

[152] F. Zylbersztejn. Developments and application of neutron noise diagnostics of sodium cooled fast reactors; developpement et application des techniques de bruit neutronique dans les reacteurs a neutrons rapides a caloporteur sodium. 2013.

[153] F. Zylbersztejn, P. Filliatre, and C. Jammes. Analysis of the experimental neutron noise from the phenix reactor. *Annals of Nuclear Energy*, 60:106–114, 2013.

Résumé étendu

Depuis le début du nouveau siècle, de nouvelles demandes énergétiques apparaissent et le réchauffement climatique dû aux énergies fossiles est devenu un enjeu majeur. L'énergie nucléaire, qui fournit aujourd'hui environ 10 % de l'électricité mondiale à partir d'environ 440 réacteurs de puissance, est la deuxième source d'énergie à faible émission de carbone au monde (28 % du total en 2019). Dans le respect des niveaux de "décarbonation profonde" qui ont été largement débattus dans les délibérations politiques internationales, l'énergie nucléaire contribue à minimiser ou à limiter la hausse des coûts du système, ce qui rend plus réaliste la réalisation d'objectifs d'émissions rigoureux.

Dans le développement futur de l'énergie nucléaire, il est nécessaire non seulement d'améliorer en permanence la sécurité et le modèle économique, mais également d'améliorer le traitement de l'approvisionnement en combustible nucléaire et de l'élimination des déchets nucléaires. Une meilleure utilisation des ressources naturelles et une réduction des déchets à vie longue sont les principaux facteurs contribuant au regain d'intérêt pour les réacteurs isogénérateurs rapides.

Les systèmes d'énergie nucléaire de génération IV présentent des avancées significatives en termes d'économie, de sécurité, de fiabilité et de durabilité par rapport aux réacteurs actuellement en service. Le réacteur rapide refroidi au sodium (SFR) possède la base technologique la plus complète parmi les réacteurs de génération IV.

Lors de l'exploitation du SFR, il peut y avoir des ruptures de gaines, la gaine constituant la première barrière de confinement du combustible à l'intérieur du cœur. La libération de matières fissiles à partir d'une rupture de gaine, peut entraîner des bouchages des canaux de refroidissement, et entraver le refroidissement du sodium et éventuellement conduire à une menace sur l'intégrité du cœur du SFR. Le "concept sodium propre" est la règle en France pour assurer la fiabilité du réacteur.

Un système de mesure de la contamination a été conçu afin de rechercher en continu la libération de produits de fission par une rupture d'aiguille combustible, comprenant deux systèmes de détection :

- Le premier est le système DRG, le système de détection de gaz, qui se caractérise par la détection d'une fissure dans la première phase de rupture de gaine, caractérisée par le dégagement de gaz de fission. Ce moyen d'inspection précoce peut éviter une menace pour la sécurité, par exemple en signalant à l'opérateur l'existence d'une fissure et lui permettant de décharger un ensemble défectueux lors d'un prochain arrêt de réacteur.

- Le second est le système DND, le système de détection de neutrons, qui sert à surveiller l'évolution du signal des neutrons retardés, émis par le DNP, qui indique la phase d'une rupture indésirable. Un seuil est fixé dans le système DND pour déclencher l'arrêt d'urgence du réacteur en cas de rupture jugée dangereuse.

Grâce à 50 ans d'expérience dans la conception, la construction et l'exploitation de SFR en France, les ruptures de gaines ont été étudiée dans le réacteur PHÉNIX (1973-2009), avec un total de 42 ruptures de gaines gaz et 15 ruptures de gaines ouvertes.

L'objectif principal de cette thèse est de développer une méthodologie générale décrivant l'ensemble du processus de détection de rupture de gaine pour une optimisation complète pour les conceptions futures. Afin de construire un modèle physique pour décrire l'ensemble du processus de détection, je définis une équation générique du signal obtenu :

$$D_{signal}(t) = \sum_{i=FP} R_i(t) * F_i(t) \times E_i + \sum_{j=BI} Q_j(t) * T_j(t) \times E_j \qquad (1)$$

Le premier terme de l'équation concerne la détection des produits de fission : avec i les isotopes des produits de fission (PF) ; $D_{signal}(t)$ est le signal détecté du détecteur ; $R_i(t)$ les produits de fission relâchés par la rupture de la gaine ; $F_i(t)$ la fonction de transfert, décrivant le transport depuis la rupture de la gaine jusqu'au détecteur ; E_i l'efficacité de détection des produits de fission.

Le second terme est lié au signal de fond : avec j les isotopes de fond (BI); Q_j la quantité d'isotopes de fond dans le réacteur ; $T_j(t)$ la fonction de transfert des isotopes de fond vers le détecteur ; E_j l'efficacité de détection des isotopes de fond.

Fondamentalement, dans un système de mesure de contamination, le signal détecté $D_{signal}(t)$ sera obtenu pour comprendre le signal libéré $R_i(t)$ par les produits de fission. L'efficacité de l'ensemble du système dépendra de la fonction de transfert $F_i(t)$ et de l'efficacité de détection E_i.

Cependant, lors des détections antérieures de rupture de gaine dans les des réacteurs SFR, par exemple RAPSODIE, PHÉNIX, SUPERPHÉNIX, l'analyse

du signal et l'interprétation de l'évolution du signal en lien avec comportement de l'aiguille combustible mérite d'être approfondie. En outre, du point de vue de la conception du système de détection, en raison des différents objectifs de surveillance et des caractéristiques de libération des produits de fission dans la détection des gaz et des neutrons, différents paramètres clé pour la conception du système de détection interviennent.

Par conséquent, je souhaite développer une méthodologie générale du processus de détection à travers l'analyse théorique et la modélisation numérique de $R_i(t)$ et $F_i(t)$ et E_i ainsi que l'étude des données expérimentales de $D_{signal}(t)$, afin d'appréhender les caractéristiques de relâchement des produits de fission ; clarifier la relation entre $D_{signal}(t)$ et $R_i(t)$; déterminer les paramètres clé des systèmes de détection de gaz et de neutrons respectivement ; optimiser la conception du système de détection de SFR à l'avenir.

Pour atteindre cet objectif, plusieurs étapes ont été mises en œuvre dans le cadre de ce travail de thèse pour faire l'analyse théorique et la modélisation numérique de chaque pièce, avec la validation des données expérimentales, lors de la détection des ruptures de gaine en SFR.

Dans la première partie du travail, le processus de détection DRG est décrit en détail. Des produits de fission d'intérêt sont identifiés, qui sont des gaz de fission rares (xénon, krypton) libérés lors de la première phase de rupture et sont des indicateurs précoces de rupture de fissure. L'ensemble du scénario de détection de gaz est développé et divisé en différentes étapes, dans lesquelles la formulation de la procédure de transport fait défaut. Ainsi, un modèle de fonction de transfert est proposé pour prédire l'élargissement temporel du signal observé. En établissant le schéma de transfert des gaz de fission et l'équation de conservation des rejets de gaz de fission, on en déduit la formule générale de la fonction de transfert. Pour les cas de fissures à ouverture rapide, la libération de gaz dans un SFR devrait être presque instantanée, en raison de la différence de pression entre l'aiguille de combustible et le sodium. On s'attend à ce que le signal observé soit principalement donné par la fonction de transfert. Les données expérimentales à grande rupture peuvent être utilisées comme évaluations expérimentales de la fonction de transfert. Par conséquent, une modélisation de la fonction de transfert est effectuée en utilisant les paramètres du réacteur PHÉNIX et comparée aux données expérimentales du cas choisi RG 14 (quatorzième rupture du catalogue). Les résultats montrent un bon accord, avec le même ordre de grandeur de l'élargissement temporel et la même forme de décroissance exponentielle. En conséquence, la fonction de transfert du système DRG est validée, ce qui est nécessaire pour la modélisation globale.

Dans la deuxième partie de ce travail, sur la base de la fonction de transfert, une méthodologie générique a été développée pour décrire l'ensemble du système de

détection de gaz dans SFR, comprenant : la quantité de gaz de fission accumulée dans le plénum de gaz, le flux de gaz qui fuit à travers la fissure, le processus de transport du combustible au détecteur, la sensibilité du détecteur à différents isotopes. Le processus global de détection est modélisé avec la simulation de chaque module :

1. en l'absence de fissure de gaine, la production de gaz de fission est calculée par les équations différentielles de Bateman avec le temps de fonctionnement du réacteur ; les gaz de fission accumulés et la pression dans le plénum de gaz sont déterminés par un code d'évolution du combustible, par exemple Germinal;

2. en cas de fissure, la perte d'étanchéité et la dépressurisation sont simulées en modélisant les fuites de gaz avec un diamètre de fissure ;

3. l'activité des gaz de fission vers le détecteur est obtenue avec la convolution du flux de fuite de gaz et de la fonction de transfert ;

4. la sensibilité du détecteur est modélisée par un code de simulation de transport de particules Monte Carlo, par exemple PHITS ;

5. le signal détecté en fonction de la dimension de la fissure est déduit.

Par conséquent, une évaluation de la sécurité des fuites pour PHÉNIX à l'aide de cette méthodologie a été réalisée, reflétant ses performances de détection précoce dans le système DRG. Avec cette application méthodologique, le signal de courant peut être dérivé en fonction de la taille de la fissure. Selon les résultats de la modélisation, des optimisations possibles pour la conception future ont été proposées.

Dans la troisième partie de ce travail, une simulation de l'émission et de la détection du signal neutronique est réalisée afin de décrire le système DND. Un schéma global de l'ensemble du processus de détection des neutrons est développé, y compris les produits de fission libérés de l'aiguille de combustible vers le sodium, le processus de transfert dans les lignes d'échantillonnage, et l'efficacité du détecteur pour les neutrons retardés. Les isotopes d'intérêt lors de la phase de rupture de gaine ouvert sont précisés, qui sont les DNP (iode, brome). Étant donné que le mécanisme de libération du DNP dépend de la température et des conditions du combustible, le mécanisme athermique, le recul direct, n'est pris en compte que dans cette partie de la modélisation. Ainsi, une simulation du transfert du signal neutronique pour la libération directe de recul de DNP est effectuée :

1. le courant de recul de la surface de rupture a été dérivé à l'aide du rapport de libération et de la plage de recul calculée par SRIM ;

2. un schéma de libération de DNP par le sodium a été établi, et la concentration de DNP collecté dans le bloc DND a été obtenue ;

3. l'efficacité du détecteur a été dérivée d'études de la littérature ;

4. le taux de comptage des neutrons retardés dans le détecteur pour une taille de rupture donnée a été calculé et les résultats de la modélisation ont été comparés aux données expérimentales.

Il en résulte que la fonction de transfert de DND est essentiellement un décalage temporel et que le signal de libération du recul est cohérent avec le signal détecté au début.

Dans la quatrième partie de ce travail, une amélioration de la modélisation de la diffusion des DNP en fonction du temps est étudiée. Le cas expérimental RG 11, avec une rupture de petite taille en début de vie, a été choisi comme cas d'étude. Les caractéristiques de la rupture et du signal neutronique du RG 11 sont analysées et il est considéré que l'augmentation du signal neutronique est due au changement d'état du combustible. Ainsi, une modélisation physique est présentée pour étudier l'influence de la couche de corrosion du combustible sur l'évolution temporelle du signal neutronique retardé :

1. un schéma de formation de la couche de corrosion a été proposé ;

2. la distribution de température à la périphérie de l'aiguille de combustible a été calculée dans COMSOL ;

3. le dégagement par diffusion thermique en fonction de la température a été calculé, ainsi que la cinétique de la couche de corrosion ;

4. la libération par diffusion améliorée lors de la formation de la couche de corrosion a été déduite.

Le résultat de la modélisation est comparé aux données expérimentales du cas RG 11 et l'interprétation possible de l'évolution des neutrons est proposée. On peut en conclure qu'un changement de température influence le mécanisme de diffusion à la périphérie de l'aiguille de combustible en raison de la formation d'une couche de corrosion ; la diffusion est cohérente avec l'évolution du signal neutronique. Ainsi, la diffusion des DNP au cours de la corrosion est susceptible d'expliquer l'évolution du signal neutronique, mais nécessitera d'autres expériences pour être quantifiée. Par ailleurs, d'autres phénomènes du combustible lors du

relargage du DNP ont été évoqués : l'élévation de température due à la couche de corrosion peut générer une bouffée de gaz pulsé à partir des bulles de gaz du combustible, ce qui peut également conduire à une augmentation du signal neutronique ; en raison de la réouverture de l'espace, le dégagement de gaz après l'arrêt est important, il n'est donc pas recommandé de recharger les barres de combustible défectueuses.

On peut généralement conclure qu'une vue d'ensemble de la détection des ruptures de gaine a été obtenue avec la méthodologie proposée. Ainsi, j'ai formulé les conclusions suivantes :

- Pour le système DRG : une fonction de transfert du système de détection de gaz a été déterminée. Une méthodologie générique a été développée pour décrire l'ensemble du système de détection de gaz, applicable à des SFR arbitraires. Pour la conception future du système de détection, la formule générale peut être appliquée pour guider le choix de conception. La méthodologie peut être utilisée comme une boîte à outils pour une optimisation complète en modifiant les variables de l'équation générale. De plus, l'application de la fonction de transfert peut contribuer à une meilleure compréhension du transfert des gaz de fission dans les SFR. La déconvolution du signal détecté pourrait être utilisée pour interpréter les données DRG en temps réel.

- Pour le système DND : une vue globale du processus de transfert des signaux neutroniques a été dérivée. Il a été constaté que l'augmentation du dégagement par diffusion lors de la formation de la couche de corrosion est susceptible d'expliquer l'évolution du signal neutronique, mais nécessitera d'autres expériences quantifiées. Pour une surveillance plus précise de la taille de la rupture, le mécanisme de libération du DNP et les comportements du combustible à la rupture devraient faire l'objet de recherches futures.

Dans la dernière partie du travail, j'ai discuté de l'application de cette méthodologie à la conception future puisque la conception est un problème d'optimisation multivariée. Dans le cadre du réacteur, le système d'instrumentation et la conception du détecteur doivent être considérés ensemble dès le début de la conception pour sélectionner les paramètres du réacteur. Une boucle d'optimisation peut être envisagée dans une procédure de conception de futurs réacteurs, dans laquelle la méthodologie générale peut être appliquée pour aider à la conception. Par exemple, un logiciel complet de conception d'instrumentation peut être développé, prenant en compte les différents choix de paramètres du système de détection, les méthodes de détection et la configuration des futurs réacteurs.

J'ai également proposé où le modèle doit être amélioré : appliquer les nouvelles méthodes de détection à la méthodologie générale, telle que les méthodes optiques, la technologie ultrasonore, les différents type de détecteurs de neutrons et les détecteurs de spectrométrie ; ajouter l'interprétation en temps réel du signal combiné, tels que le neutron, gamma, acoustique, pression ; obtenir des comportements de carburant plus précis en réalisant des expériences sur le carburant, tel que la façon dont le sodium pénètre dans la gaine, la chimie du sodium en contact avec le combustible et l'effet de la formation de JOG sur la libération de DNP. J'ai aussi proposé quelles expériences peuvent être faites dans les travaux futurs : les tests de fonction de transfert dans la maquette d'eau, les boucles d'expérimentation pour les tests de capacité des détecteurs, les applications de la technologie du jumeau numérique.

De par ses résultats prometteurs et ses applications, j'espère que la méthodologie générale développée dans cette thèse sera un apport précieux pour les chercheurs et les ingénieurs travaillant sur la détection des ruptures de gaine des SFR.

Acknowledgments

Most importantly, I express my deepest gratitude towards my supervisor FILLIATRE Philippe and co-supervisor DESGRANGES Lionel, for the continuous support and encouragement from the starting of the thesis work. During the research, they gave me the freedom to explore on my own and at the same time helped me plan the work with their immense knowledge and experience. I am always inspired by their valuable guidance and timely reviews. They are not only my teachers and work partners, but also life mentors and friends. I am very glad and lucky to work with them during these three years.

I would like to thank the committee members for their presence in the defense, their careful reading of my thesis, and the remarks they addressed to me to improve my work.

I also would like to present my sincere gratitude to my department, service and laboratory: DES/IRESNE/DER/SPESI/LDCI (Laboratoire de Dosimétrie, Capteurs et Instrumentation). Thanks for CEA Cadarache and the TECNA project which gave me a wonderful and memorable experience. Thank you to my colleagues for the constructive suggestions and amiable help: THIOLLAY Nicolas, LAMOTTE Maxime, DE IZARRA Grégoire, IRAZOQUI Kevin and others.

I am grateful to my lovely friends in CEA and in Aix en Provence, for accompanying me through my thesis study in pleasure: BOUCHON Baptiste, CAZENAVE Damien, KEDZIERSKA Barbara, Chaowei Xu, Xiaolong Zhang, Haifu Huang, Yifan Peng, Linkai Wei, Chunhui Dang, Shuqi Xu, Shengli Chen, PARK Yeseul and others.

Last but not least, I am thankful to my parents, family and friends in China for their support and concerns.

Publications

Ding, C., P. Filliatre, and L. Desgranges. "Gas detection in sodium cooled fast reactors: determination of a transfer function." In EPJ Web of Conferences, vol. 253, p. 05002. EDP Sciences, 2021.

Ding, C., P. Filliatre, L. Desgranges, and D. Friant. "How could fuel corrosion influence the delayed neutron signal time evolution in sodium cooled fast reactors?" Nuclear Engineering and Design 398 (2022): 111977.

Ding, C., P. Filliatre, and L. Desgranges. "General methodology for gas monitoring of cladding failure in sodium-cooled fast reactors" Nuclear Engineering and Design. (under review)

Filliatre, P., C. Jammes, C. Ding, L. Desgranges, and R. Coulon. "Conception of delayed neutron detector blocks in a sodium cooled fast reactor." Nuclear Engineering and Design 371 (2021): 110933.

Abstract

The Generation IV nuclear energy systems present significant advancements in economics, safety, reliability and sustainability, in which Sodium cooled Fast Reactor (SFR) has the most comprehensive technological basis. During the operation of SFR, cladding failures may happen: the release of fissile materials from the failure can result in coolant channel blockages which may lead to a threat on the core integrity in SFR. A contamination measuring system has to be designed in order to continuously search for the release of fission products by a fuel pin failure. Gaseous fission products release will be at the first stage of failure and will be detected by DRG system (Gas detection system). When the crack of cladding is enlarged, the fuel will be in contact with sodium and the neutron signal will be detected in the DND system (Delayed neutron detection system).

This thesis presents an overall view of cladding failure detection, from the behavior of the fission products within the fuel to the signal interpretation of the detector. A general methodology of detection process is developed: first, the transfer function of DRG system is determined; second, a description of the whole process of gas detection is given and applied to analyze the reliability of early detection of DRG system; third, a modeling of the whole process of DND system for the basic release of direct recoil is performed and the neutron transfer process is deduced; finally, the enhanced thermal diffusion release due to corrosion layer formation is simulated and the interpretation of the neutron signal evolution related to the fuel behavior is proposed.

The methodology is grounded by a theoretical analysis of the physical phenomena at stake, its results are confronted to a reassessment of the experimental data from the previous PHENIX reactor. Its form is versatile enough to be applied to future design of reactors: its guidance ability for the conception of their cladding failure detection systems has been exemplified.

Keywords: Gas detection, Transfer function, Neutron detection, Corrosion layer formation, PHENIX reactor, Sodium-cooled fast reactors

Résumé

Les réacteurs nucléaires de génération IV présentent des avancées significatives en terme d'économie, de sécurité, de fiabilité et de durabilité. Parmi ceux-ci, le réacteur à neutrons rapides refroidi au sodium (SFR) bénéfice de la plus grande expertise technologique. Lors de l'exploitation d'un SFR, des ruptures de gaine peuvent survenir : la libération de matières fissiles par la rupture peut entraîner des bouchages de canaux de refroidissement pouvant conduire à une menace sur l'intégrité du cœur. Un système de mesure de la contamination doit être conçu afin de rechercher de manière continue les produits de fission libérés par une rupture d'aiguille combustible. Les rejets de produits de fission gazeux correspondent au premier stade de défaillance et seront détectés par le système DRG (Système des ruptures de gaine). Lorsque la fissure de la gaine s'élargit, le combustible sera en contact avec le sodium et le signal neutronique sera détecté dans le système DND (Système de détection de neutrons différés).

Cette thèse présente une vision d'ensemble de la détection des ruptures de gaine, depuis le comportement des produits de fission dans le combustible jusqu'à l'interprétation du signal du détecteur. Une méthodologie générale du processus de détection est développée : premièrement, la fonction de transfert du système DRG est déterminée ; deuxièmement, une description de l'ensemble du processus de détection de gaz est donnée et appliquée pour analyser la fiabilité de la détection précoce du système DRG ; troisièmement, une modélisation de l'ensemble du processus du système DND pour la libération de base du recul direct est effectuée et le processus de transfert de neutrons est déduit ; enfin, la libération par diffusion thermique, renforcée par la formation d'une couche de corrosion, est simulée et l'interprétation de l'évolution du signal neutronique liée au comportement du combustible est proposée.

La méthodologie est fondée sur une analyse théorique des phénomènes physiques mis en jeu ; ses résultats sont confrontés à une réévaluation des données expérimentales du précédent réacteur PHENIX. Son formalisme est suffisamment général pour être appliqué à la conception future de réacteurs : sa capacité à orienter la conception de leurs systèmes de détection de rupture de gaine est illustrée.

Mots clés : Détection de gaz, Fonction de transfert, Détection de neutrons, Formation de corrosion, Réacteur PHENIX, Réacteurs rapides refroidis au sodium